NASA CR - 72323

C O N T R A C T O R R E P O R T

THE EFFECT OF PERIODIC PRESSURE AND TEMPERATURE FLUCTUATIONS ON UNSTEADY HEAT TRANSFER IN A CLOSED SYSTEM

by

Daniel W. Wendland

prepared for

NATIONAL AERONAUTICS AND SPACE ADMINISTRATION

March 1, 1968

Contract NsG-601

Technical Management
NASA Lewis Research Center
Cleveland, Ohio
Chemistry and Energy Conversion Division
Paul R. Wieber

University of Wisconsin
Department of Mechanical Engineering
Madison, Wisconsin

Acknowledgments

A number of individuals and organizations should be credited with helping support and guide this project:

Professor Phillip S. Myers and Professor Otto A. Uyehara for their insight and advice; Associate Professor Gary L. Borman for mathematical guidance and assistance;

The National Science Foundation for five years of personal financial support;

The National Aeronautics and Space Administration, for project financial and technical support;

Tom LeFeuvre, Ray Goluba, and other graduate student friends, for their helping hands and willing minds; and

My wife Kathleen, for long hours of editing and typing, and for her continual encouragement.

The Effect of Periodic Pressure and Temperature Fluctuations on Unsteady Heat Transfer in a Closed System

DANIEL W. WENDLAND

SUMMARY

The purpose of this project was to study the nature of the unsteady heat transfer from a closed gas system to a plane metal surface with the gas experiencing periodic pressure and temperature oscillations. The gas system was defined by a piston-cylinder-head compression chamber; the piston was driven by a variable-speed motor to generate the gas pressure and temperature fluctuations. Gas pressure histories were measured with a piezoelectric pressure transducer. Gas temperatures were measured with a 3.81 micron hot-wire anemometer probe used as an uncompensated resistance thermometer. Instantaneous metal surface (the surface of the head of the chamber) temperature was measured with a fast-response surface thermocouple with a one-micron junction thickness.

A mathematical technique was developed to calculate instantaneous metal surface heat transfer rates: experimentally measured surface temperature histories were introduced into a CDC 3600 digital computer program which calculated, listed, and plotted surface heat transfer histories.

In the experimental observations, the gas pressure history had an amplitude of about 365 psi and a mean value of about 197 psi; the pressure maximized at about 2 1/2 degrees before the volume minimum (TDC). These histories were essentially unaffected by system frequency throughout the experimental range (15 to 58 Hz). The bulk gas temperature histories had amplitudes on the order of 600 F°, mean values near 370°F, and peaked at about three degrees before TDC; these histories were somewhat frequency-sensitive. Some of the frequency-sensitivity is attributed to phase lags of the gas temperature transducer.

As the driving frequency was changed, two regimes of response in periodic metal surface temperature to these gas property variations were noted. At moderate and high frequencies (25 to 58 Hz) the wall surface temperature was fairly sharply peaked, maximizing at about zero crankangle degrees (i.e., piston TDC). A theoretical model viewing the thermal boundary layer as a time-varying resistance predicted essentially this behavior. An even better prediction was obtained with a model derived from the one-dimensional energy equations and containing resistive, capacitive, convective, and pressure work terms. These models are not included in this report, as a far superior theoretical model was developed in the last months of the research period. For information on these secondary models, the reader is referred to the appendices of the author's Ph.D. thesis, published in January, 1968 at the University of

Wisconsin.

The superior theoretical model mentioned above was formulated from thermodynamic principles and contained little or no empirical information. The model predicted wall heat transfer histories which were very similar to the heat transfer histories calculated from the medium and high frequency experimental data. The model, termed the Adiabatic Plane Model, also predicted negative, zero, and infinite heat transfer coefficients, and a phase lag of wall surface temperature with respect to bulk gas temperature of less than one crankangle degree.

At very low frequencies (up to perhaps 18 Hz), the wall temperature response was smooth and nearly sinusoidal, lagging the gas temperature peak by as much as 80 crankangle degrees; the peak location was highly frequency-sensitive. A theoretical model for the boundary layer proposing only resistive and capacitive effects can predict this type of temperature response. This model is explained in the appendices of the thesis mentioned above.

At intermediate frequencies, the two regimes combine and the wall surface temperature shows two maxima per cycle.

In summary, three conclusions can be drawn from this investigation:

1) the metal surface temperature and surface heat transfer rate are not in phase with the gas tem-

perature because of compression and expansion of the gas; the heat transfer coefficient based on Newton's Law of Cooling is therefore of doubtful utility, as the coefficient assumes negative, zero, and infinite values;

2) the lag of surface temperature behind gas temperature and pressure histories at moderate and high frequencies was found to be small (on the order of two or three crankangle degrees, or about .04 radians) and insensitive to frequency;

3) the surface heat transfer rate was found to lead the gas temperature at moderate and high frequencies by from eight to ten crankangle degrees (0.18 radians).

TABLE OF CONTENTS

LIST OF FIGURES

LIST OF TABLES

NOMENCLATURE

Symbol	Meaning
A	area; in^2, ft^2
A_k, B_k	Fourier coefficients
b	Biot factor, h_{mean}/k_{wall}; ft^{-1}
C_p, C, c_p, c_v	specific heats; $Btu/lb_m{}^\circ R$
d	wire diameter; microns, inches
f	frequency; Hertz
h	film coefficient; $Btu/hrft^2{}^\circ R$
H	enthalpy per unit area; Btu/ft^2
i, j, k, K	an index
k	thermal conductivity; $Btu/hrft\ ^\circ R$
L	connecting rod length; ft
m	mass per unit area in Adiabatic Plane Model; elsewhere, used as mass in lb_m
M	total mass per unit area in Adiabatic Plane Model; lb_m/ft^2
n	an index, polytropic coefficient
N	number of iterations, number of laminae, the last lamina
p, P	pressure; lb_f/in^2
$\dot{q}$	heat flux; Btu/ft^2sec, Btu/in^2sec
R	crank radius, ft; specific gas constant, electrical or thermal resistance
t	time; temperature in °F in heat transfer program discussion
T	temperature; °R, °F

Symbol	Meaning
u, v, w	velocity; ft/sec
V	volume, length^3; in Adiabatic Plane Model, V_n is volume per unit area, ft^{3n}/ ft^2
w	mass; lb_m
$\dot{W}$	rate of work
x	distance; ft, inches, mm
Nu	Nusselt Number; Nu_δ is Nusselt Number based on length δ
Pr	Prandtl Number
Re	Reynolds Number; Re_δ is Reynolds Number based on length δ
RPM	driving frequency; revolutions/ minute
TDC	top dead center position of piston (0 crankangle degrees)
BDC	bottom dead center position of piston ($\pm$ 180 crankangle degrees)
T_{egh}	effective gas temperature for head
T_{egp}	effective gas temperature for piston
Δx^+	distance between centers of laminae n+1 and n
Δx^-	distance between centers of laminae n and n-1
α	thermal diffusivity, ft^2/hr; proportionality constant
γ	ratio of specific heats, c_p/c_v
δ	boundary layer thickness; mm, ft
ε	phase angle
η	a coefficient

Symbol	Meaning
θ, Θ	time; wire time constant; temperature amplitude, °F
λ	mean free path
μ	viscosity
υ	kinematic viscosity
ρ	density, mass/volume
σ_k	Lanczos Smoothing Factor
τ	time
ϕ	phase shift; velocity function (Eqn. 81)
$\Delta\phi$	phase difference between two functions
ω	angular velocity
Ω	variable substituted for time, p. 154

Superscripts

$\sim$	swing (i.e., maximum - minimum)
$\cdot$	time rate of change

Subscripts

aj	air jacket (i.e., head exterior)
atm	atmospheric
bb	blowby
E	Eichelberg (pertaining to film coefficient)
g	gas
∞	at a great distance
int	internal

Subscript	Meaning
m	mean
mu	makeup
s	surface
ss	steady state
w	wall surface
δ	pertaining to edge of boundary layer

INTRODUCTION

One of the classical problems in the study of heat transfer is the case of energy exchange between a fluid and the plane surface of a solid plate or wall. Typically, the fluid at a great distance from the plate is at a constant temperature, and the plate is at a different temperature. The fluid traditionally moves in steady flow parallel to the plate, heat transfer occurs between plate and fluid, and velocity and temperature profiles are established in the fluid. In laminar flow, conditions at a given point of reference with respect to the solid surface do not change with time. In turbulent flow, relatively small perturbations in fluid properties are superimposed upon the unchanging flow conditions. Steady-state heat transfer at the plate surface at a distance x from the leading edge of the plate is described by:

$$q(x)/A = h(x) \cdot [T_s - T_\infty] \qquad (1)$$

where: $h(x)$ is the local heat transfer coefficient,
T_s is the local plate surface temperature, and
T_∞ is the fluid temperature at a great distance.

Theoretical arguments and experimental studies have produced many correlations for h in terms of fluid properties and the fluid velocity (or Nusselt Number in terms of Prandtl Number and Reynolds Number).

This investigation, too, is concerned with energy transport between a fluid and a wall. There are several conditions in this study, however, which differ significantly from the "classical" conditions:

1) The fluid motion is normal to the wall, not parallel to it.

2) The system is closed, not open; one mass of fluid (in this case, gas) undergoes a series of thermodynamic processes.

3) The gas conditions (pressure, temperature, velocity) far from the solid surface (in fact, throughout the system) are cyclical with time.

4) The plate, or wall, conditions (surface temperature, surface heat flux) are also cyclical.

This type of gas-solid interaction is of interest in two general areas: the study of unsteady heat transfer in rocket combustion chambers, and research in internal combustion engines (and in compressors).

In the piston engine, much of the energy of combustion and compression is lost through heat transfer. The precise nature of this unsteady heat transfer is still largely unknown; steady-state measurements (i.e., cooling water temperatures and flow rates) tell nothing about the time distribution of the energy loss from the gas around the working cycle. In a motored engine, the gas temperature may change by six or seven hundred Fahrenheit degrees during the cycle, while the response in compression chamber wall surface temperature will be on the order of a few degrees. Temperature gradients in the gas immediate to the wall may

be as high as 15,000 F^{o}/inch, the time rate of change of gas temperature may be as high as 2.5×10^{5} F^{o}/second (12 F^{o} per crankangle degree at 3600 rpm), and the time rate of change of gas pressure may reach 1.3×10^{5} psi/second.

In the rocket combustion chamber and nozzle, an oscillatory combustion phenomenon often occurs in which the gas pressure can swing by several hundred psi and the gas temperature by over 1000 F^{o} at frequencies from 50 - 250 Hz ("chugging") to several kHz ("screaming"). This represents rates of change of gas temperature and pressure several orders of magnitude greater than those encountered in engine work. Heat transfer takes place from hot gas to the walls; when the gas - wall temperature gradients are high and the thermal resistance of the gas near the walls is low, the heat flux rates are often high enough to burn through the nozzle.

Heat transfer also takes place from the hot gases to the vaporizing fuel and oxidizer droplets near the injector. The vaporization rate of the droplets responds in some fashion to the gas pressure and temperature changes; an increase in vaporization rate may support or oppose the impinging pressure waves, depending on the phase relationships.

The thermal response of surfaces to changes in gas con-

ditions is complicated by two factors:

1) as the gas has a heat capacity, capacitive energy storage and release will take place in the gas immediate to the wall at a rate proportional to the time rate of change of local temperature, and

2) since the gas pressure is changing with time, work done by the volume of gas near the wall will represent a source or a sink of energy.

Thus the behavior of the temperature and the energy fluxes in the wall and in the gas near the wall surface is of great interest. This is a broad area for inquiry: the cyclic frequencies can range to 10,000 Hz, the energy fluxes to hundreds of thousands of Btu/hrft^2, the temperatures to several thousand degrees R. The medium can range from air to luminous combustion gases. It is also a very difficult area for inquiry: rapidly changing local temperatures must be measured in complex flow situations under conditions far from ideal.

Practical considerations make it necessary to limit an investigation to a small range in operating variables and flow conditions. This investigation limits itself to fairly low frequencies (as far as rocket combustion instability is concerned), moderate pressure and temperature ratios (or swings), and a closed gas system. A study concerned with higher frequencies ($\tilde{=}$ 500 Hz), smaller pressure and temperature ratios, and an open system will be published in 1968 by R. W. Goluba*.

*Ph. D. candidate, University of Wisconsin (1968)

I. SURVEY ON PRESSURE WAVES AND HEAT TRANSFER

Prior to 1950, little interest was shown in the influence of pressure waves, mechanical vibration, and fluid velocity pulsations on heat transfer. Since that time, however, and particularly in the last ten years, quite a bit of effort has been expended in this direction. This is probably due to a number of factors: the discovery that certain frequencies and amplitudes of mechanical vibration can improve the performance of heat exchangers, the occurrence of vibration in rocket combustion and heat transfer, and the recent availability of high frequency-response recording equipment to study these effects.

Interest has centered, largely, on two types of systems. In the first, a horizontal or vertical plane surface or small cylinder in a fluid environment is mechanically induced to vibrate, and the influence of this motion on free or forced convection from object to fluid is noted. Typically, the heat transfer rate changes little until a critical vibration intensity (the product of frequency and amplitude) is reached, at which point the heat transfer rate increases by some 50%. The critical vibration intensity generally correlates with a transition in the type of boundary layer adjacent to the surface. Shine (1) presents a good example of this work and a bibliography of the same.

The second, and more pertinent, system category is one in

which pressure and/or velocity pulsations in a fluid environment impinge on a stationary surface (horizontal or vertical, plane or cylindrical), and the rate of heat transfer in free or forced convection is measured as a function of pulsation frequency and intensity. These researches can generally be categorized by the intensity, or amplitude, of the disturbance.

The great preponderance of papers found in the literature deal with very low amplitude (under one psi), or acoustic, oscillations in pressure and the attendant pulsations in fluid velocity. A very few investigations deal with high amplitude (up to, say, 100 or 200 psi) disturbances which are generated by sirens, resonators, or mechanical devices. A small but increasing number of studies are being made with very high amplitude (on the order of 500 psi) pressure waves whose source is an oscillatory combustion.

The low amplitude, or acoustic, disturbances have received much attention. Little theoretical work has been done in the area; most investigations are directed toward the mechanisms of heat transfer in the boundary layer with and without acoustic stimulation. Early investigators were concerned primarily with flow patterns in resonant tubes and not with heat transfer. Lord Rayleigh (2) performed a theoretical analysis of the flow patterns in Kundt's tube and predicted that resonant vibrations would produce quarter wave length vortices. This was later experimentally veri-

fied by Andrade (3). C. K. Hwu (4) investigated the effect of acoustic vibrations on the forced convective heat transfer for air flowing in a horizontal tube. An increase of up to 50% in laminar flow heat transfer was noted when the tube length and acoustic frequency were such that a standing wave was set up in the tube.

Fand (5) has done much work with a heated horizontal cylinder in an intense sound field. Free convection from the cylinder was found to be invariant with sound intensity below about 135 db (i.e., peak to peak pressure swing of 0.046 psi); from 136 db to 142 db at 1 kHz to 6 kHz driving frequency (i.e., 0.052 psi to 0.103 psi peak to peak), the rate of heat transfer increased sharply. Above 146 db (0.164 psi peak to peak), the increase was less rapid. Harrison, et. al., (6) studied the influence of stationary sound waves on a vertical heated tube in both free and forced convection. Up to 54% increase in film coefficient was observed. Kubanskii (7,8) has presented a number of excellent papers in this area. An electrically heated horizontal cylinder was subjected to an intense sound field during free convection in air. With frequencies from 8 kHz to 30 kHz, a 75% increase in heat transfer rate was noted for the intensity range of 145 db to 152 db (0.146 psi to 0.326 psi peak to peak). The same horizontal tube in forced convection was exposed to standing sound waves at right angles to the tube. The heat transfer was either not

changed or increased by about 50%, depending on the relation between the nodes of the standing wave and the tube axis. A practical application of this increase in heat transfer was noted by Boucher (9), who reported that the application of sound waves of 145 db intensity and 6 kHz frequency greatly increased the drying rate of liquid sprays, raw cotton, rubber pellets, and many other materials.

Researchers at the Georgia Institute of Technology have done much work in the area of acoustics and heat transfer since 1958 under the sponsorship of the Aeronautical Research Laboratory at Wright Field. Their work is summarized in papers by Jackson (10), Purdy (11), and Eastwood (12). The outside surface temperature of a 10.5 foot, 4.125 inch outside diameter horizontal copper tube is maintained at 210°F by a jacket of saturated steam. Air flows through the tube at about atmospheric pressure. A resonant acoustic vibration is generated at the downstream end by a 50-watt driver (or horn) operating in the frequency range 150-350 Hz. The greatest sound intensity obtained was 162.5 db (approximately 1.1 psi peak to peak) at 222 Hz.

Experimental results indicate that the resonant sound waves produce a spatially periodic variation in the local heat transfer coefficient. Two distinct spatial distributions of the heat transfer coefficient were discovered as the Reynolds number was changed. For Reynolds numbers below

about 20,000 the local heat transfer coefficient maximized at the velocity antinodes (which are also the pressure nodes). Above a Reynolds number of about 40,000 the heat transfer maxima are at the velocity nodes (which are the pressure antinodes). The intermediate Reynolds numbers produce a gradual transition between the two types of heat transfer, the actual changeover taking place at Re=35,000.

A locus of critical sound intensity levels exists below which essentially no change in the heat transfer takes place. The critical sound intensity level also shows two distinct zones of behavior with Reynolds number; in each zone, the critical intensity level is directly proportional to Reynolds number. For the low Reynolds number case, an increase in sound intensity level above the critical value produces a slight (at most, 20%) increase in the overall heat transfer level. For the high Reynolds number case, increases in intensity above the critical tend to decrease the overall heat transfer level. The reason for the shift in behavior with increasing Reynolds number is ascribed to changes in secondary flow patterns.

Other papers describing experimental and analytical investigations of the influence of low-amplitude pressure waves on heat transfer are given by Westervelt (13), Illingworth (14), and Lemlich (15), to list a few.

Large amplitude (50 psi to 150 or 200 psi peak to peak)

steep-fronted pressure waves are being studied by several groups. At the University of Wisconsin, R. W. Goluba (16) is working with siren-generated pressure waves in a one-inch diameter tube. The upstream siren is a rotating disk which chops the flow and produces a resonating, steep-fronted pressure wave at 500 to 1100 Hz. The mean tube pressure is from 200 psi to 300 psi; the peak to peak pressure amplitudes generated are from 100 psi to 120 psi. Transient tube wall surface temperatures are very similar to the gas pressure histories in shape, from 0.25 to 0.75 F° in amplitude, and generally in phase with the gas pressure. Generalized correlations for heat transfer have not yet been obtained by Goluba.

At Princeton University, studies under the direction of Crocco (17) of large-amplitude waves have been in process for nearly ten years. The oscillations (about 50 psi peak to peak amplitude) are steep-fronted: the disturbance caused by a rotating chopper located downstream of the test section has steepened into a shock front by the time it reaches the test area. Heat transfer increases of up to 200% have been observed, and are generally associated with flow reversals; recall that secondary flows also played an important role in the Georgia Institute of Technology investigations. Although no generalized correlations have been developed by the Princeton group, the increase of heat transfer with resonant pressure oscillations has been found

to vary with oscillation frequency and amplitude, the through-flow Mach number, and the mean tube pressure. The local oscillating pressure, however, was shown not to be the driving parameter for the heat transfer increase; the amplitude of the local oscillating velocity provided a much better correlation. These large amplitude oscillations are normally associated with flow reversal. The Princeton group has had difficulty separating amplitude effects from secondary effects due to wave shape changes and deformations in radial velocity profiles.

Many investigations, both analytical and experimental, are currently being conducted to determine the driving mechanisms and suppression techniques for large amplitude, steep-fronted pressure waves in oscillatory combustion. Much of this information remains in the classified literature.

Among the experimental contributions, Blackshear (18) presents a good, basic study of "screech" mechanisms in a small afterburner. Barrère (19) has published a lengthy experimental examination of low frequency combustion instability including reproductions of instantaneous gas pressure and temperature recordings. Cheng (20) of the Guggenheim Laboratories authored an experimental study of small amplitude, low frequency pressure oscillations in the combustion chamber of a liquid-fueled rocket with different nozzle profiles. Marble (21) traces "chugging" in a bi-propellant system to fuel and oxidizer flow rate oscilla-

tions and presents a servo-stabilization mechanism to sense and reduce the "hunting" of the system.

Schlieren photographs of high frequency oscillations in a bluff-body flame are given by Kaskan (22) and are associated with a transverse oscillation mode. Truman, et. al., (23) has also done a study of the transverse mode of vibration, but in high thrust engines. Finally, Rogers (24) and Berman (25) have published experimental studies of high frequency instability, the former in ramjet combustors and afterburners, the latter in rocket nozzles. The publication by Rogers contains good illustrative and background material.

Theoretical studies, primarily on the coupling of pressure and velocity disturbances to heat transfer, have been contributed by a number of authors. Cheng (26), mentioned earlier for an experimental study, has presented a theoretical study on the self-excitation of high frequency combustion instability in solid propellant rockets. In an earlier paper, Cheng (27) elucidates on the effect of non-uniform time lags between the introduction of combustibles into a system and their conversion to burned gas on the high frequency instability of the system.

Crocco, with Cheng, presented a long theoretical dissertation (28) on the role of unstable pressure oscillations in combustion instability with "concentrated combustion." Fi-

nally, Priem (29) has attempted to correlate high frequency combustion instability in liquid-fueled rocket combustors by means of similarity parameters. There are many more references to be found in the literature pertaining to combustion-related pressure oscillations.

To conclude this brief review, a number of papers are given in which the relationship of flame front energy generation to pressure waves is investigated.

Chu (30) has formulated expressions for the pressure field generated by a moderate rate of heat release within a fluid. Two general models are considered: in the first, the nature of the steep-fronted pressure wave generated by heat release in a tube section is determined; in the second, the pressure field due to a point energy source in a three-dimensional environment is calculated. Blackshear (31) discusses instability in burners: The dynamics and amplification of pressure waves passing through a flame front are analyzed. A change in the flame front area is found to act as a generator of pressure waves. Schalla (32) corroborates this finding: a source of pressure oscillations is present in any system in which the gas experiences an increase in heat release rate. Using ethylene-air mixtures, Schalla found acoustic pressure disturbances (on the order of 0.10 psi amplitude, 120 Hz frequency) generated when the air flow was across sharp gradients in composition.

The amount of publication in the area of heat transfer augmentation due to periodic pressure and velocity oscillations can be expected to increase in the future.

II. EXPERIMENTAL APPARATUS

GENERAL STATEMENT ON APPARATUS

The object of this investigation is to examine the effects of periodic pressure and temperature oscillations in a closed gas system on the heat transfer between the gas and a metal wall. A piston-cylinder-compression chamber combination is used to generate the periodic fluctuations in pressure and temperature. This compression chamber was taken as a reasonable source of low-frequency fluctuations for a number of reasons:

1) A pressure ratio as high as 25 could be produced, and it could be easily changed by changing the compression ratio of the system;

2) A broad low-frequency range of 9 to 60 cps could be encompassed;

3) The area available for instrumentation was not small;

4) The head (i.e., metal wall) material could easily be changed.

The project started with an already set-up CFR engine (spark ignition, variable compression ratio), but the instrumentation area was severely limited by the water jacket. An air-cooled Briggs and Stratton model 142300 engine was installed, but oil droplets from the piston rings and cylinder walls coated and/or destroyed the delicate instrumentation. A Pioneer model 700 chain saw crankcase was substituted: it was designed to need no oil in the crankcase,

and the crankshaft and connecting rod bearings could run on a dab of grease. To keep the cylinder walls free of oil, the steel piston rings were removed, the ring grooves were widened and deepened, and teflon piston rings supported by O-rings were installed. A sprayed teflon film replaced oil as the cylinder wall lubricant.

The head was a half-inch thick plate of either cast iron or aluminum. No valves were used, as air turbulence was to be minimized; one-dimensional air flow normal to the head surface was desired. As blowby occurred past the piston rings, makeup air was supplied through two small holes in the cylinder wall which were exposed by the piston near the bottom of its stroke.

CRANKCASE AND CYLINDER

The cylinder bore was 2.3125 inches, and piston stroke was 1.5625 inches. Two 1/8 inch diameter holes in the honed cast iron sleeve were exposed by the top piston ring at 38 crankangle degrees before bottom dead center to supply makeup air to compensate for blowby losses. Fig. 1 shows the makeup air supply system. The pressure of the makeup air system was variable from zero to about 25 inches of mercury.

PISTON

The piston was cylindrical. Its two main piston rings

of teflon* were 1/8 inch wide and 0.0740 inches thick, pressed to the cylinder wall by two 0.100 inch diameter O-rings. After considerable piston slap was noted from the scuffing and dirt build-up on the piston, the piston and cylinder were replaced and a thin teflon ring was added to the piston skirt. This reduced the scuffing so that after eight hours of operation at an average speed of 2000 rpm, only minor piston scuffing was noted. In nine hours' running, an average of only .003 inches of wear occurred on the three teflon rings.

The cylinder walls and piston sides were sprayed with Rocol I. F. L. spray teflon*, a new product designed as a dry lubricant for die and press work.

HEAD

The head was a half-inch thick plate, about four inches square, with a one-inch threaded hole in the center for temperature measuring instrumentation and a pressure pick-up mounting hole slightly off-center. At the cycle frequencies studied, the head acted as a semi-infinite plate to the temperature fluctuations on the inside surface: only steady-state heat transfer occurred at the outside surface. The compression chamber side of the head was counterbored 0.020 inches concentric with the bore at the

*See List of Manufacturers and Addresses in rear of text

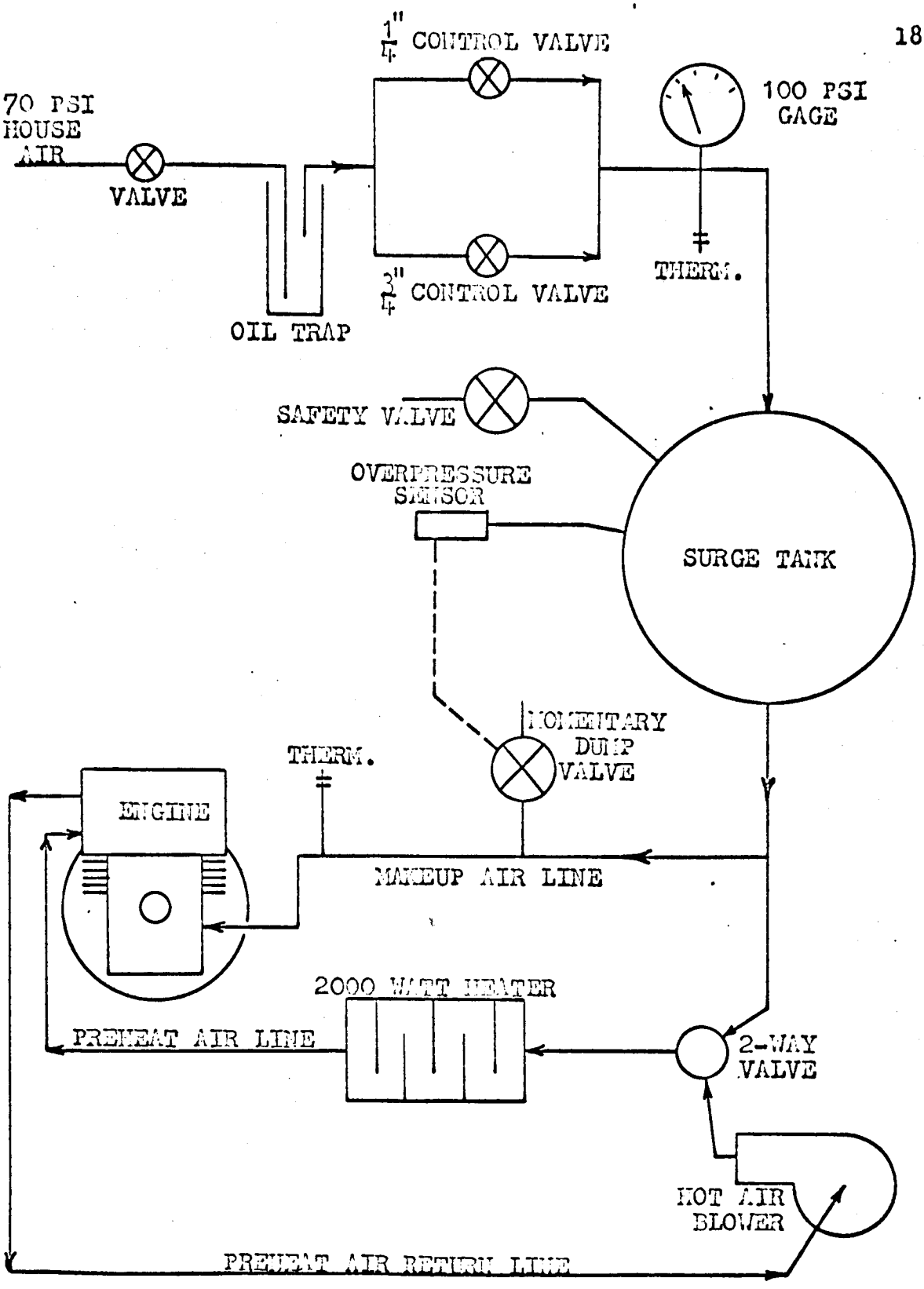

Fig. 1 Makeup and Preheat Air Systems

bore diameter to establish a compression ratio of 10.06. The off-center location of the pressure pickup necessitated the machining of a small, semicircular volume in the head; an identical volume was machined symmetrically across the bore in the interest of aerodynamic symmetry. These volumes (hereafter termed "ears") are visible in Fig. 2. The expression used in this work for compression chamber volume is:

$$V_{gas} = V_{clearance} + \frac{\pi B^2}{4} \left[R(1-\cos\omega t) + \frac{R^2}{4L} (1-\cos 2\omega t)\right] \quad (2)$$

where $V_{clearance} = 0.72534$ inches^3,

B = Bore = 2.3125 inches,

R = Crank Radius = 1.1875 inches,

L = Connecting Rod Length = 4.42 inches, and

ωt = angle referenced to top dead center.

GENERAL OVERVIEW ON INSTRUMENTATION

The principal variables measured are gas pressure, bulk gas temperature (sometimes simply termed gas temperature), wall surface temperature, and driving frequency. Gas pressure is measured by a 601H Kistler piezoelectric pressure transducer. Gas temperature is measured by a small-wire resistance thermometer. Wall (i.e., head) surface temperature is measured by a surface thermocouple. Driving frequency, and crankangle position of the piston (i.e., the

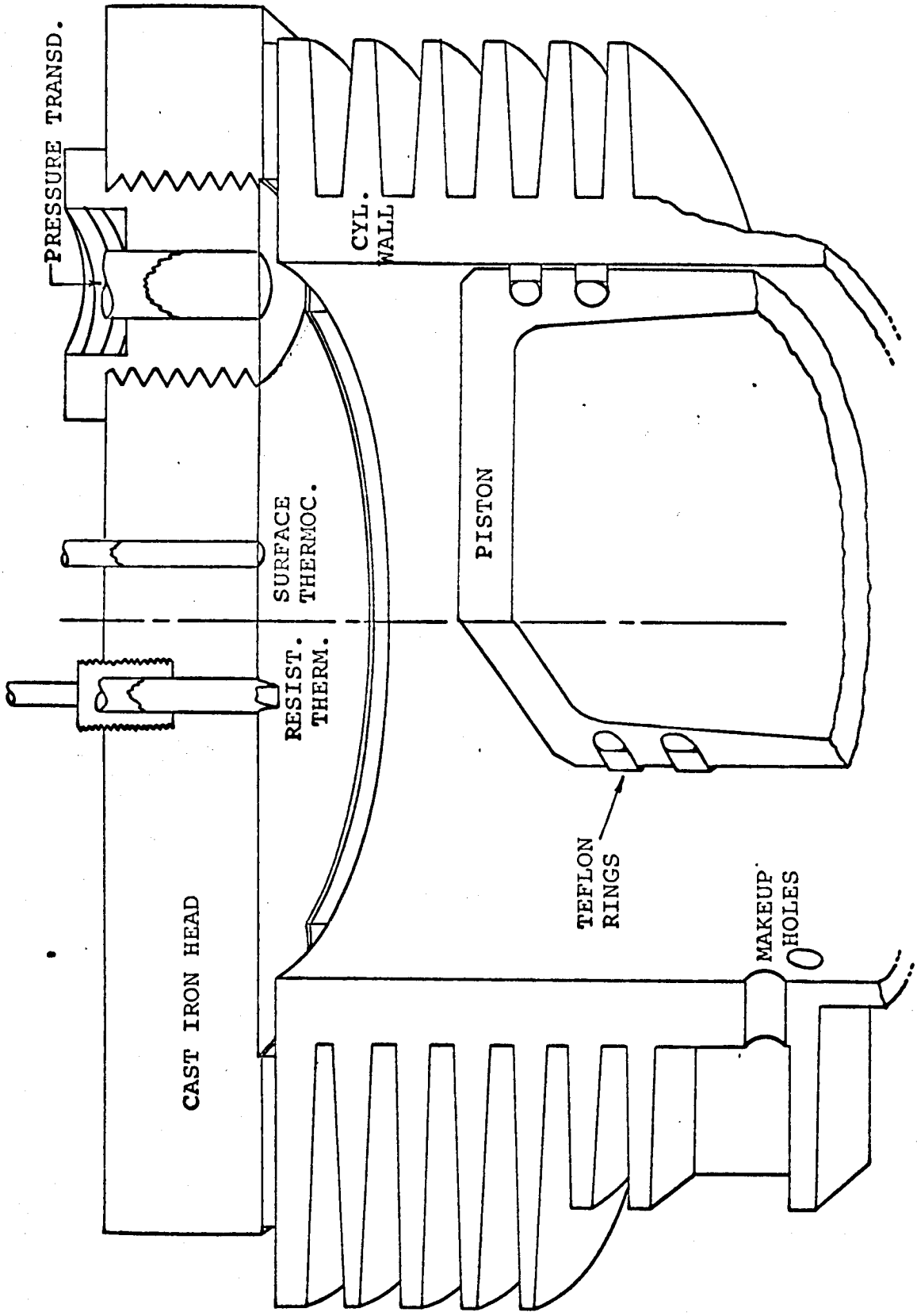

ASSEMBLY WITH ORIGINAL HEAD

Fig. 2

time reference), is measured by an Electro* magnetic pickup excited by a set of grooves in a crankshaft flywheel.

A separate set of breaker points actuated by a cam on the crankshaft, with associated circuitry, provides a 10-volt square wave at the driving frequency for oscilloscope synchronization. The more important of these instruments will be covered in succeeding sections.

ASTRODATA AMPLIFIERS

While some of the transducers in the experimental setup had output voltages on the order of a few volts (timing mark pickup, pressure transducer - charge amplifier combination), the temperature-sensing transducers yielded millivolt or microvolt level signals which required amplification before display. Preliminary work in this study was done with the hand-built direct-coupled amplifiers designed and fabricated by Overbye (33); because of stability and noise problems, it was deemed necessary to substitute a commercial product. Low noise Astrodata* direct-coupled amplifiers were obtained. Each amplifier had a gain variable from 3 to about 3100, differential input and output channels, and input and output grounds independent of chassis ground. The stated noise figure was less than 2

*Trade name: see List of Manufacturers and Addresses

microvolts rms referred to the input from 0.05 Hz to 10 kHz. The quoted frequency response was flat ±0.5% from dc to 1 kHz, down 3 db at 10 kHz.

In testing the amplifiers prior to installation, it was discovered that they caused a frequency-dependent phase shift of the output signal to occur relative to the input signal. The measured mean lag of several amplifiers is given in Fig. 3 as a function of frequency with an indication of the spread at each measured point. It is apparent that below about 5 kHz (i.e., the 83rd harmonic at 3600 rpm, or 60 Hz), the phase lag for a given amplifier is very closely linear. The phase lag could be expressed as:

$$\phi \begin{matrix}\text{lag of output with} \\ \text{respect to input}\end{matrix} = \alpha \left[\frac{f}{1000}\right] \qquad (3)$$

where f is the frequency in Hz and α is the measured slope in degrees per kHz. The measured slope over the range $0 \leq f \leq 5000$ Hz varied among the 11 amplifiers tested from 18.7 degrees/kHz to 19.7 degrees/kHz. Five amplifiers with slopes within a percent of 19.3 degrees/kHz were selected and used in the project. In all cases the phase shift was essentially independent of gain.

Since the phase lag is linear, the output signal must be a faithful (though delayed) reproduction of the input, for if the fundamental of the input wave, say 50 Hz, is delayed by 0.965 degrees, and the seventh harmonic (i.e., 350 Hz) is

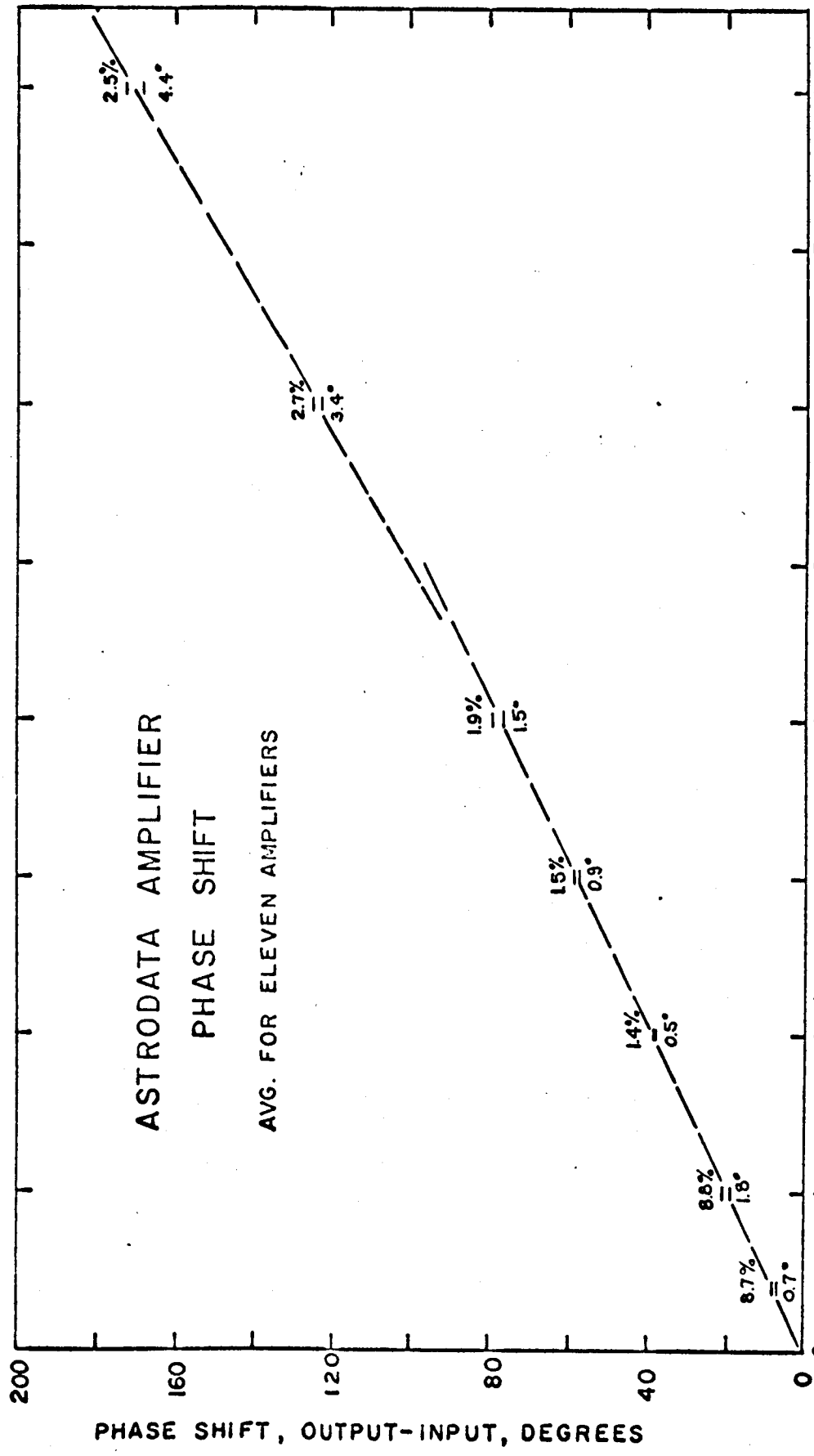
ASTRODATA AMPLIFIER
PHASE SHIFT
AVG. FOR ELEVEN AMPLIFIERS
2.5% = 4.4°
2.7% = 3.4°
1.9% = 1.5°
1.5% = 0.9°
1.4% = 0.5°
8.8% = 1.8°
8.7% = 0.7°
PHASE SHIFT, OUTPUT-INPUT, DEGREES
200
160
120
80
40
0
FREQUENCY, KILOHERTZ
0
1
2
3
4
5
6
7
8

Fig. 3

delayed by 6.755 degrees, the time delay of the two is identical (0.0536 milliseconds) since the period of the higher harmonic is one seventh as long. This does introduce a complication, however. If a phase-shifted surface temperature is displayed on the oscilloscope with a non-phase-shifted timing mark trace (since the latter required no amplifier), the two traces are obviously displaced horizontally on the display and cannot be easily related. The problem is solved by using Astrodata amplifiers in the timing mark and pressure circuits at low gain, and having them serve as "phase shifters." Then all signals displayed simultaneously are phase shifted in equal amounts, including the timing-mark base.

Before the advent of reliable solid state direct coupled amplifiers, it would have been very difficult, if not impossible, to record or study the small signals studied in this project.

VII. EXPERIMENTAL DATA

The experimental data gathered in this investigation consisted chiefly of temperature, pressure, and heat flux histories for the equilibrium cycle of the system using air as the working fluid. At each of the eight fixed driving frequencies in the range 15 to 58 Hz (915 to 3452 rpm), from two to five cycles (not necessarily successive cycles) of data were taken; each cycle of data consisted primarily of the bulk gas temperature and pressure histories and the head surface temperature history. The instrumentation used for these measurements has already been described. A table listing the figure numbers for most of the experimental measurements is given below: these figures are found in Appendix A; data for three intermediate speeds are not included.

Figure Numbers for Experimental Data Histories

RPM	HERTZ	GAS TEMP.	PRESSURE	T_{WALL}	Q_{WALL}
579.	9.65	-	-	A1	A1
915.0	15.25	A2	A3	A4	A5
1246.8	20.78	A6	A7	A8	A9
1512.7	25.21	A10	A11	A12	A13
2434.8	40.58	A14	A15	A16	A17
3452.0	57.53	A18	A19	A20	A21

A comparison of most of the cycle-averaged surface temperature histories and the corresponding surface heat transfer

histories is presented in Fig. 13.

GAS TEMPERATURE

EXPERIMENTAL OBSERVATIONS

A sampling of the recorded gas temperature histories is presented in the histories of Appendix A (specifically Figs. A2, A6, A10, A14, and A18). The noise level (both 60 Hz and high frequency) was so low as to be negligible, except for two brief segments of the cycle when the synchronization breaker points actuated, at about -105 and +26 crankangle degrees, for four degree intervals. There was a moderate amount of cycle-to-cycle variation in the bulk gas temperature history, due probably to departures from one-dimensionality and random gas motion due to rocking of the piston and the induction of makeup air. The cyclic variation occurred primarily near top dead center (TDC) and 80 degrees to either side of bottom dead center (BDC), and decreased somewhat with increasing frequency.

The shape of the gas temperature history was essentially unchanged as driving frequency increased, except for an increase in amplitude and a slight shift in the crankangle at which the history maximized. Fig. 12 details this shift in bulk gas temperature maximum as recorded by the resistance thermometer: at 10 Hz the peak is at about -2.5 crankangle degrees; at 60 Hz the peak is at -1.5 degrees.

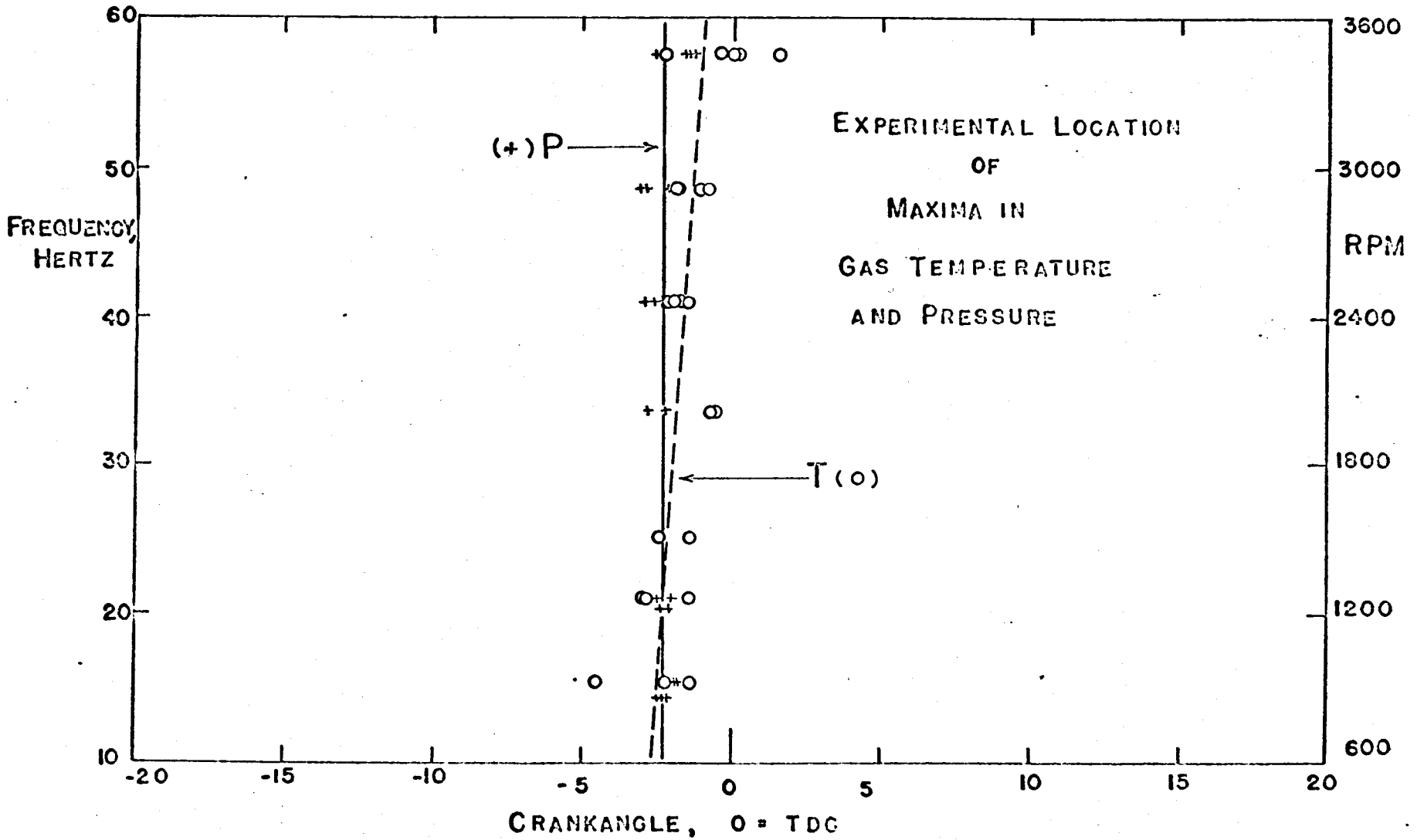
EXPERIMENTAL LOCATION
OF
MAXIMA IN
GAS TEMPERATURE
AND PRESSURE
(+) P
T (o)
FREQUENCY, HERTZ
RPM
CRANKANGLE, 0 = TDC
60
50
40
30
20
10
3600
3000
2400
1800
1200
600
-20
-15
-10
-5
0
5
10
15
20

Fig. 12

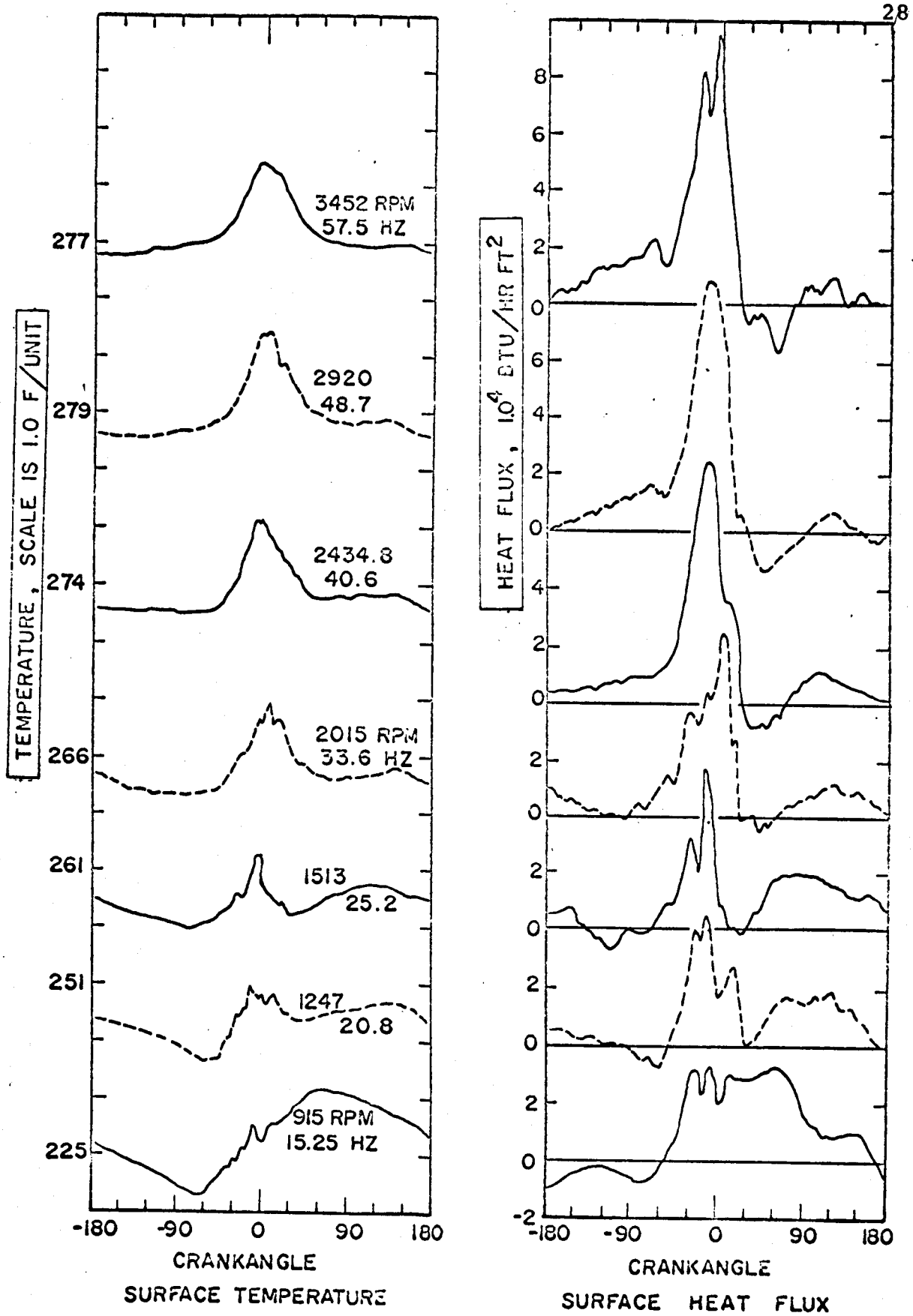
TEMPERATURE, SCALE IS 1.0 F/UNIT
277
279
274
266
261
251
225
3452 RPM
57.5 HZ
2920
48.7
2434.8
40.6
2015 RPM
33.6 HZ
1513
25.2
1247
20.8
915 RPM
15.25 HZ
-180
-90
0
90
180
CRANKANGLE
SURFACE TEMPERATURE
HEAT FLUX, 10^4 BTU/HR FT^2
8
6
4
2
0
-2
-180
-90
0
90
180
CRANKANGLE
SURFACE HEAT FLUX

FIG. 13

The bulk gas temperature swing increases over this frequency range from about 560 F° to about 630 F°. All gas temperature measurements were made with 3.81 μ tungsten resistance wires.

PEAKING OF GAS TEMPERATURE

According to Fig. 12, at low driving frequencies the instantaneous gas temperature as measured by the resistance wire leads both the gas pressure maximum (-2.5 crankangle degrees) and the gas volume minimum, but at high driving frequencies the wire temperature peak lags the pressure peak slightly.

The pressure transducer and its charge amplifier have very high frequency response: the Kistler model 566 electrostatic charge amplifier has a nominal 150 kHz upper limit; the 601H transducer has a flat response to within 1% up to at least 15 kHz (about the 300th harmonic of the highest frequency studied in this work). The recorded pressure history can be considered as a faithful reproduction of the chamber pressure. The resistance thermometer time constant is not accurately known, however, and some possibility exists that at high frequencies the temperature of the small wire may lag the gas temperature by a few crankangle degrees. Since both the gas pressure and the gas temperature are bulk averaged quantities, a simple first-law analysis may shed some light on how the wire tem-

perature relates to the gas temperature.

The first law for a simple closed system is:

$$PV = mRT \ .$$

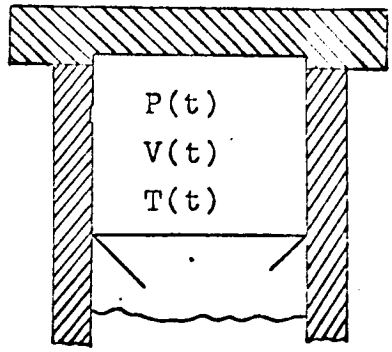

We can differentiate with respect to time and assume that the specific gas constant R is indeed constant:

$$\frac{P}{R}\frac{dV}{dt} + \frac{V}{R}\frac{dP}{dt} = \frac{d}{dt}(m \cdot T) \ . \qquad (19A)$$

If we restrict ourselves to the entire compression stroke, the dV/dt term is always negative.

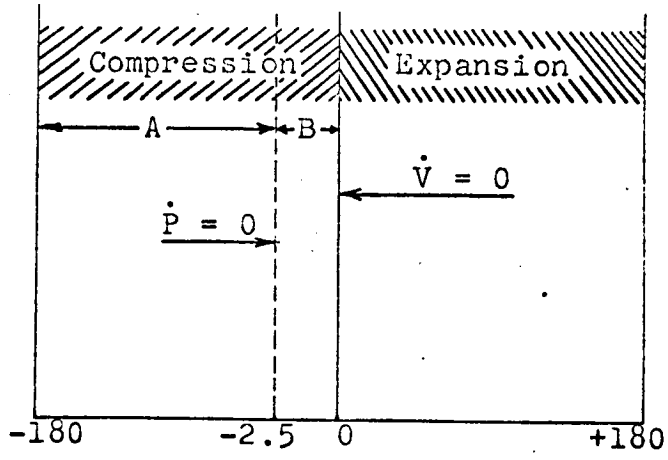

If we further restrict ourselves to the short time interval "B" between and including the pressure peak (about 2.5 degrees before TDC) and the volume minimum (TDC, or 0 crankangle degrees) in the compression stroke, the dP/dt term is also negative or at most zero. Then in the domain "B", the quantity d(m·T)/dt must be negative. For a constant

mass system, the gas temperature must be decreasing; then, the gas temperature must peak in the domain "A" prior to the pressure peak.

If the system is complicated by the possibility of mass loss through blowby, the argument is not as simple. Examine the instant at which the pressure reaches its maximum (i.e., -2.5°). The term $\frac{V}{R} \frac{dP(-2.5°)}{dt}$ is zero. The term $\frac{P}{R} \frac{dV(-2.5°)}{dt}$ is, for typical conditions encountered in this investigation, approximately:

$$\frac{P}{R} \frac{dV(-2.5°)}{dt} \cong \frac{(388 \text{ psi})(-.0032 \text{ in}^3/\text{cr. degree})}{(53.3 \text{ ft lb}_f/\text{lb}_m \text{°R})}$$

$$\frac{P}{R} \frac{dV(-2.5°)}{dt} \cong -.00200 \text{ lb}_m \text{ °R/cr. degree.}$$

The equation now reads,

$$-20 \times 10^{-4} \text{lb}_m \text{ °R/degree} \cong T \frac{dm}{dt} + m \frac{dT}{dt} \quad . \qquad (19B)$$

The approximate size of the first term on the right side is, from the SIMUL simulation program, negative but small:

$$T \frac{dm(-2.5°)}{dt} \cong -(1290°R)(.315 \times 10^6 \frac{\text{lb}_m}{\text{cr.degree}})$$

$$T \frac{dm(-2.5°)}{dt} \cong -.0004 \text{ lb}_m \text{ °R/cr. degree.}$$

Then the term containing dT/dt in Eqn. 19B is negative when the pressure reaches its maximum for the case allowing blowby mass flow out of the system.

The gas temperature, bulk averaged, is thus seen to peak before the pressure whether or not there is mass loss from the system. The experimental observation illustrated in Fig. 12 can be interpreted as follows: at high frequencies, the resistance wire temperature lags the gas temperature by two or three crankangle degrees.

GAS PRESSURE

Figs. A3, A7, A11, A15, and A19 present gas pressure histories at frequencies from 15 to 58 Hz. No noise was ever identified on a pressure trace. There was very little cycle-to-cycle variation; what occurred took place primarily in the low pressure period of the cycle and perhaps was related to makeup air addition. As driving frequency increased, the cyclic variation in pressure history gradually decreased.

The shape of the gas pressure history was the least affected by increased driving frequency of all the histories measured. The mean pressure swing changed from 365.8 psi at 15 Hz to 364.2 psi at 58 Hz. The pressure maximum remained at -2.5 crankangle degrees with a maximum cyclic variation of perhaps one degree.

SURFACE TEMPERATURE

Figs. A1, A4, A8, A12, A16, and A20 present wall surface temperature histories measured at a point near the center of symmetry of the head at frequencies from 9 to 58 Hz. A summary of most of the surface temperature histories (each history being the average of several cycles) with the corresponding heat transfer histories is given in Fig. 13. At low speeds (up to about 15 Hz) the wall surface temperature peaks unexpectedly late. The lag of the surface temperature peak (with respect to a fixed reference, such as TDC, or the pressure history peak) increases with increasing speed. At high speeds (35 Hz to the maximum of the equipment, 58 Hz), the wall surface temperature peak is at or very near to top dead center. At intermediate frequencies the two trends overlap and a clear double peaking is observed in head (or wall) surface temperature. A plot showing the trends of the crankangle position of this temperature peak with frequency is shown in Fig. 14. An interpretation of these data is deferred until later. These histories represent very small signal levels: a 2 F° swing in surface temperature produces a voltage swing of only 60 microvolts. As a consequence, noise suppression was important; the steps taken to increase the signal-to-noise ratio were discussed earlier. The observed 60 Hz ripple was less than 5% of the signal size, and the high frequency noise level was held to less than about 8% of

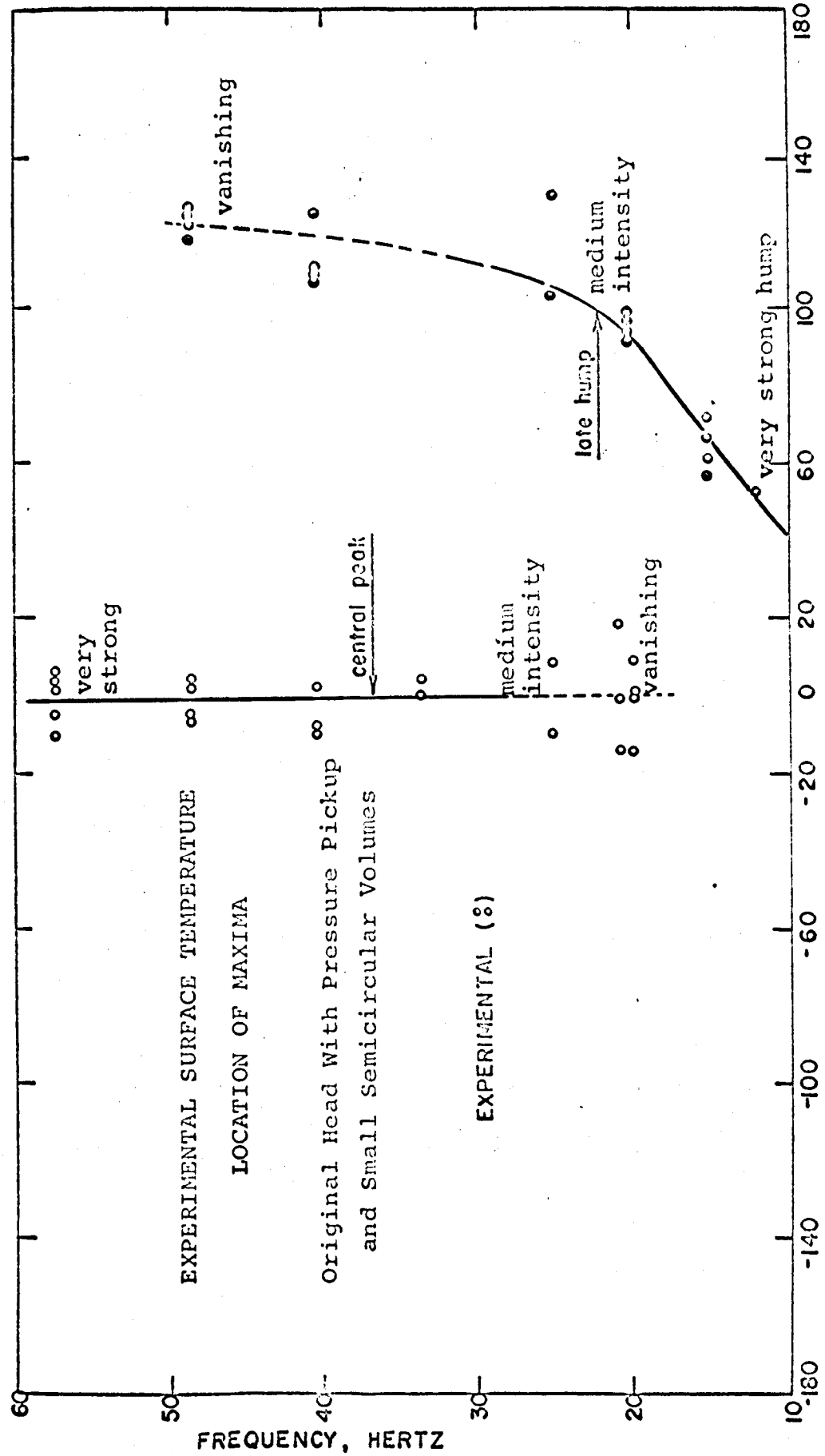
EXPERIMENTAL SURFACE TEMPERATURE
LOCATION OF MAXIMA
Original Head With Pressure Pickup
and Small Semicircular Volumes
EXPERIMENTAL (8)
very strong
vanishing
central peak
medium intensity
vanishing
late hump
medium intensity
very strong hump
FREQUENCY, HERTZ
CRANKANGLE
60
50
40
30
20
10
180
140
100
60
20
-20
-60
-100
-140
-180

FIG. 14

the signal size.

There was considerable cycle-to-cycle variation in the surface temperature data; for this reason, several cycles were recorded at each speed and the results later were averaged for interpretation. In spite of cyclic variation in the surface temperature histories, very definite patterns emerged from the data; these patterns are discussed later.

SURFACE HEAT TRANSFER

LISTING OF DATA

Surface heat transfer histories are given in Figs. A1, A5, A9, A13, A17, and A21. The method of calculation of these histories from the surface temperature histories is explained in the next section. In spite of the cycle-to-cycle variation in the surface temperature data, the surface heat transfer histories averaged over a number of cycles show definite patterns of change with increasing driving frequency. This is best seen in the summary figure, Fig. 13, together with the very low speed data of Fig. A1.

COMPUTATION OF INSTANTANEOUS HEAT TRANSFER

Statement of Method

The instantaneous heat transfer at the compression chamber surface was obtained by the application of one-dimensional semi-infinite solid theory to the measured chamber surface temperature. It would, in principle, be possible to measure instantaneous surface heat transfer rates at the temperature levels and cyclic frequencies covered in this work with recently developed heat flux transducers*, but this course of action was not taken for a number of reasons:

1) It is possible to calculate the required heat transfers accurately, though at the expense of time and effort, from the measured surface temperature history.

2) Available transducers are on the order of 1/4 to 1/2 inch in diameter, and instrument spacing would mean that the temperature and the heat flux were measured perhaps one inch apart in a 2.3125 inch chamber.

3) Available transducers usually have ceramic or pyrex backup materials, severely disturbing the one-dimensional heat flow and making dubious a correlation between heat flux and surface temperature.

4) Instantaneous heat flux recording would require another channel in the already filled display (a four-channel oscilloscope).

For these reasons and others, the calculation route to instantaneous surface heat transfer was taken.

*Heat Technology Laboratories in List of Manufacturers and Addresses

The basic principle of calculation is as follows: the surface temperature history is taken from a film record and converted to an array of ordinates and associated crankangle times. The history is taken as being given by these points and linear line segments between the points. A Fourier analysis is performed to break the surface temperature history down into its harmonic elements; a limit for the number of harmonics is chosen (a number less than the number of original ordinates); the higher harmonics are not used. Semi-infinite solid theory is applied to this harmonic synthesis, and an expression for the instantaneous temperature profile into the wall is generated. Instantaneous surface heat transfer is calculated from a differentiation of the temperature profile, evaluated at the plate (i.e., head) surface.

This technique is the same as used by Overbye (33) and others. It involves fairly standard heat transfer philosophy; there are, however, significant differences in calculation and application between the method used and that of Overbye, resulting in greater flexibility and accuracy. Credit for the origin of these differences and their transformation into a method of calculation should be given to T. LeFeuvre*. A more detailed study of this method will be found in LeFeuvre's Ph.D. dissertation (1968).

*Ph.D. candidate, Department of Mechanical Engineering, University of Wisconsin

One-Dimensionality Approximation

Heat transfer is assumed to be one-dimensional, normal to the plane of the head surface, throughout this work. The surface thermocouple from whose signal the flux is calculated is close to the center of a half-inch thick plate of cast iron which constitutes the head. Fig. 15 shows that the resistance thermometer probe is the only nearby object which could disturb the heat flow (other than the instrument plug-head thread interface), and it is four thermocouple diameters away. The washer-shaped thermocouple junction is backed by iron, the same material as the head. It is essential* that the thermocouple backing material be identical to that of the head if the output signal is to be representative of the typical surface temperature of the head. The central oxidized nickel or constantan wire does constitute a different thermal resistance in parallel with the iron resistance ($k_{constantan}$ = 17 Btu/hrft°F, k_{iron} = 29 Btu/hrft°F), but the wire area normal to the flux direction is only 1.3% of the junction area.

Semi-Infinite Solid Approximation

The use of semi-infinite solid laws is valid if the surface temperature fluctuations are damped to negligible amplitude before reaching the exterior surface. Overbye de-

*Periodical #TB-161, Nanmac Corporation

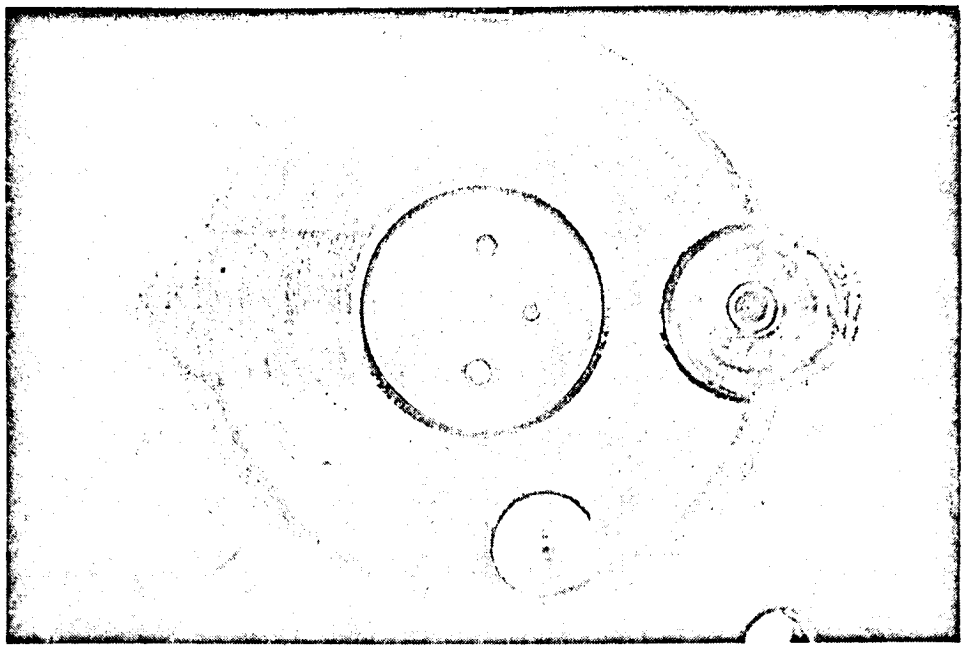

Two Views of Underside of Head

Instrumented with resistance wire at top and one surface thermocouple on the right in central plug, and a Kistler pressure pickup in the plug at right in one of the semicircular volumes in the head.

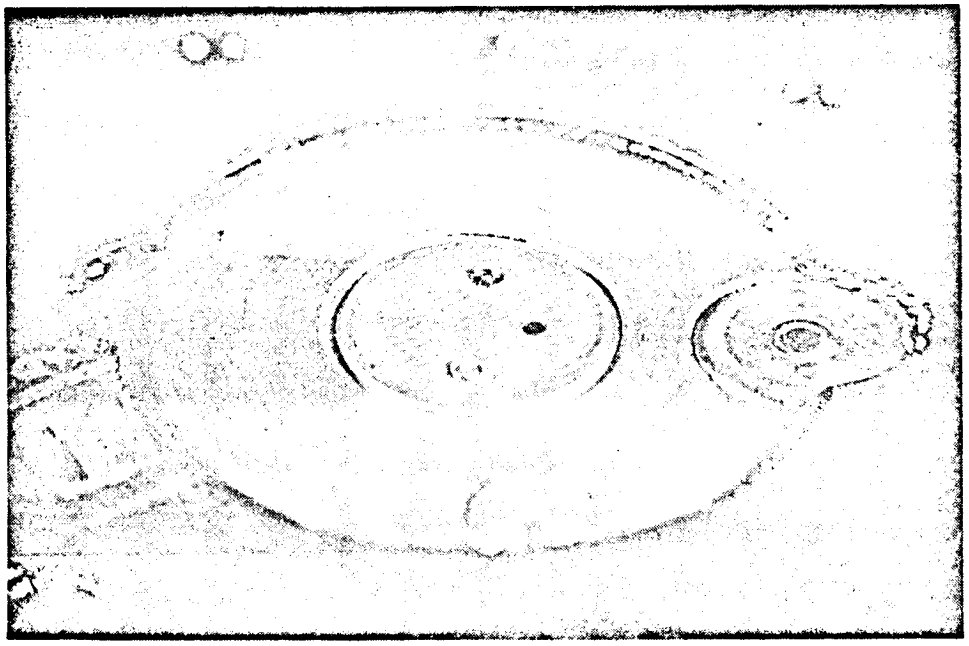

Figure 15 - Underside of Head

tected no perturbations in exterior temperature at low frequency operation (low frequency harmonics penetrate deeper than higher harmonics) with a 35 F° swing on the inside of a cast iron wall less than 3/8 inch thick. This experimenter made the same observation with better electronics, a 2 F° inside swing, and a half-inch wall.

According to Schneider (67), the envelope of a temperature history which is periodic at the surface decays with depth into a semi-infinite solid according to:

$$\text{Envelope size} \sim \exp\left(-x\sqrt{\omega/2\alpha}\right)$$

where ω is the frequency of the lowest harmonic,
α is the thermal diffusivity of the material, and
x is the distance into the material.

If we set a 1000:1 diminution as the standard for the semi-infinite solid, the critical depth for "complete" damping is given by x_c in the following expression:

$$\exp\left(-0\cdot\sqrt{\omega/2\alpha}\right) = 1000\cdot\exp\left(-x_c\sqrt{\omega/2\alpha}\right), \quad \text{or,}$$

$$x_c = +\sqrt{2\alpha/\omega}\ \log_e\ 1000. \qquad (20)$$

For cast iron (α = 0.666 ft^2/hr), several values of x_c for various ω are summarized below:

ω (rpm):	800	1000	1500	2000	4000
x_c(in.):	.174	.156	.127	.110	.078

It is clear that semi-infinite solid theory can be applied to a half-inch slab of cast iron with confidence.

Theory

Fourier Series Approximation

A wall which can be taken as a semi-infinite solid sees a steady periodic temperature history at its surface. We assume that the oscillation has been maintained long enough so that the original transient state due to starting the cyclic surface temperature has built up into a steady type of periodic flow.

The first concern is to determine the time-dependent temperature profile in the wall. The heat transfer literature contains many derivations for temperature profiles induced in slabs and cylinders by surface temperature variations expressed in terms of elementary functions. In the case of experimental periodic temperature variations not easily expressed in terms of simple functions, the best procedure is to reduce the experimental curve to an equivalent trigonometric series. The profile into the wall for each series term is obtained by application of the Fourier heat equation:

$$\frac{\partial t}{\partial \theta} = \alpha \frac{\partial^2 t}{\partial x^2} \qquad (21)$$

where: t is temperature, °F,
θ is time, hours,
α is thermal diffusivity, $ft^2/hr.$, and
x is distance into the wall from the surface, ft.

Let us consider an experimental temperature-time history at the metal surface consisting of N+1 temperature ordinates $t_n(0,\theta_n)$ at corresponding times θ_n. The abscissas θ_n need not be equally spaced.

We take the function $t(0,\theta)$ to be defined by the array of N+1 points and linear line segments between the points; for reasons not discussed here, the ordinate of the first point is discarded and the value for the N+1st point is substituted so that the end point ordinates are equal. A Fourier analysis will provide a trigonometric equivalent to the function; we will limit ourselves to the first K terms:

$$t(0,\theta) = A_{ow} + \sum_{k=1}^{K} [A_k \cos(k\omega\theta) + B_k \sin(k\omega\theta)] \qquad (22)$$

where $t(0,\theta)$ is the approximated temperature function,
k is the harmonic number, k = 1,2,3, ...K,
ω is the frequency in radians/hour,
θ is the time in hours,
A_{ow} is the average of the given ordinates,
A_k is the amplitude of the kth cosine harmonic,
B_k is the amplitude of the kth sine harmonic.

The A and B coefficients are given by:

$$A_{ow} = \frac{1}{\Theta} \int_{\theta_0}^{\theta_N} t(0,\theta)\, d\theta \qquad (23)$$

$$A_k = \frac{2}{\Theta} \int_{\theta_0}^{\theta_N} t(0,\theta) \cos(\theta\pi k/K)\, d\theta \text{ , and} \qquad (24)$$

$$B_k = \frac{2}{\Theta} \int_{\theta_0}^{\theta_N} t(0,\theta) \sin(\theta\pi k/K)\, d\theta \qquad (25)$$

where $k = 1,2,3,4, \ldots K$

$\theta_0 \leqslant \theta \leqslant \theta_N$

$\Theta \equiv [\theta_N - \theta_0]$; ($\theta_0$ would generally be taken = 0).

A more convenient, but less accurate, definition for the coefficients is more often used in which the integral definitions for A_{ow}, A_k, and B_k become sums over the N ordinates:

$$A_{ow} \equiv \frac{1}{N} \sum_{n=1}^{N} t_n(0,\theta_n) \text{ ,} \qquad (26)$$

$$A_k \equiv \frac{1}{N} \sum_{n=1}^{N} t_n(0,\theta_n) \cos(n2\pi k/K), \qquad (27)$$

$$B_k \equiv \frac{1}{N} \sum_{n=1}^{N} t_n(0,\theta_n) \sin(n2\pi k/K). \qquad (28)$$

In this form, however, the function is broken into a series of steps; the height of each step is the ordinate value at the end of the step, and the trigonometric functions are evaluated at the step ends. The approach used here replaces the steps with linear ramps and actually performs the integrals.

Applying the separation of variables technique suggested by Schneider (67), with the boundary conditions:

$$t(0,\theta) = A_{ow} + \sum_{k=1}^{K} A_k \cos(k\omega\theta) + B_k \sin(k\omega\theta), \qquad (29)$$

and $t(L,\theta) = A_{aj}$

where L is the wall thickness in feet, and
A_{aj} is the external (air jacket) temperature, °F,

we get the steady state solution,

$$t_{ss}(x,\theta) = A_{ow} - \frac{(A_{ow} - A_{aj})x}{L} \qquad (30)$$

and the transient solution,

$$t_{tr}(x,\theta) = \sum_{k=1}^{K} \exp(-px) \left[A_k \cos(k\omega\theta - qx) + B_k \sin(k\omega\theta - qx)\right]. \qquad (31)$$

when the p and q are evaluated by subjecting this solution to the test of the Fourier heat equation, we find that

$$p = q = \sqrt{k\omega/2\alpha} \tag{32}$$

and the complete solution for the temperature profile induced in the wall is:

$$t(x,\theta) = A_{ow} - \frac{(A_{ow} - A_{aj})x}{L} + \tag{33}$$

$$+ \sum_{k=1}^{K} \exp\left[-x\sqrt{\frac{k\omega}{2\alpha}}\right] \left\{ \begin{array}{l} A_k \cos(k\omega\theta - x\sqrt{\frac{k\omega}{2\alpha}}) + \\ B_k \sin(k\omega\theta - x\sqrt{\frac{k\omega}{2\alpha}}) \end{array} \right\} .$$

This equation satisfies the boundary conditions at $x = 0$ and $x = L$: when $x = 0$ it reduces to

$$t(0,\theta) = A_{ow} + \sum_{k=1}^{K} [A_k \cos(k\omega\theta) + B_k \sin(k\omega\theta)] \tag{34}$$

and when $x = L$, recalling the infinite plate assumption that the time dependent portion of the solution is negligibly small,

$$t(L,\theta) = A_{aj} . \tag{35}$$

Differentiating the equation for the induced temperature profile with respect to depth into the wall, we get:

$$\frac{\partial t(x,\theta)}{\partial x} = -\left[\frac{A_{ow} - A_{aj}}{L}\right] + \sum_{k=1}^{K}\sqrt{\frac{k\omega}{2\alpha}} \cdot \exp\left[-x\sqrt{\frac{k\omega}{2\alpha}}\right] \cdot$$

$$\cdot \left\{ \begin{array}{l} (A_k - B_k)\sin(k\omega\theta - x\sqrt{\frac{k\omega}{2\alpha}}) + \\ \\ (-B_k - A_k)\cos(k\omega\theta - x\sqrt{\frac{k\omega}{2\alpha}}) \end{array} \right\} \quad (36)$$

Setting x equal to zero,

$$\left.\frac{\partial t(x,\theta)}{\partial x}\right|_{x=0} = \frac{A_{ow} - A_{aj}}{L} - \sqrt{\frac{\omega}{2\alpha}} \cdot \sum_{k=1}^{K}\sqrt{k} \left\{ \begin{array}{l} (B_k - A_k)\sin(k\omega\theta) + \\ (B_k + A_k)\cos(k\omega\theta) \end{array} \right\}. \quad (37)$$

Since the surface heat transfer is defined from the metal side of the surface by

$$q_{surface} = -(\text{cond.}) \cdot \left.\frac{\partial t(x,\theta)}{\partial x}\right|_{x=0}, \quad (38)$$

the heat transfer rate, in units of Btu/hr ft^2, is given by

$$q_{surface} = \text{cond.}\left[-\left[\frac{A_{ow} - A_{aj}}{L}\right] + \sqrt{\frac{\omega}{2\alpha}} \cdot \sum_{k=1}^{K}\sqrt{k} \left\{ \begin{array}{l} (B_k - A_k)\sin(k\omega\theta) + \\ (B_k + A_k)\cos(k\omega\theta) \end{array} \right\}\right] \quad (39)$$

The first term of this expression represents the steady-

state heat transfer rate and the series summation constitutes the transient heat transfer rate at the wall surface.

Converged Fourier Series Approach

When approximating a periodic function with a Fourier series with a "reasonable" number of terms, a series representation often "overshoots" any steep-fronted segments and oscillates about the function. Hamming (68) points out, for example, that when approximating a square wave of unity amplitude, a ten-harmonic Fourier fit overshoots by nearly 9%, then

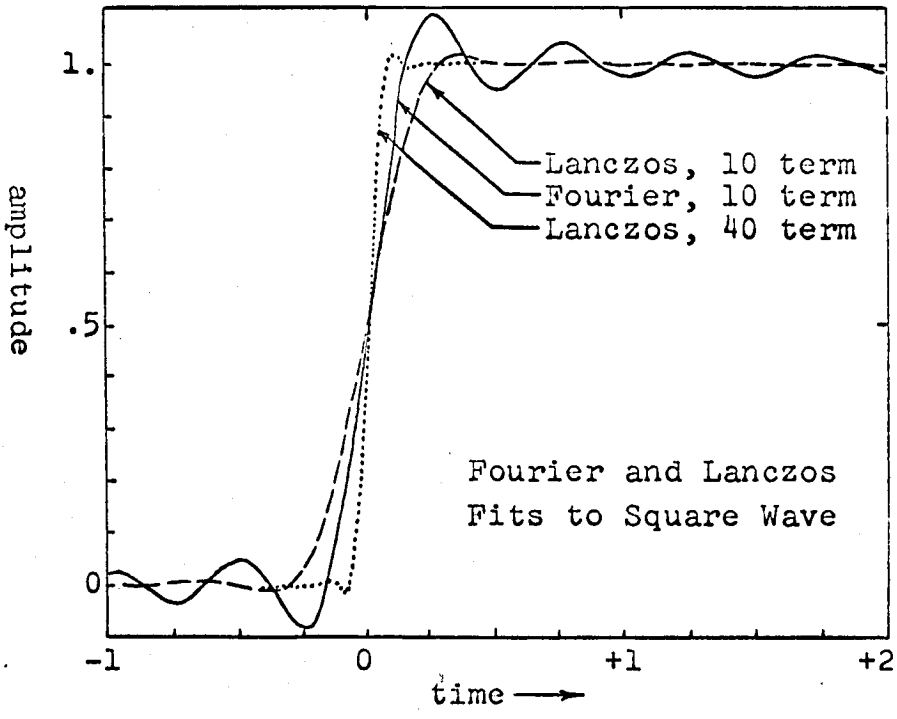

oscillates about as shown in the sketch above. This behavior is often termed the "Gibbs Phenomenon."

In treating experimental wall temperatures to Fourier analysis with 50 harmonics, and computing instantaneous surface heat transfer, the resultant histories appeared to contain oscillations of regular frequency as shown in the lower half of Fig. 16. These oscillations were attributed to the Gibbs Phenomenon, as increasing the number of terms in the analysis from 50 to 70 terms decreased their amplitude.

A number of mathematical "tricks" exist to smooth the Fourier representation, generally at the expense of high frequency response. If each coefficient A_k and B_k is multiplied by the so-called Lanczos Smoothing Factor,

$$\sigma_k = \frac{\sin \pi k/K}{\pi k/K} \quad , \qquad (40)$$

where $k = 1,2,3, \ldots K$,

the first overshoot in the previous sketch is reduced from 0.08949 to 0.01187, and the first minimum is reduced from 0.04859 to 0.00473 (for the 10-harmonic representation, i.e., $K = 10$). The factor is very close to unity for the first harmonic and decreases to zero for the Kth harmonic, as seen in Fig. 17.

Applying the Lanczos factors to the harmonic coefficients in the calculation of the wall surface heat flux damped the regular oscillations, as shown in the top half of Fig. 16. Essentially the same result could have been achieved

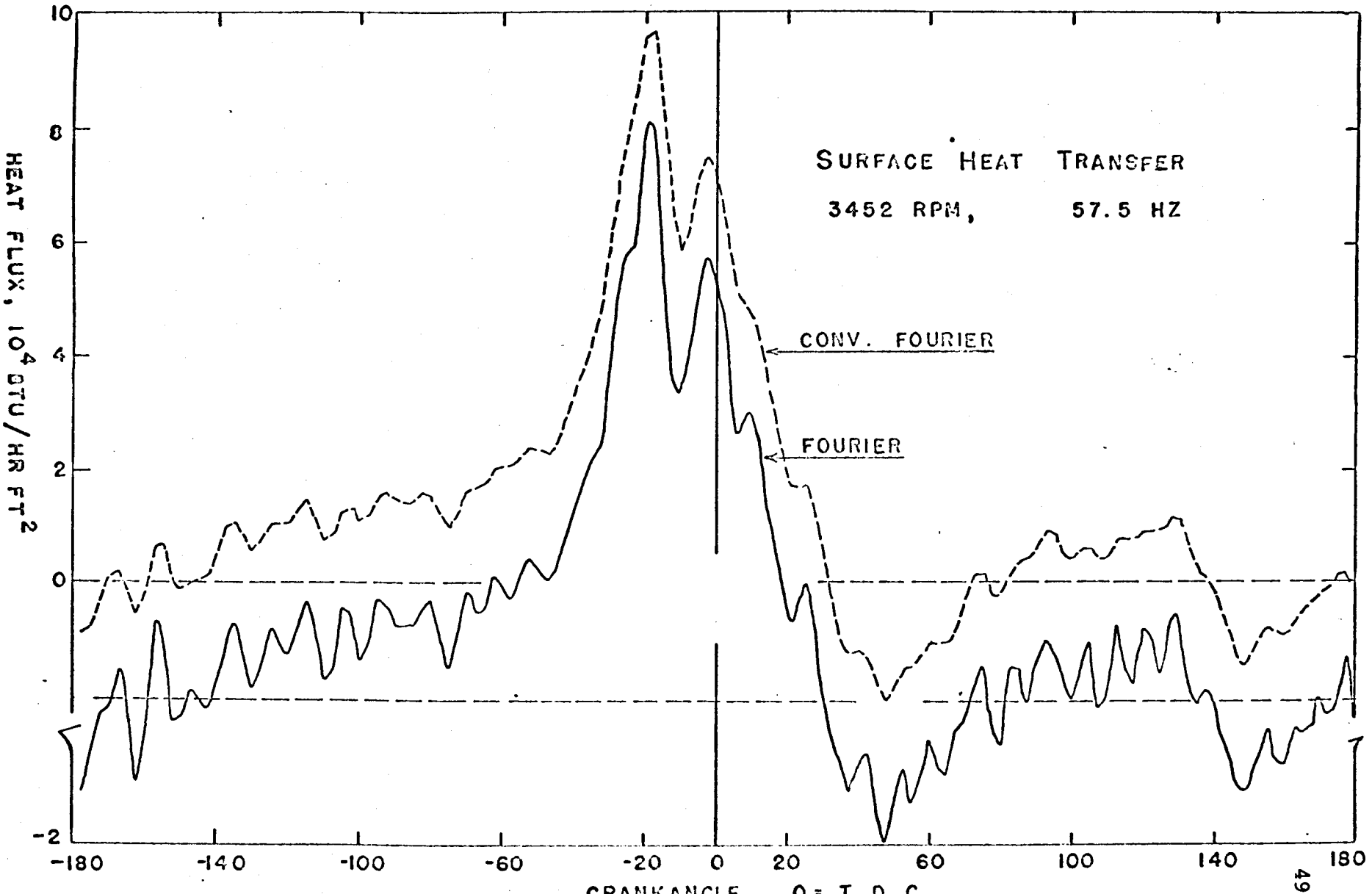
SURFACE HEAT TRANSFER
3452 RPM, 57.5 HZ
CONV. FOURIER
FOURIER
HEAT FLUX, 10^4 BTU/HR FT^2
CRANKANGLE, 0 = T.D.C.
10
8
6
4
2
0
-2
-180
-140
-100
-60
-20
0
20
60
100
140
180

FIG. 16

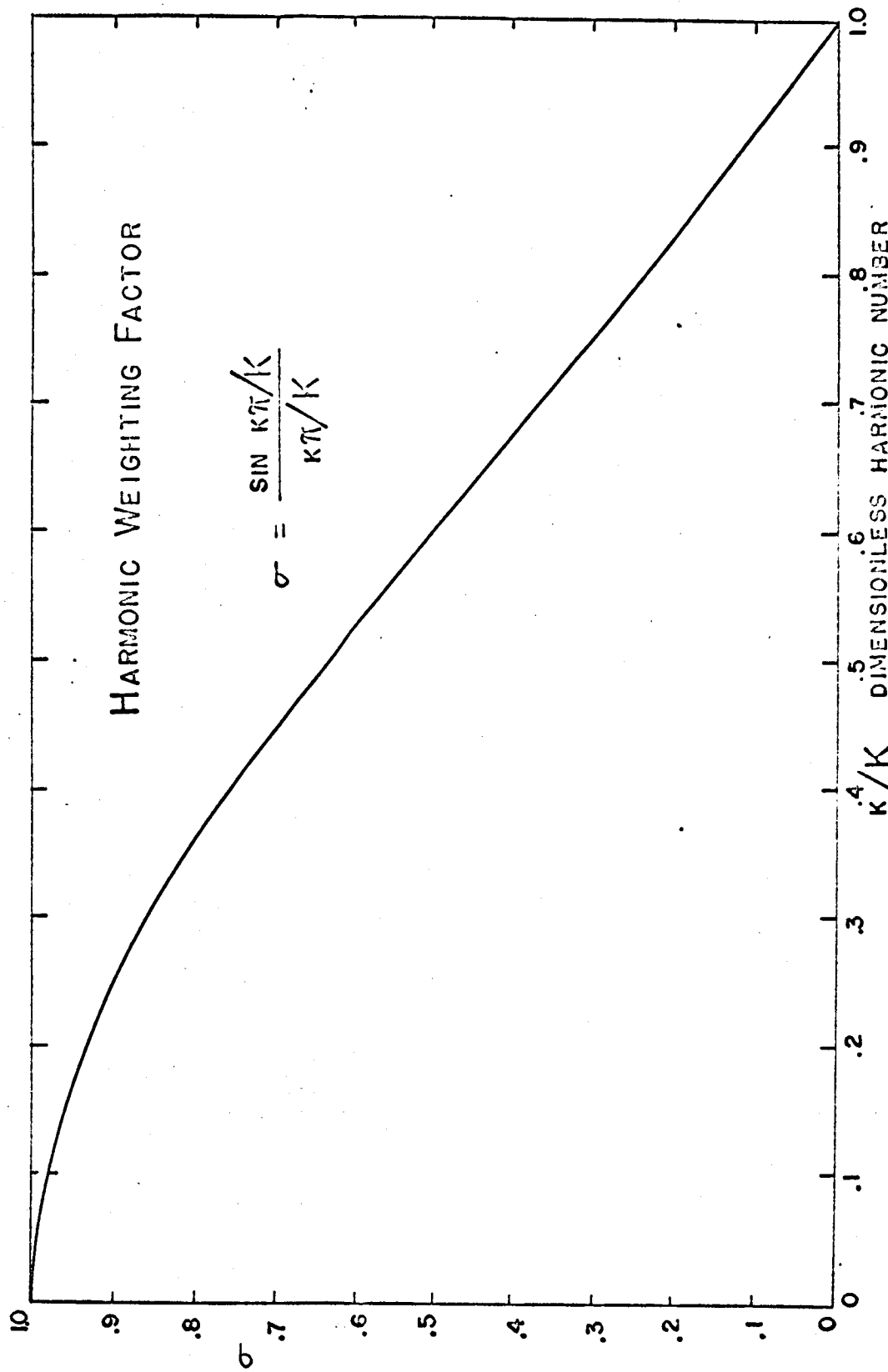
HARMONIC WEIGHTING FACTOR
$\sigma = \frac{\sin k\pi/K}{k\pi/K}$
σ
0
.1
.2
.3
.4
.5
.6
.7
.8
.9
1.0
k/K DIMENSIONLESS HARMONIC NUMBER

Fig. 17

by increasing the number of terms K to over 100, but at the expense of increased computer time. For want of a better name, this computation technique is herein termed the "converged Fourier" method as contrasted to the "Fourier" method.

With the application of this factor, the surface temperature history becomes, instead of Eqn. 29,

$$t(0,\theta) = A_{ow} + \sum_{k=1}^{K} \frac{\sin(\pi k/K)}{\pi k/K} \left\{ A_k \cos(k\omega\theta) + B_k \sin(k\omega\theta) \right\} \tag{41}$$

and the temperature profile into the wall is now:

$$t(x,\theta) = A_{ow} - \left\{ \frac{(A_{ow} - A_{aj})x}{L} \right\} + \tag{42}$$

$$+ \sum_{k=1}^{K} \exp\left[-x\sqrt{\frac{k\omega}{2\alpha}} \right] \cdot \frac{\sin(\pi k/K)}{\pi k/K} \cdot \left\{ \begin{array}{l} A_k \cos(k\omega\theta - x\sqrt{\frac{k\omega}{2\alpha}}) + \\ B_k \sin(k\omega\theta - x\sqrt{\frac{k\omega}{2\alpha}}) \end{array} \right\}.$$

The instantaneous heat transfer rate at the surface can be evaluated from:

$$q_{\text{converged, surface}} = \text{cond.} \left[\left[\frac{-A_{ow} - A_{aj}}{L} \right] + \right. \tag{43}$$

$$+\sqrt{\frac{\omega}{2\alpha}}\sum_{k=1}^{K}\sqrt{k}\left[\frac{\sin(\pi k/K)}{\pi k/K}\right]\left\{\begin{matrix}(B_k - A_k)\sin(k\omega\theta) & + \\ (B_k + A_k)\cos(k\omega\theta) & \end{matrix}\right\}\Bigg].$$

As the number of terms considered, K, increases, the small differences between the measured wall surface temperature, the "Fourier" fit (Eqn. 29), and the Lanczos smoothed or "converged" Fourier fit (Eqn. 41) will decrease. For 50 terms, the average error of the fits with respect to the measured curve is on the order of 1% of the total swing (i.e., about .02 F°).

CALCULATED FILM COEFFICIENT

Newton's Law of Cooling, expressing the rate of heat transfer across a film at the interface of a fluid and a solid,

$$q/A\Big|_{surface} = h\cdot(T_{fluid} - T_{solid\ surface}), \qquad (44)$$

has been commonly applied for many years in the study of free and forced convection. Its use is quite conventional and proper in many practical steady-state applications. However, caution must be observed in using this equation to describe the heat transfer rate in a system with rapidly changing conditions. The heat flux q/A is evaluated at the solid surface. When the properties of the film next to the surface are such that a phase lag occurs in the response of the wall surface temperature with respect to a gas tempera-

ture change, the film coefficient h can assume negative, zero, and infinite values. This effect is described briefly by Overbye(33). A more recent and complete exposition on negative and infinite values of h is given in a text by Y. V. Kudryavtsev (69). The theoretical models in this text incorporating capacitive energy storage in the boundary layer exhibit this behavior (see Fig. 58 for the RC Model, explained in Section VIII. B. 4.).

The experimental data, too, produce the peculiarly behaving h. Fig. 18 depicts the behavior of the coefficient calculated from:

$$h_{experimental} = \frac{q/A}{(T_{gas} - T_{wall\ surface})} . \qquad (45)$$

When h is positive, the heat flux and temperature difference agree in sign. When h is negative, they differ in sign. When h is zero, the heat flux is zero. When h is infinite, the film temperature difference is zero.

The coefficient h assumes infinite values whenever the surface heat flux does not change sign precisely when the temperature difference across the film changes sign.

AERODYNAMIC COMPLICATIONS

Ideally, all gas motion and property gradients in this investigation take place in only one dimension, normal to

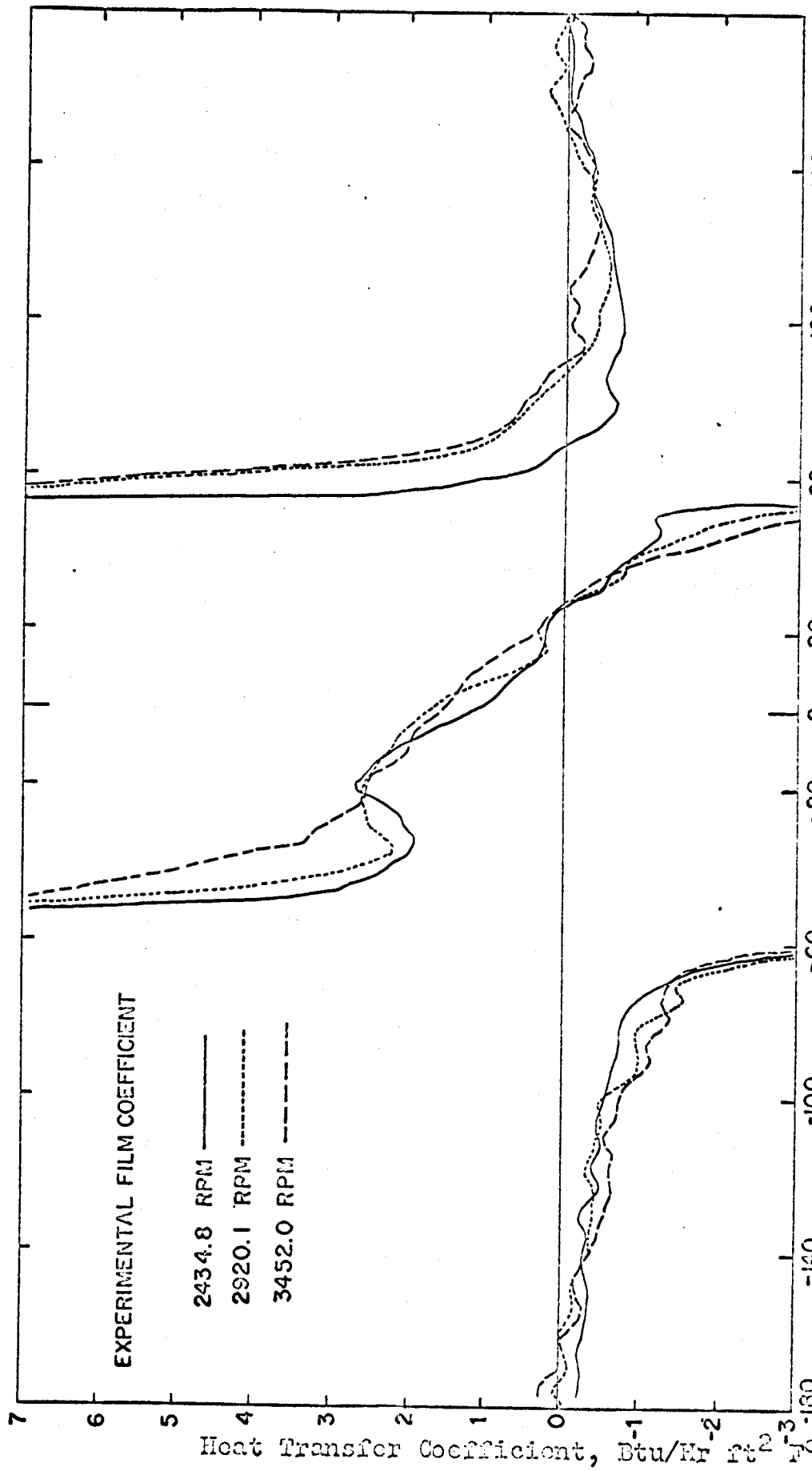
EXPERIMENTAL FILM COEFFICIENT
2434.8 RPM
2920.1 RPM
3452.0 RPM
Heat Transfer Coefficient, Btu/Hr Ft² F
7
6
5
4
3
2
1
0
-1
-2
-3
180
140
100
60
20
0
-20
-60
-100
-140
-180
T.D.C.
CRANKANGLE

FIG. 18

the head surface. The theoretical studies are all based on models in which a boundary layer is bounded on one side by a wall (the head) and on the other side by a spatially homogeneous gas mass (the bulk gas) in which there are no temperature gradients. The resistance thermometer, protruding about 0.100 inches (about 3 mm) into the gas, measures this bulk gas temperature. When several resistance thermometers were inserted the same depth into the gas at different places, the temperature histories seen were identical, showing the independence of temperature from r and θ. However, in order to have a gas mass with uniform density, there must be some small-scale gas motion in the bulk to mix the cool gases near the cylinder walls with the warmer "core" gases. It was therefore thought desirable to measure the head surface temperature at a number of positions simultaneously to see if the temperature history varied appreciably with location on the head surface. To this end, a head was constructed with nine surface thermocouples distributed as shown in Fig. 19. Surface temperature data were taken over the frequency range for three conditions as described below.

CYLINDRICAL CHAMBER

The head of Fig. 19 differs from the original head (see Fig. 2) in that the two semi-circular clearance volumes, or "ears" (one to accomodate the pressure transducer, one

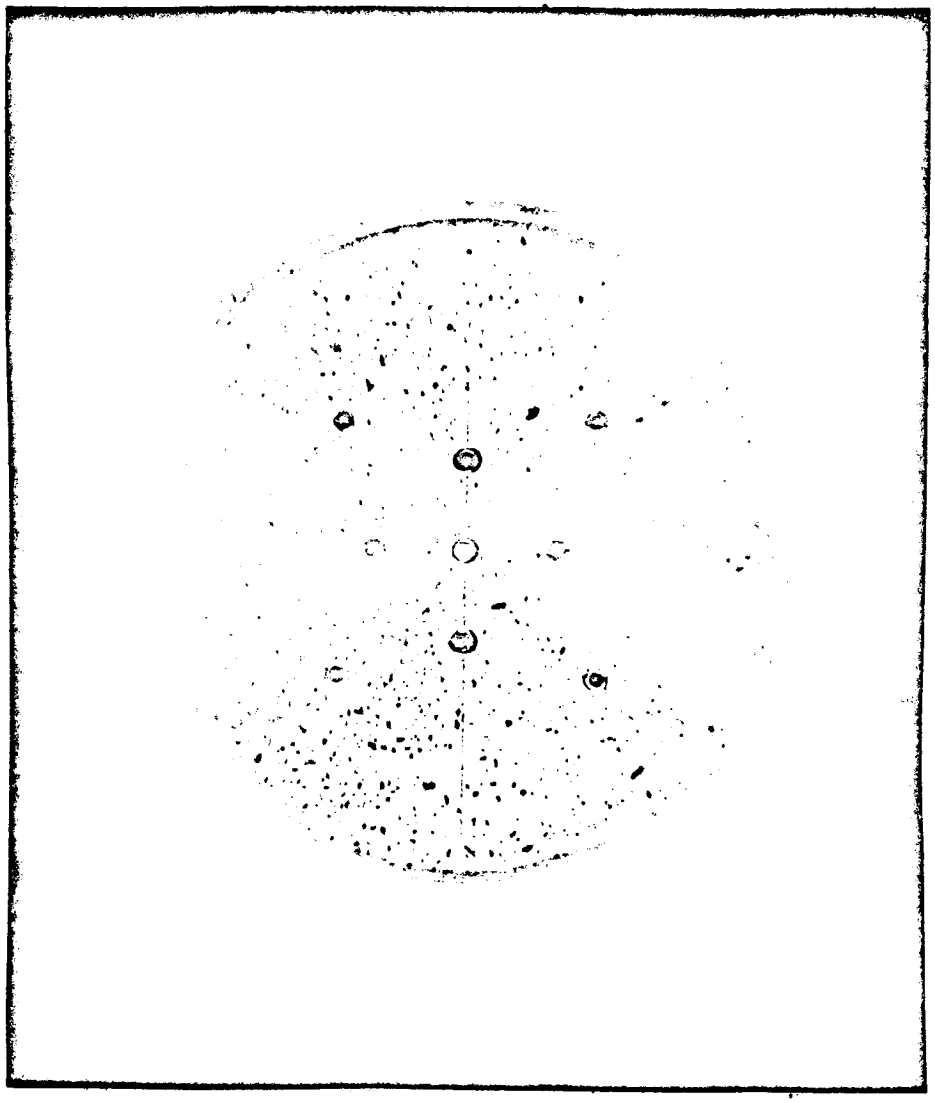

Underside of modified head with nine surface thermocouples, after running for 2 hours at 2000 rpm. The black specks are teflon residue from rings and cylinder walls.

Fig. 19

on the opposite side of the chamber for symmetry), were not needed, and therefore not included. As a consequence, this compression chamber was truly cylindrical and the fluid did not experience any "squish" flow (into the ears during compression, out of the ears during expansion). The nine surface thermocouples all experienced essentially the same histories as described by Figs. A1, A4, A8, A12, A16, and A20 for driving frequencies up to 22 Hz. Above this frequency the history was much the same as in the figures except that a "parasitic" oscillation at about the fifth or sixth harmonic of the fundamental appeared superimposed upon the history, growing in amplitude with speed until at 58 Hz its swing was about 40% of the main temperature swing. Fig. 20 shows the crankangle locations of the peaks of the "primary" and the "parasitic" temperatures on the head surface; this figure can be compared directly to Fig. 14 for the original head. Fig. 21 presents an example of the surface temperature behavior at 3175 rpm (53 Hz), showing the superimposed oscillation. The "parasitic" wall surface temperature oscillation is presumed to be due to changes in the heat transfer coefficient induced by cyclic air flow pattern in the chamber. All nine thermocouples reported this temperature oscillation, although its amplitude varied somewhat about the head surface.

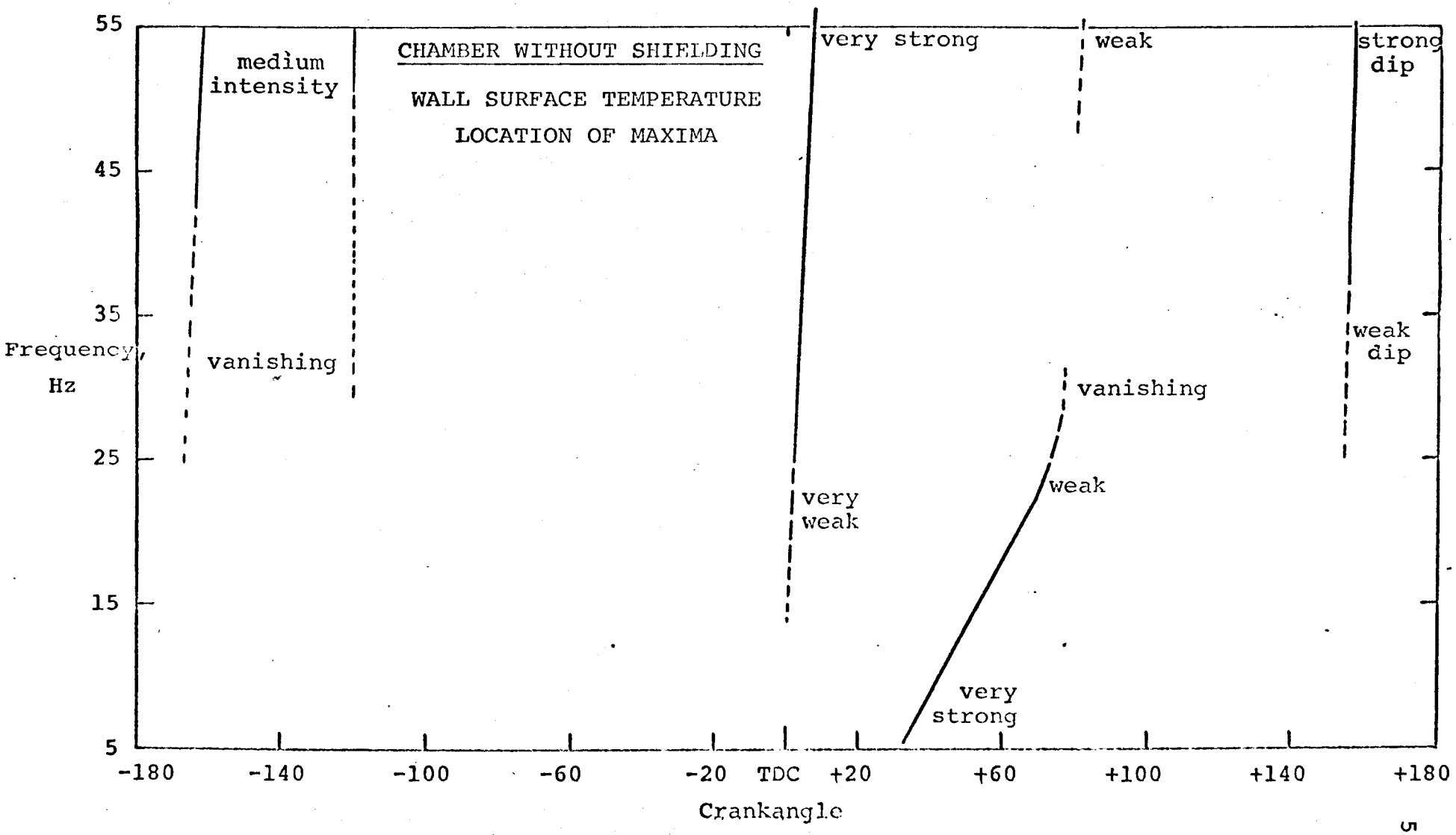
CHAMBER WITHOUT SHIELDING
WALL SURFACE TEMPERATURE
LOCATION OF MAXIMA
medium intensity
vanishing
very strong
very weak
weak
vanishing
weak
very strong
strong dip
weak dip
55
45
35
25
15
5
Frequency, Hz
-180
-140
-100
-60
-20
TDC
+20
+60
+100
+140
+180
Crankangle

Fig. 20

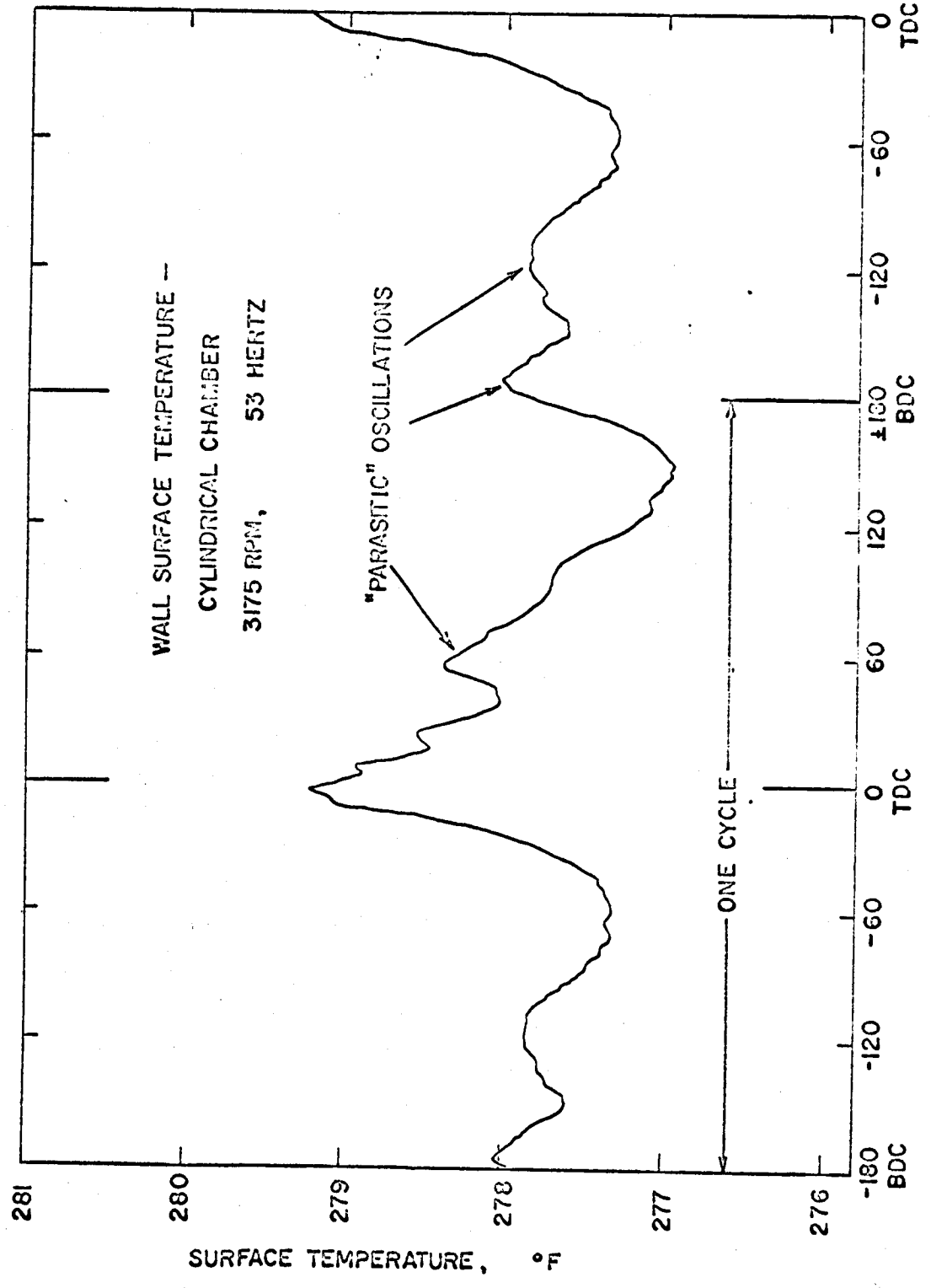
WALL SURFACE TEMPERATURE —
CYLINDRICAL CHAMBER
3175 RPM, 53 HERTZ
"PARASITIC" OSCILLATIONS
ONE CYCLE
SURFACE TEMPERATURE, °F
CRANKANGLE
281
280
279
278
277
276
-180 BDC
-120
-60
0 TDC
60
120
±180 BDC
-120
-60
0 TDC

FIG. 21

CYLINDRICAL CHAMBER WITH CLOSED MAKEUP PORTS

On the suspicion that air flow through the small makeup fluid ports in the cylinder wall bottom was serving as a driving mechanism for the recurring air flow (which was in turn inducing the periodic "parasitic" heat transfer and surface temperature swing), the holes were plugged and a set of data runs made. The size of the temperature and pressure swings decreased with time as blowby past the piston rings caused the system mass to decrease, but the wall surface temperature oscillations were not decreased in ratio to the overall wall surface temperature swing. The cyclic air flow is therefore not totally dependent on makeup air flow for its driving function. An alternative driving mechanism is the scraping of the cool boundary layer off the cylinder walls by the piston and the mixing of this denser mass with the bulk gas.

CYLINDRICAL CHAMBER WITH SCREENING

A screen of fine-mesh nylon was constructed 0.120 inches from the head interior surface and parallel to it to break up the cyclic air flow patterns and reduce their effect on surface temperature and surface heat transfer. This construction is illustrated in Fig. 22. The screen had two layers: a support of Nitex 35-500 nylon monofilament (32 filaments/inch, 300 micron filament diameter, 500 micron

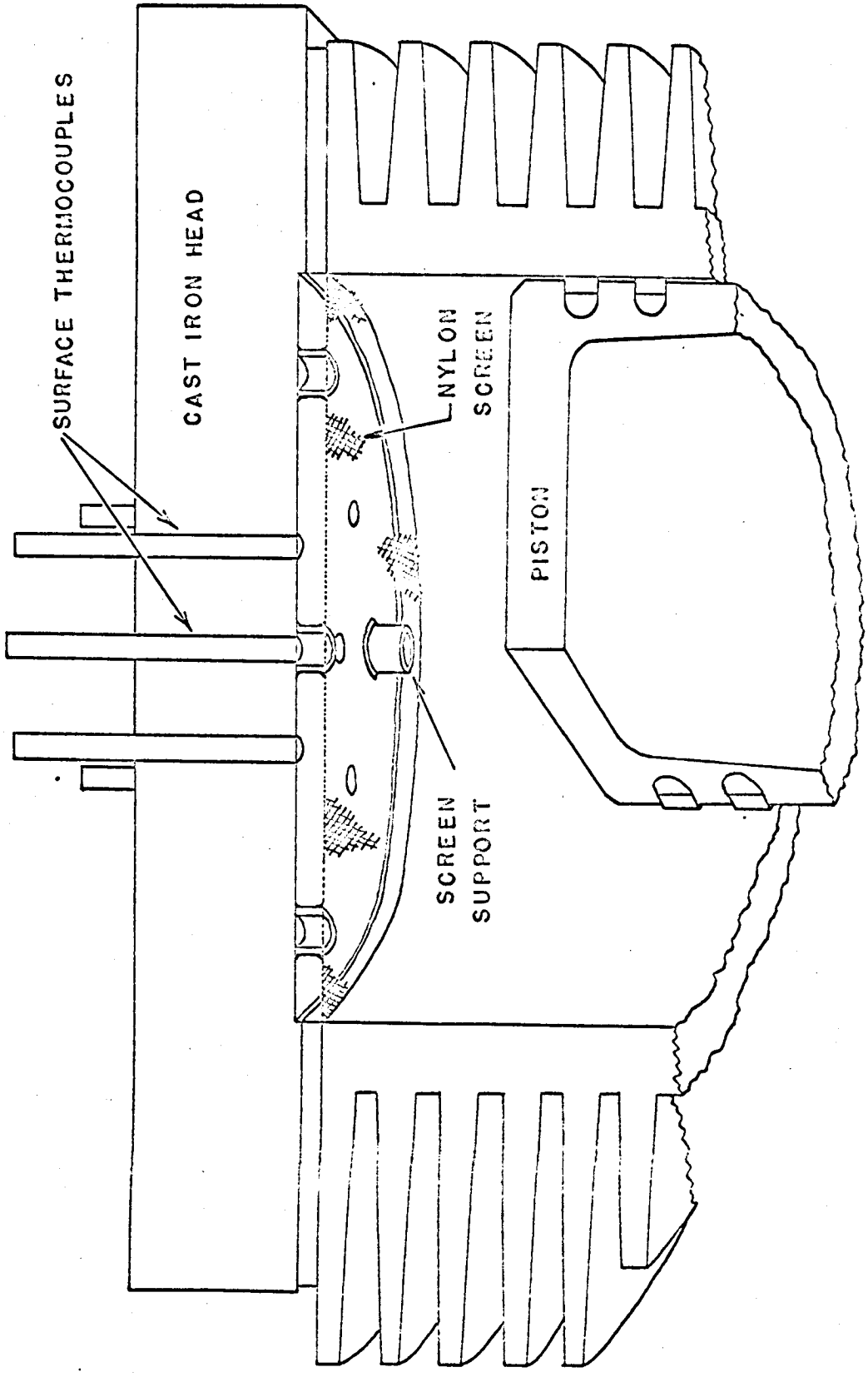

FIG. 22 ASSEMBLY WITH SCREEN IN POSITION

opening, 39% open area), and a fine mesh of soft nylon screening of about 100 micron opening, 150 filaments/inch. The screen was fastened around the circumference of the chamber and was supported at five locations on the face of the head by small plastic tubes (see Fig. 22).

The parasitic oscillations on the surface temperature histories were reduced by 50 to 80% in amplitude from the previous runs with the unshielded "cylindrical" chamber. The maxima of the small oscillations occurred at the same crankangle locations as before, as indicated by Fig. 23. This figure can be compared directly with Fig. 20 for the unshielded chamber and Fig. 14 for the original head.

CONCLUSIONS ON AIR MOTION

The three data sets discussed above shared with the original set of Figs. A1, A4, A8, A12, A16, and A20 (or, in summary, Fig. 12) the same general trends in head surface temperature history: a lagging surface temperature hump at low driving frequency; a peak near piston top dead center (0 crankangle degrees) at all high speeds; a double peak combining the two phenomena at intermediate speeds. The original set was completely free of the "aerodynamic" effects of the last three, and was taken to represent simple one-dimensional flow normal to the head surface. The oscillations were probably due to cyclic air flow

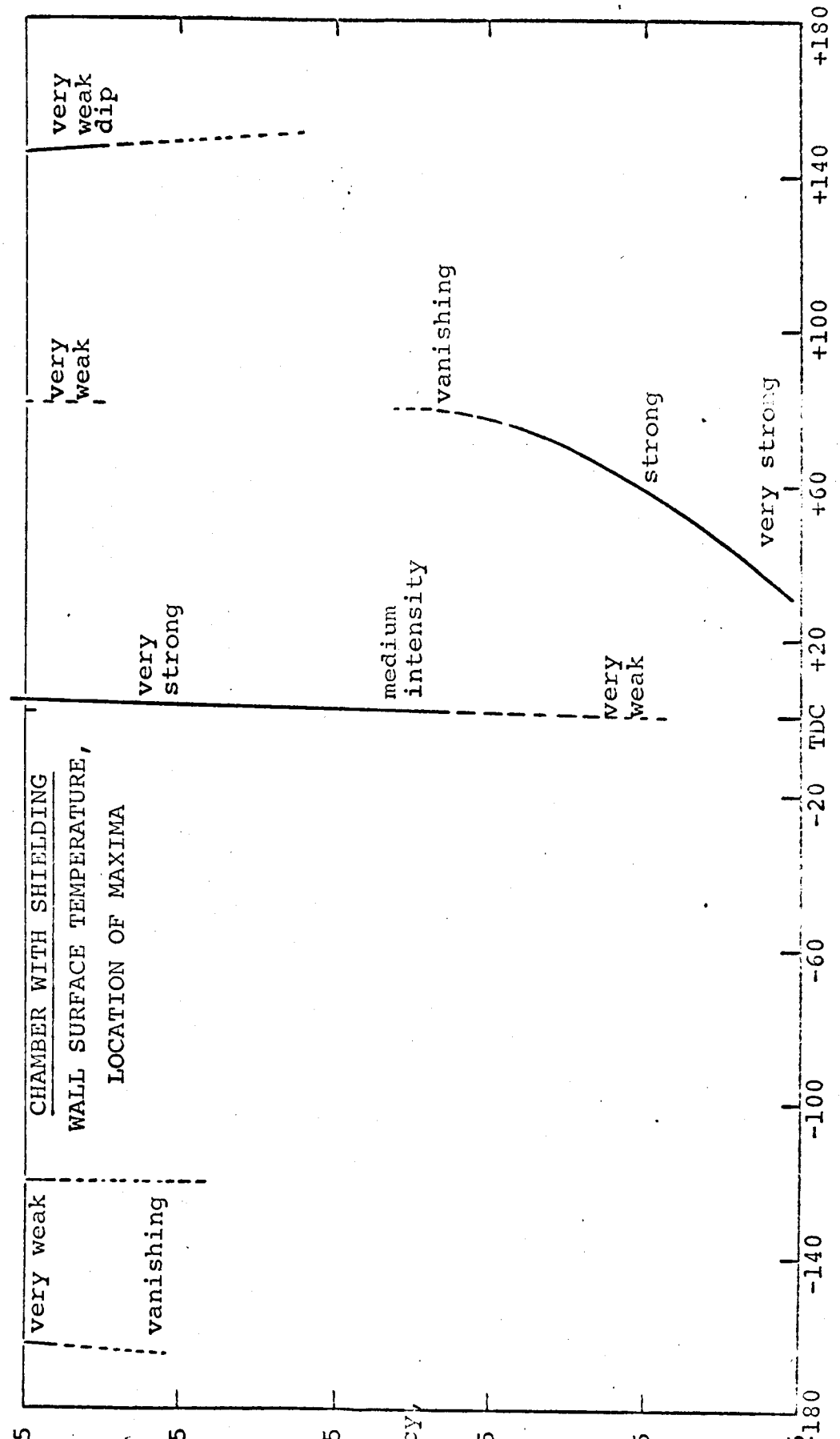
CHAMBER WITH SHIELDING
WALL SURFACE TEMPERATURE,
LOCATION OF MAXIMA
very weak
vanishing
very strong
medium intensity
very weak
vanishing
very weak
dip
very strong
strong
Frequency Hz
55
45
35
25
15
5
-180
-140
-100
-60
-20 TDC +20
+60
+100
+140
+180
Crankangle

Fig. 23

patterns sustained by very small pressure gradients in the bulk gas; the "squish" effect of the small semi-circular volumes (0.98% of the total clearance volume) was sufficient to break up these resonant air flow patterns in the original tests.

VIII. THEORETICAL MODELS

A number of theoretical models were developed to treat several domains in the system. All of the models take the form of digital computer programs, and each employs some type of relaxation or cyclic iteration technique to proceed from a guessed initial state to a cyclic history of states which satisfies the pertinent energy and continuity equations.

One of the theoretical models, termed the Adiabatic Plane Model, was considerably superior to the other models; it will be discussed in detail on the following pages. The five secondary models, which preceded the other chronologically, will be briefly described at this point. A more complete listing of the assumptions, methods of calculation, and results of the secondary models can be found in the Appendix section of the author's Ph.D. thesis.*

The first of the "secondary" models is named SIMUL, and treats the entire working fluid and the surrounding hardware: head, piston, and cylinder walls. This model was successful in predicting the steady periodic behavior of the working fluid treated as a homogeneous mass: bulk gas temperature and pressure histories, and heat flux histories through the surrounding metal surfaces (based on constant

*Ph.D. thesis, Daniel W. Wendland, U. of Wis., Jan. 1968

internal metal surface temperatures) were calculated.

The remaining four "secondary" models consider the head (sometimes termed the "wall") and the boundary layer adjacent to it on the compression chamber, or working fluid, side. In each, the intent is to examine the combination of various energy terms in the boundary layer with the energy flux entering the external edge of the boundary layer. The metal surface heat transfer rate is the result of this interaction of energy fluxes, and the metal surface temperature responds to changes in this heat flux. Each of these models was successful, to a varying degree, in predicting the metal surface temperature and surface heat transfer responses to gas temperature and pressure driving functions. They are not presented here, however, since the Adiabatic Plane Model rests on a far surer theoretical base and makes a better prediction of the metal surface thermal response.

ADIABATIC PLANE MODEL

In each of the secondary models of either the entire working fluid and the surrounding metal walls or of the head and its gas-side boundary layer, a considerable amount of empirical information was necessary to make the analysis possible. This empirical information was typically in the form of a time-varying spatial or energy flux boundary condition. In the total system model (SIMUL), the heat transfer rates at the metal surfaces were taken to be proportional to the Eichelberg heat transfer coefficient and to the bulk gas - wall surface temperature difference, both time-varying quantities. In the four models of the boundary layer - wall system, the Eichelberg coefficient was again used, and the time-varying boundary layer thickness was estimated around the cycle. The latter was accomplished by specifying the value of the Nusselt Number based on the instantaneous heat transfer coefficient and the instantaneous boundary layer thickness; this value, Nu_δ, was generally held constant around the system cycle. It was occasionally necessary to assume that the velocity profiles from piston to head were linear. Since some of the assumptions do not have strong theoretical bases, it was decided to construct a model for the system which draws its resources from basic thermodynamics and contains a bare minimum of simplifying assumptions and "engineering"

data. This theoretical construct is known as the Adiabatic Plane Model.

The system is the working fluid constrained by the head, cylinder walls, and the moving piston. The first major assumption,

1) the system is one dimensional, normal to head and piston,

ignores heat transfer to the cylinder walls and its influence on the gas properties, and can be defended on two grounds: first, the experimental system to which this model is an analogue was designed so that the gas motion would be as close to one-dimensional as possible; second, our interest is not so much in a gas being compressed and expanded in a particular piston-cylinder combination, but rather in the unsteady thermodynamic state of a gas experiencing pressure and temperature fluctuations and exchanging energy with a plane solid wall.

The second assumption is that:

2) the head surface temperature is constant.

The constancy of the metal surface temperature is not too bad an assumption, since the expected surface temperature swing is less than 1% of the gas temperature swing. The assumption of constancy is not fundamental in the analysis, in any case, and it will be shown later how a known varia-

ble surface temperature could easily be introduced to the system model.

The third major assumption is that:

3) there is a plane midway between piston and head at which the gradient of gas temperature with distance is zero.

This would follow from symmetry if we made the piston and head surface temperatures constant and equal. However, even if the piston surface temperature is not quite equal to the head temperature (the simulation program predicts it to be some 50 to 80 F° higher), its time variation is on the order of a few degrees--less than 1% of the gas temperature swing. The time-varying location of the adiabatic plane (or plane of zero temperature gradient) may be slightly different from the instantaneous position of the plane constrained to be halfway from piston to head. However, the temperature gradients in this region are very small (see figures in this section) and the error introduced by this boundary condition is small.

It is simplest, then,(and least expensive in terms of computer time) to consider the system to be bounded by the head and by a plane moving midway between head and piston. At the plane, the heat flux is zero; at the wall, the temperature is constant.

The final major assumption is that:

4) the fluid pressure is a function solely of time.

This assumption is quite reasonable at cyclic frequencies of a few hundred Hz, since the rate of change of chamber pressure is relatively slow, and the system can quickly "smooth out" any small pressure gradients existing in the gas. As frequency increases, fluid velocities begin to approach sonic values, and pressure gradients can stand in the gas.

Other assumptions are as follows:

5) The fluid is a perfect gas with the molecular weight and basic properties of air.

6) The gas specific heat and thermal conductivities can be approximated by linear temperature functions: at temperatures below 500°F,

$$k_{gas} = .0132 + (2.36 \times 10^{-5}) \cdot T \text{ (Btu/hr ft °F)}$$

$$c_{p_{gas}} = .2400 + (1.71 \times 10^{-5}) \cdot (T-90) \text{ (Btu/lb °F)},$$

and at temperatures above 500°F,

$$k_{gas} = .0250 + (1.70 \times 10^{-5}) (T-500)$$

$$c_{p_{gas}} = .2470 + (3.20 \times 10^{-5}) (T-500),$$

where T is the local instantaneous gas temperature in degrees F.

7) The mass of the system is constant.

8) The fluid is inviscid.

9) The fluid is not subject to inertia forces; the kinetic energy is small.

10) There is no gravity field, or, the one dimension of the system is perpendicular to the direction in which gravity is acting.

Assumption 7 becomes important when one compares the results of this model with the experimental data, taken in a working fluid whose mass changed slightly around the cycle. The ninth and tenth assumptions state that the energy dissipation due to fluid friction and the fluid's kinetic energy are negligibly small.

THE MATHEMATICAL FORMULATION

The gas, with total mass M, is subdivided into N elements, or laminae, as shown in Fig. 24. Each lamina has a constant mass, one Nth of the total mass, and is at a time-dependent temperature T throughout. All laminae share the same pressure history by assumption 3.

There are N+1 equations describing the thermodynamic state of this system at any time t. The first equation says simply that the sum of the volumes of the laminae at the time t must be equal to the volume contained at that time between head and plane (i.e., half the piston displacement volume at time t). Since the system is one-dimensional, all equations are written per unit area. The area is taken as unity for convenience. Then the first governing equation is:

$$\sum_{n=1}^{N} V_n(t) = V_d(t) \qquad (46)$$

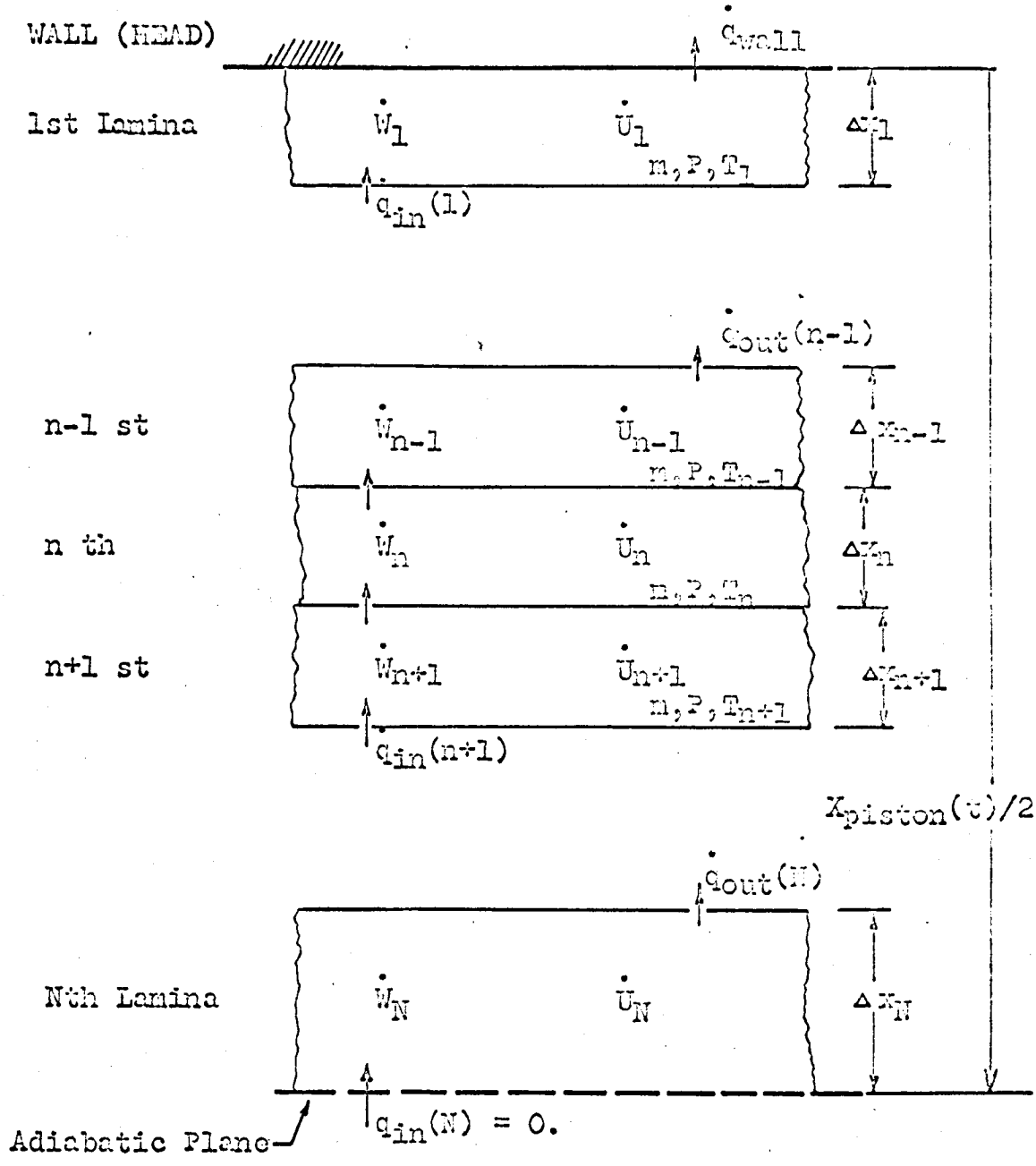

Fig. 24 . The Adiabatic Plane Model

where $V_n(t)$ is the volume of the nth lamina at time t, and

$V_d(t)$ is the volume between head and plane (in units of inches^3/inches^2) at time t.

The other N governing equations are energy rate balances at time t for the N laminae. For the nth lamina, with thickness Δx_n (equal to V_n, since the units are inches^3/inches^2), the simplified first law for the general element n at time t is:

$$\dot{q}_{n_{in}}(t) - \dot{q}_{n_{out}}(t) = mc_v \frac{dT_n(t)}{dt} + P(t) \frac{dV_n(t)}{dt}, \quad (47)$$

where m is the mass of element n per unit area. The units of this equation are energy/length^2 time.

The last term, which expresses the rate of work, can be changed with the help of the perfect gas law:

$$P(t) \frac{dV_n(t)}{dt} = P(t) \frac{d}{dt}\left[mR \frac{T_n(t)}{P(t)}\right] \quad (48)$$

$$P(t) \frac{dV_n(t)}{dt} = mRT_n(t)\left[\frac{1}{T_n(t)} \frac{dT_n(t)}{dt} - \frac{1}{P(t)} \frac{dP(t)}{dt}\right] \quad (49)$$

Applying the relationship for a perfect gas, $c_p = c_v + R$, the first law for the nth element is:

$$\dot{q}_{n_{in}}(t) - \dot{q}_{n_{out}}(t) = \left[mc_p \cdot \frac{dT_n(t)}{dt}\right] - \left[\frac{mRT_n(t)}{P(t)} \cdot \frac{dP(t)}{dt}\right]. \quad (50)$$

The first term in this equation represents the energy input rate by conduction to the nth mass, or lamina, as it and the observer moves in the system; the second is the output rate. The third term is the rate of change of enthalpy in the nth chunk, and the last is a work-related term.

THE FINITE DIFFERENCE EXPRESSIONS

Development of Equations

In the finite difference versions of the constraining equations, the choice of forward difference, backward difference, and central difference expressions for the first derivatives in the individual terms is guided by stability and convergence considerations. The forms selected below are the result of a series of trials with different forms for the terms which resulted in varying degrees of instability or stability.

The work-related term is expressed as a central difference. If we use j to represent the present time (at which all quantities are known or assigned), j-1 to be the immediate (and also known) past, and j+1 to indicate the immediate (and unknown) future, then the term becomes:

$$\text{Work-Related Term} \cong -\frac{mRT_n(j)}{P(j)}\left[\frac{P(j+1)-P(j-1)}{2\Delta t}\right] \qquad (51)$$

where Δt is the duration of the time interval.

The enthalpy term is expressed in forward difference form so that the temperature at time j+1 can be evaluated:

$$\text{Enthalpy Term} \cong mc_p \left[\frac{T_n(j+1) - T_n(j)}{\Delta t}\right]. \qquad (52)$$

The use of the forward difference form is fairly standard practice in this type of evaluation. The central difference form for this term was checked out, but its use resulted in rapid instability at all speeds considered. If the time interval is chosen to be sufficiently small, the error associated with the forward difference form for this term is small.

The conduction rates are expressed for time j:

$$\dot{q}_{n_{in}}(j) = k\left[\frac{T_{n+1}(j) - T_n(j)}{\Delta x^+(j)}\right], \qquad (53)$$

and

$$\dot{q}_{n_{out}}(j) = k\left[\frac{T_n(j) - T_{n-1}(j)}{\Delta x^-(j)}\right], \qquad (54)$$

where $\Delta x^+(j)$ is the distance from the center of element n+1 to the center of element n at time j, and $\Delta x^-(j)$ is the distance between centers of elements n and n-1.

Because $\Delta x_n(j)$ and $V_n(j)$ are numerically equal (since depth

is really volume per unit area), $\Delta x^+(j)$ can be written:

$$\Delta x^+(j) = \frac{\Delta x_{n+1}(j)}{2} + \frac{\Delta x_n(j)}{2}, \tag{55}$$

or, by the perfect gas law,

$$\Delta x^+(j) = \frac{mR}{2P(j)} [T_{n+1}(j) + T_n(j)], \tag{56}$$

and similarly,

$$\Delta x^-(j) = \frac{mR}{2P(j)} [T_n(j) + T_{n-1}(j)]. \tag{57}$$

Then the input conductive flux is:

$$\dot{q}_{n_{in}}(j) = \frac{2kP(j)}{mR} \left[\frac{T_{n+1}(j) - T_n(j)}{T_{n+1}(j) + T_n(j)} \right], \tag{58}$$

and the output conductive flux is:

$$\dot{q}_{n_{out}}(j) = \frac{2kP(j)}{mR} \left[\frac{T_n(j) - T_{n-1}(j)}{T_n(j) + T_{n-1}(j)} \right]. \tag{59}$$

Combining into the complete finite difference form for the nth, or general, element,

$$\frac{2kP(j)}{mR} \left[\frac{T_{n+1}(j) - T_n(j)}{T_{n+1}(j) + T_n(j)} - \frac{T_n(j) - T_{n-1}(j)}{T_n(j) + T_{n-1}(j)} \right] =$$

$$mc_p \cdot \left[\frac{T_n(j+1) - T_n(j)}{\Delta t}\right] - \frac{mRT_n(j)}{P(j)} \cdot \left[\frac{P(j+1) - P(j-1)}{2\Delta t}\right] . \quad (60)$$

The analogous equation for the Nth, or last element reflects the adiabatic wall boundary condition, $\dot{q}_{n_{in}}(j) = 0$:

$$\frac{2kP(j)}{mR} \cdot \left[- \frac{T_N(j) - T_{N-1}(j)}{T_N(j) + T_{N-1}(j)}\right] =$$

$$mc_p \cdot \left[\frac{T_N(j+1) - T_N(j)}{\Delta t}\right] - \frac{mRT_N(j)}{P(j)} \cdot \left[\frac{P(j+1) - P(j-1)}{2\Delta t}\right] . \quad (61)$$

The analogous equation for the first element reflects the constant wall temperature boundary condition in the following way: since

$$\dot{q}_{1_{out}}(j) = k\left[\frac{T_1(j) - T_{wall}}{\Delta x_1^-(j)}\right], \quad (62)$$

and the appropriate Δx is the distance from the center of element 1 to the wall surface, or

$$\Delta x_1^-(j) = \frac{V_1(j)}{2} = \frac{mRT_1(j)}{2\,P(j)} \quad (63)$$

then the first law equation for the first element is:

$$\frac{2kP(j)}{mR} \left[\frac{T_2(j) - T_1(j)}{T_2(j) + T_1(j)} - \frac{T_1(j) - T_{wall}}{T_1(j)}\right] =$$

$$mc_p \cdot \left[\frac{T_1(j+1) - T_1(j)}{\Delta t}\right] - \frac{mRT_1(j)}{P(j)} \cdot \left[\frac{P(j+1) - P(j-1)}{2\Delta t}\right] \quad .(64)$$

There is nothing in these equations which says that T_{wall} must stay constant; it was chosen to be so because the wall surface temperature history is unknown and the consequences of making it a constant are probably minor. If a wall surface temperature history is available, it can easily be expressed as a subscripted variable and introduced to Eqn. 64.

The N+1 equations determining the thermodynamic behavior of the system are as follows: Eqn. 46, the volume constraint; Eqn. 61, the first law for element N; Eqn. 64, the first law for element 1, and the N-2 versions of Eqn. 60 for the N-2 general elements. The unknowns are also N+1 in number: the pressure P(j+1) at the immediate future time, and the future temperatures of the N elements, $T_n(j+1)$, n=1,2,3,...N.

Two questions were encountered during the development of this model regarding: 1) the basic form of Eqn. 47 and 2) whether the system is completely determined by the N+1 equations listed above. These questions are assuaged in the following sections.

Displacement Work

As the adiabatic plane mirrors the piston motion (but at "half scale"), the gas laminae are compressed and displaced. Their centers of gravity are moved, leading to the speculation that the work term in Eqn. 47 should somehow contain an additional displacement or "pumping" work factor.

The correct form for the work term consistent with the assumptions contained in this model can be deduced from a simple thought experiment. Consider a medium in one-dimensional space, in which the fluid pressure is a function only of time. Planes 1 and 2 move with instantaneous velocities $u_1(t)$ and $u_2(t)$ in this fluid. The instantaneous rate of work on plane 1, with area A, is:

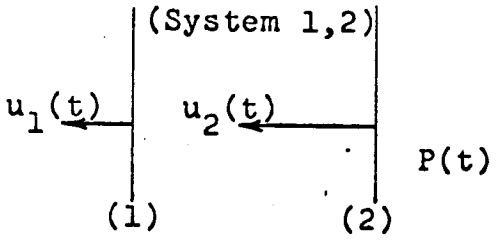

$$\dot{w}_1(t) = P(t) \cdot A \cdot u_1(t). \qquad (65)$$

Similarly, the rate of work on plane 2 is:

$$\dot{w}_2(t) = P(t) \cdot A \cdot u_2(t). \qquad (66)$$

The net rate of work on the mass contained between the

planes is the difference:

$$\dot{w}_{1,2}(t) = P(t)\cdot A\cdot[u_2(t) - u_1(t)] \qquad (67)$$

Now, $[u_2(t) - u_1(t)]$ is the relative velocity of the sides of the subsystem 1,2. Then the rate of change of volume of the subsystem could be expressed:

$$\frac{dV_{1,2}(t)}{dt} = A\cdot[u_2(t) - u_1(t)] \qquad (68)$$

and the net work rate for the lamina 1,2 is

$$\dot{w}_{1,2}(t) = P(t)\,\frac{dV_{1,2}(t)}{dt}\,, \qquad (69)$$

which is precisely the form used in Eqn. 47 and which describes the work rate on a stationary mass. The displacement work rate is identically equal to zero; this follows as a direct consequence of basic assumptions 3 and 8: the absence of a potential field in which the subsystems move.

Complete Determination of the System

When the system is viewed as a whole, it is clear that the only input work is the work done by the adiabatic plane on the whole gas, the only output heat transfer is conduction at the head, and the difference must be the rate of change

of internal energy of all the gas laminae. Expressed in equation form, it must be true that:

$$-\dot{q}_{wall}(t) = \frac{d}{dt} H_{total}(t) - V_{total}(t) \frac{dP(t)}{dt} . \quad (70)$$

The system is correctly determined, then, if the N+1 guiding equations contain Eqn. 70 as a corollary.

The N first law equations for the N laminae can be written in the form of Eqn. 50:

$$\dot{q}_{1_{in}}(t) - \dot{q}_{wall}(t) = mc_p\left[\frac{dT_1(t)}{dt}\right] - \left[\frac{mRT_1(t)}{P(t)} \cdot \frac{dP(t)}{dt}\right]$$

$$\dot{q}_{n_{in}}(t) - \dot{q}_{n_{out}}(t) = mc_p\left[\frac{dT_n(t)}{dt}\right] - \left[\frac{mRT_n(t)}{P(t)} \cdot \frac{dP(t)}{dt}\right] \quad (71 A,B,C)$$

$$- \dot{q}_{N_{out}}(t) = mc_p\left[\frac{dT_N(t)}{dt}\right] - \left[\frac{mRT_N(t)}{P(t)} \cdot \frac{dP(t)}{dt}\right]$$

If we add these N equations, noting that the conductive flux into the nth element is the conductive flux out of the (n+1)st, the result is a gross cancellation on the left side, yielding:

$$- \dot{q}_{wall}(t) = mc_p \sum_{n=1}^{N} \frac{dT_n(t)}{dt} - \frac{mR}{P(t)} \cdot \frac{dP(t)}{dt} \cdot \sum_{n=1}^{N} T_n(t). \quad (72)$$

The first term on the right side is really:

$$mc_p \sum_{n=1}^{N} \frac{dT_n(t)}{dt} = \sum_{n=1}^{N} \frac{dH_n(t)}{dt} = \frac{dH_{total}(t)}{dt} . \quad (73)$$

The last term on the right side is simplified with the help of the other basic governing equation, Eqn. 46:

$$V_d(t) = \sum_{n=1}^{N} V_n(t) = \sum_{n=1}^{N} \frac{mR}{P(t)} \cdot T_n(t) = \frac{mR}{P(t)} \sum_{n=1}^{N} T_n(t) \quad (74)$$

Then the last term in Eqn. 72 is:

$$- \frac{mR}{P(t)} \frac{dP(t)}{dt} \sum_{n=1}^{N} T_n(t) = - V_d \frac{dP(t)}{dt} . \quad (75)$$

Having re-expressed the terms of Eqn. 72, we collect them:

$$- \dot{q}_{wall}(t) = \frac{dH_{total}(t)}{dt} - V_d \frac{dP(t)}{dt} . \quad (76)$$

This is the same as Eqn. 70; thus, the N+1 chosen equations correctly determine the system.

SOLUTION OF THE FINITE DIFFERENCE EQUATIONS

The unknowns in the defining equations, Eqns. 46, 61, 64, and the N-2 versions of 60, are the future temperature array $T_n(j+1)$, n = 1,2,3,...N and the future chamber pres-

sure P(j+1). The method of solution chosen is as follows:

1) Select the initial temperature array $T_n(j=0)$ and the initial pressure P(j=0) from experience.

2) Guess the future pressure at time 1 from the polytropic relationship:

$$P(j=1) = P(j=0) \left[\frac{V_d(j=0)}{V_d(j=1)}\right]^n \qquad (77)$$

where n has some reasonable value, from 1.35 to 1.40 (in the program, n = 1.4 was chosen arbitrarily).

3) Each of the N energy rate finite difference equations has two unknowns: the pressure P(j+1) and the temperature $T_n(j+1)$. The pressure having been guessed, each of the energy equations can be solved for the temperature. This yields the temperature array $T_n(j=1)$, n = 1,2,...N, for the guessed pressure at that time.

4) The volume constraint equation, Eqn. 74, is written in the form:

$$P_{\substack{\text{better}\\\text{guess}}}(j=1) = \frac{mR}{V_d(j=1)} \sum_{n=1}^{N} T_n(j=1) \; . \qquad (78)$$

and the calculated temperature array is inserted,

producing the $P_{better\ guess}$ consistent with the constraints. This P(j=1) is compared to the guessed pressure from step 2. If it agrees within .002 psi (generally it agrees within about 0.5 psi on the first iteration), it was a close enough guess. If not, this new pressure is used in step 3 and the iteration begins anew. Convergence generally requires from three to six iterations.

5) In this fashion the temperature array (or profile) and gas pressure are calculated around the cycle from the "experience-selected" initial conditions. The temperature array and pressure value at the cycle end (-180 crankangle degrees, or BDC) are compared to the initial conditions. If the pressure has converged to within 0.1 psi, the cycle is deemed converged. If the pressure has not yet converged, the final conditions are used as initial conditions in step 1 and we begin again. With judicious selection of initial conditions, about five or six cycles are needed to achieve complete convergence.

The computer program as written required about 27 seconds for compilation, and about two minutes, 12 seconds per cycle on the CDC 1604 computer, when N is set at about 70 elements. Thus, the program was relatively expensive to

run. More sophisticated programming could reduce the time somewhat, but the very large number of iterations required dictates that the execution time will be fairly long.

CONVERGENCE AND STABILITY

With this program as with all finite difference treatments of differential equations, the matters of convergence and stability are of real concern. Two basic parameters can be varied independently to change the rate and/or accuracy of computation: the width of the spatial element, Δx_n, and the time increment between steps, Δt. In the present case, the time increment is related to system frequency, rpm, and the time division of the individual cycle (here taken as one crankangle degree, with 360 degrees per cycle). The spatial width Δx_n of the elements varies with the element chosen and also with time.

The stability criterion for the Diffusion Equation is generally taken to be:

$$\frac{k_{gas}\Delta t}{\rho c_p (\Delta x)^2} < 0.5 \quad . \tag{79}$$

However, ρ is varying from place to place and with time, k and c_p are temperature-dependent, and the Δx of the elements are different and time-varying. In the face of these fac-

tors, a more pragmatic approach to stability was adopted.

The time increment can be written (having fixed 360 as the number of increments per cycle) as

$$\Delta t = C_1/\text{rpm},$$

where C_1 is some constant, and the Δx increment can be roughly taken to be:

$$x = C_2/N,$$

where C_2 is some number and N is the total number of laminae. Then in an approximate fashion, the stability requirement can be expressed as:

$$\frac{N^2}{\text{rpm}} < \text{some number } C, \qquad (80)$$

where C is determined by trial and error. The table below gives the results of several trials:

STABILITY CORRELATION TABLE

Run Number	RPM	N	Calculated C	Solution Condition
1124	400	42	4.410	Unstable
1187	400	40	4.000	Unstable
621	600	71	8.402	Unstable
993	600	35	2.042	Stable
1064	800	50	3.125	Unstable
890	800	42	2.205	Stable
629	4000	150	5.625	Unstable
544	4000	71	1.260	Stable
784	9000	71	0.560	Stable

It appears that the value of C for marginal stability lies between 2.205 and 3.125. For a conservative C of 2.205, the maximum N for a stable calculation is:

$$N_{max} = 1.49 \sqrt{rpm} \qquad (81)$$

As N is decreased below about 30, the Δx "screen" gets rather coarse, and the program results become a less faithful solution to the differential equations.

MODEL RESULTS AND CONCLUSIONS

As this model differs from the experimental apparatus in a number of ways, care must be exercised in making direct comparisons between model and experimental dependent variable arrays. The one-dimensional assumption neglects heat transfer to the cylinder sleeve. The presence of viscous energy dissipation and very small spatial pressure gradients is ignored. In the experimental setup, the energy dissipated at the piston rings and piston surface in rubbing on the non-lubricated cylinder walls was thought to contribute in determining the general thermal level of the working fluid. This energy dissipation is not included in the present model. The mass of the model gas is constant; in the experimental setup, some mass was lost through blowby during the high pressure portion of the cycle and regained through the makeup ports in the low pressure portion of the cycle. This fluid flow is analyzed in the system simulation pro-

gram (SIMUL), not presented here. A final important difference is the lack of makeup air in the model, which contributed a fresh "charge" of 140°F air to each experimental cycle. This had two effects: first, a certain amount of energy was added to the system with the makeup air; second, enough mass was added to keep the pressure near BDC at a level near atmospheric, from which compression could proceed.

Table 1 on the following two pages lists the independent and dependent variables for the model as a function of frequency; a few parallel experimental variables are included for purposes of comparison. Peak crankangle times listed in the table are interpolated between the computed one degree steps, and because the solution has a step, or segmented, nature, they should not be thought of as being accurate to the nearest 0.1 crankangle degree.

The method of calculation of the bulk-averaged temperature is described later. The polytropic coefficients based on the bulk averaged temperature and the volume (1.365 at 800 rpm, 1.370 at 4000 rpm) are in reasonable agreement with the experimental coefficients (1.359 at 915 rpm, 1.374 at 3452 rpm).

The information (temperature swings and ratios of max/min) listed for elements 1 and 2 should be approached with caution, since the masses and volumes of the elements de-

Table 1

CHANGE OF VARIABLES WITH FREQUENCY -
ADIABATIC PLANE MODEL AND EXPERIMENTAL DATA

ADIABATIC PLANE MODEL

RPM	600	800	4000	9000
Frequency, Hertz	10	13.3	66.7	150
N, no. of elements	35	42	71	71
Chosen Wall Temp., °F	200	215	276	276
Swings in Variables				
T (bulk averaged), °F		580.0	665.0	
T (first element), °F*	126.1	120.5	149.8	216.9
T (second element), °F**	293.0	284.7	343.3	445.5
T (Nth element), °F	624.5	665.1	850.0	891.1
Pressure, psi	130.2	133.8	152.9	159.4
$\dot{q}$ at wall, Btu/hr ft^2	11.9K	14.0K	33.9K	52.6K
Ratios of Max/Min				
T (bulk averaged)		2.350	2.380	
T (first element)	1.218	1.202	1.234	1.360
T (second element)	1.616	1.575	1.655	1.936
T (Nth element)	2.505	2.500	2.442	2.434
Pressure	24.81	24.95	25.16	25.22
Pressure at BDC, psia	5.47	5.59	6.34	6.58

EXPERIMENTAL COUNTERPARTS

RPM	915	3452
Frequency, Hertz	15.27	57.5
Measured Wall Temperature °F	225	277
Swings in Variables		
Gas Temperature (from wire), F°	560	630
Gas Pressure, psi	365.4	364.0
Wall Heat Flux (Btu/hr ft^2)	45.3K	94.5K
Ratios of Max/Min		
Gas Temperature	2.113	2.188
Gas Pressure	23.9	30.5
Pressure at BDC, psia	17.61	12.04

*element next to the wall

**second element from the wall

Table 1 (continued)

ADIABATIC PLANE MODEL

RPM	600	800	4000	9000
Frequency, Hertz	10	13.3	66.7	150
Peak Crankangle Times*				
T (element N), cr. degrees	-0.2	-0.1	+0.2	+0.2
Pressure, "	-0.3	-0.2	-0.1	-0.0
$\dot{q}$ at wall surface, "	-10.2	-10.3	-9.8	-9.6
Polytropic Calculations				
n from T_{bulk}, V_{total}		1.365	1.370	
n from P, V_{total}	1.392	1.392	1.382	1.381
Cycle averaged T_N, °F	134.5	174.7	372.3	441.4
Cyclic mean $\gamma(T_N)$	1.398	1.396	1.388	1.386
Ratio of $n(P,V_{tot})/\gamma$	0.982	0.986	0.993	0.996

EXPERIMENTAL COUNTERPARTS

RPM	915	3452
Frequency, Hertz	15.27	57.5
Peak Crankangle Times		
Gas Temperature	-2.0	+2.2
Gas Pressure	-1.0	-1.0
$\dot{q}$ at wall surface	-8.5	-8.5
Wall Surface Temperature	+67.5**	-2.4
Polytropic Calculations***		
n from T_{gas}, V_{total}	1.320	1.335
n from P_{gas}, V_{total}	1.359	1.374

*Computer iterations are at one crankangle degree intervals, and values listed in tenths of a degree represent interpolations.

**This is the late "hump" which occurs only at low speeds.

***The experimental polytropic calculations are performed for a system whose mass is time-varying, and are to be interpreted with caution.

pend on N, the number of elements chosen. As this varies with frequency (because of stability requirements), these data are strictly interpretable only within a frequency (or rpm) column. Note that the temperature swing of the first element is generally about half that of the second element, and is on the order of one or two hundred degrees. If we would wish the model to precisely describe the finer details of the temperature distributions, we would have to increase N to several hundred, greatly increasing the computing time. Since temperature ratios on the order of 2.5 represent isentropic behavior and a unity temperature ratio isothermal behavior, it can be seen from the listed temperature ratios how we proceed from isentropic behavior near the Nth element to nearly isothermal at the first.

Fig. 25 shows the histories of the adiabatic plane temperature (actually the temperature T_N, half the thickness of the Nth lamina from the adiabatic plane and never more than 0.2 F° from the plane temperature) with frequency as the parameter. This temperature peaks consistently within ±0.2 crankangle degrees of TDC. The swing and level increased with increasing frequency, and the temperature ratio decreased very slightly. The shapes of these curves and the crankangle locations of their maxima compare well with most of the experimental observations. The polytropic coefficient calculated from the T_N ratio and the overall volume ratio decreased from 1.3922 at 10 Hz to 1.3808 at 150 Hz.

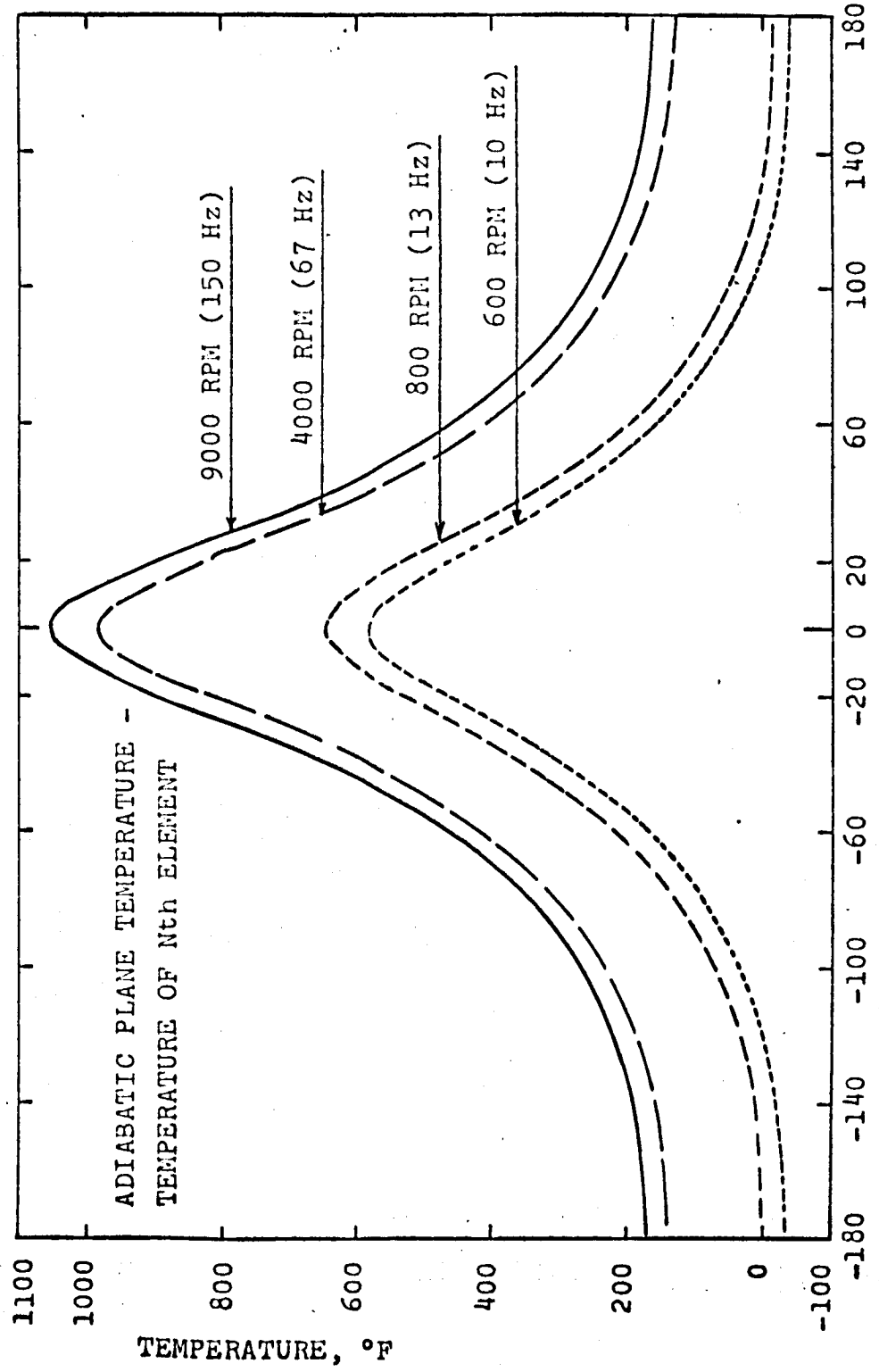
9000 RPM (150 Hz)
4000 RPM (67 Hz)
800 RPM (13 Hz)
600 RPM (10 Hz)
ADIABATIC PLANE TEMPERATURE -
TEMPERATURE OF Nth ELEMENT
TEMPERATURE, °F
1100
1000
800
600
400
200
0
-100
-180
-140
-100
-60
-20
0
20
60
100
140
180
CRANKANGLE

Fig. 25

Fig. 26 gives several gas pressure histories as predicted by the model. The pressure was closely symmetric with crankangle in the compression and expansion strokes, and peaked within a few tenths of a crankangle degree of TDC at all speeds. The pressure swings and levels dropped as speed decreased below a few thousand rpm. As the lowest pressure in the cycle,(i.e., at BDC) dropped from 6.58 psia at 150 Hz to 5.47 psia at 10 Hz, the cycle pressure ratio remained fairly constant at from 24.8 to 25.2. The polytropic coefficient calculated from the pressure ratio and the overall volume ratio increased from 1.373 at 10 Hz to 1.3808 at 150 Hz. The pressure ratios compared well with the experimental and SIMUL values. The pressure swings were reduced because in the model the BDC pressures were much lower than in the experiment. The minimum pressures in the model (and hence the pressure and temperature swings) could easily be elevated by increasing the mass of the elements, which is established in the initial part of the program. In the experimental apparatus, this was done in the introduction of makeup air.

It is interesting to note the polytropic calculations for the Adiabatic Plane Model on the top of the second page of Table 1. The cycle averaged adiabatic plane temperature rises from 134.5°F to 441.5°F from 10 Hz to 150 Hz. The ratio of specific heats, γ, evaluated at the cyclic mean temperature, decreases from 1.398 at 10 Hz to 1.386 at 150

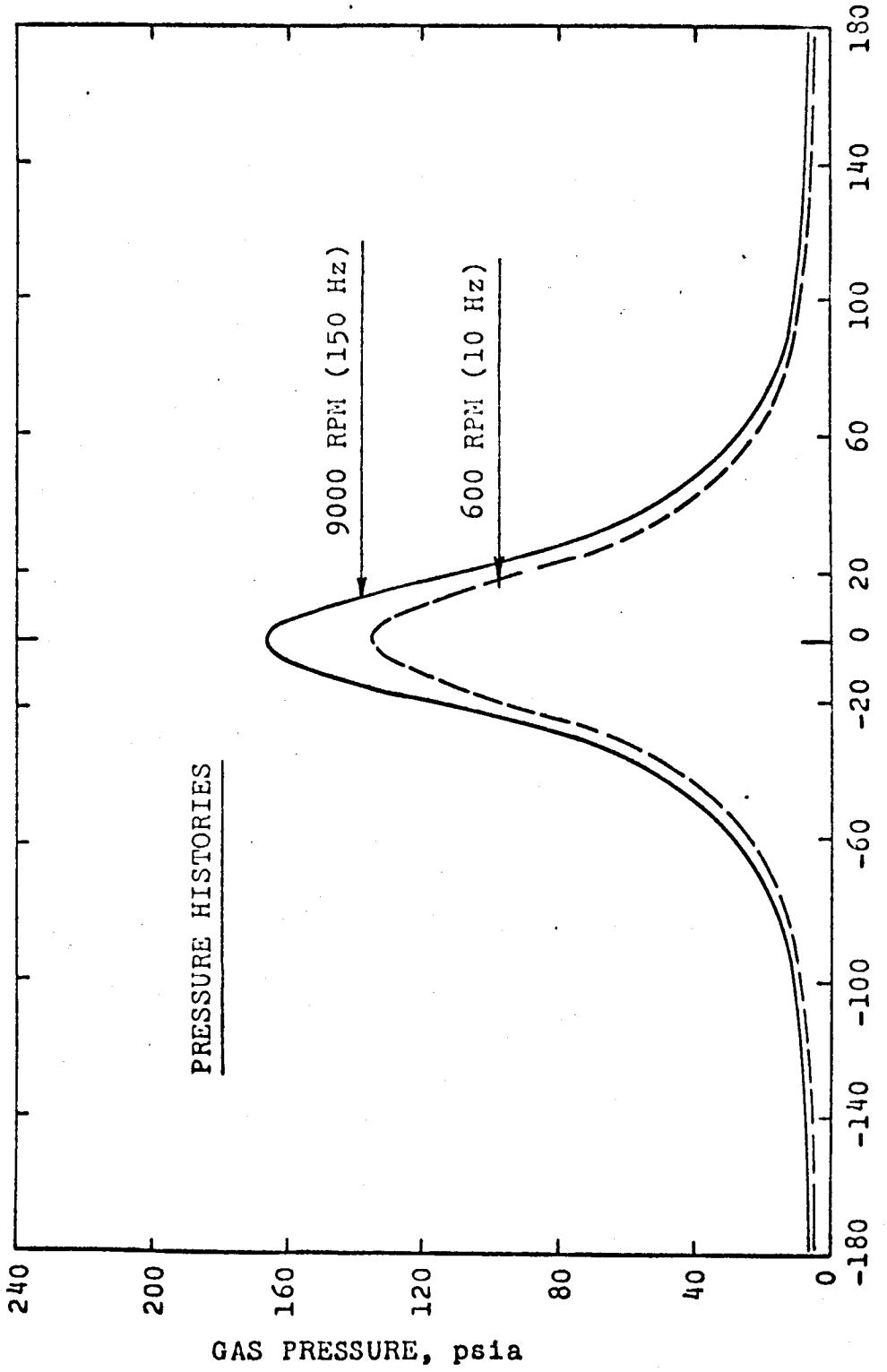
PRESSURE HISTORIES
9000 RPM (150 Hz)
600 RPM (10 Hz)
GAS PRESSURE, psia
240
200
160
120
80
40
0
-180
-140
-100
-60
-20
0
20
60
100
140
180
CRANKANGLE

Fig. 26

Hz. The "degree of isentropicity" is best judged from the ratio of the cycle polytropic coefficient based on P and V_{total}, to γ. The cycles appear to approach the isentropic standard as frequency increases; this agrees with intuitive reasoning, in that heat transfer should be of less importance at high speeds, when the time interval for transferring heat per cycle is small.

Fig. 27 presents the wall surface heat flux histories as a function of frequency. The histories reached their peaks at -10.0 ±0.4 crankangle degrees, in close agreement with the high frequency experimental data. The history shapes were very close to those of the high frequency (>25 Hz) experimental heat flux histories (see Fig. 13 for experimental plots), although the amplitudes were slightly smaller. Since the surface temperature maxima were found in experimental and analytical studies to lag the corresponding surface heat flux maxima by from 9 to 11 crankangle degrees for this shape of history, the transient surface temperature which could be calculated from these model heat flux histories would peak at ±1.6 degrees from TDC. This correlates very closely with the high speed experimental observations.

Figs. 28 and 29 give the temperature profiles in the gas between the head and the adiabatic plane. Observe that a true boundary layer thickness would be somewhat difficult to evaluate from these data, although the steepest temper-

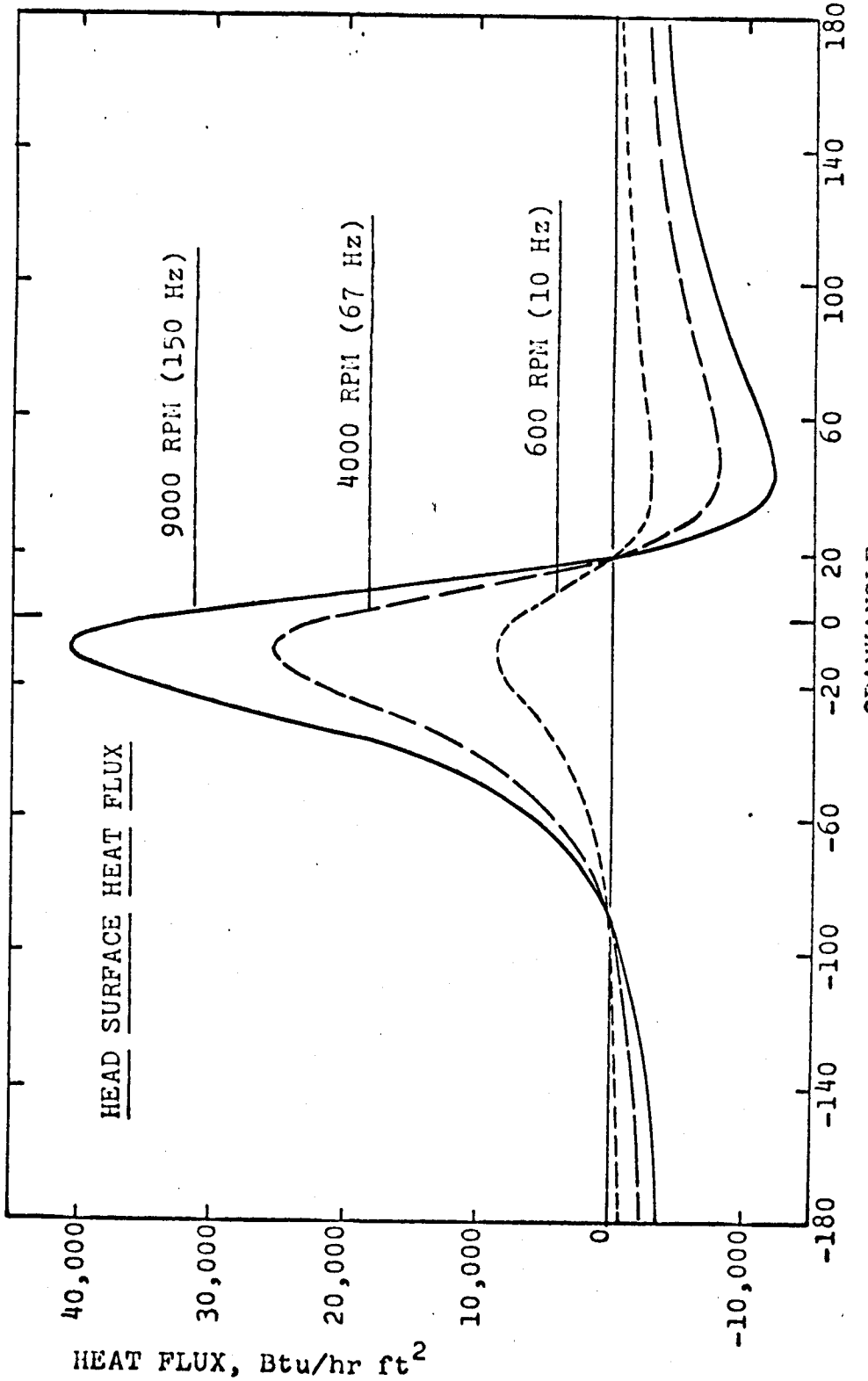
HEAD SURFACE HEAT FLUX
9000 RPM (150 Hz)
4000 RPM (67 Hz)
600 RPM (10 Hz)
HEAT FLUX, Btu/hr ft^2
40,000
30,000
20,000
10,000
0
-10,000
-180
-140
-100
-60
-20
0
20
60
100
140
180
CRANKANGLE

Fig. 27

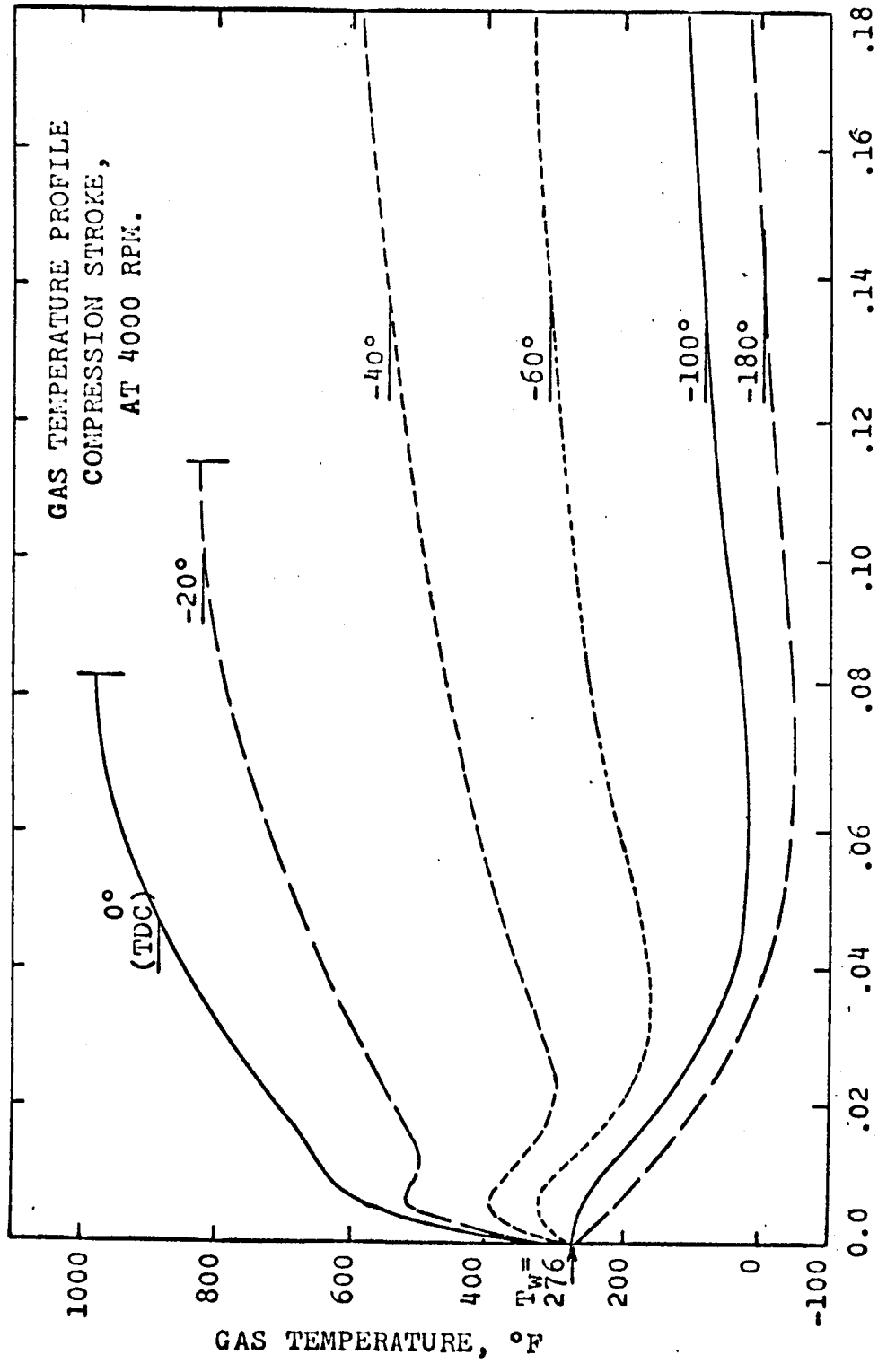
GAS TEMPERATURE PROFILE
COMPRESSION STROKE,
AT 4000 RPM.
0°
(TDC)
-20°
-40°
-60°
-100°
-180°
1000
800
600
400
T_w=
276
200
0
-100
GAS TEMPERATURE, °F
0.0
.02
.04
.06
.08
.10
.12
.14
.16
.18
DISTANCE INTO GAS FROM WALL SURFACE, inches

Fig. 28

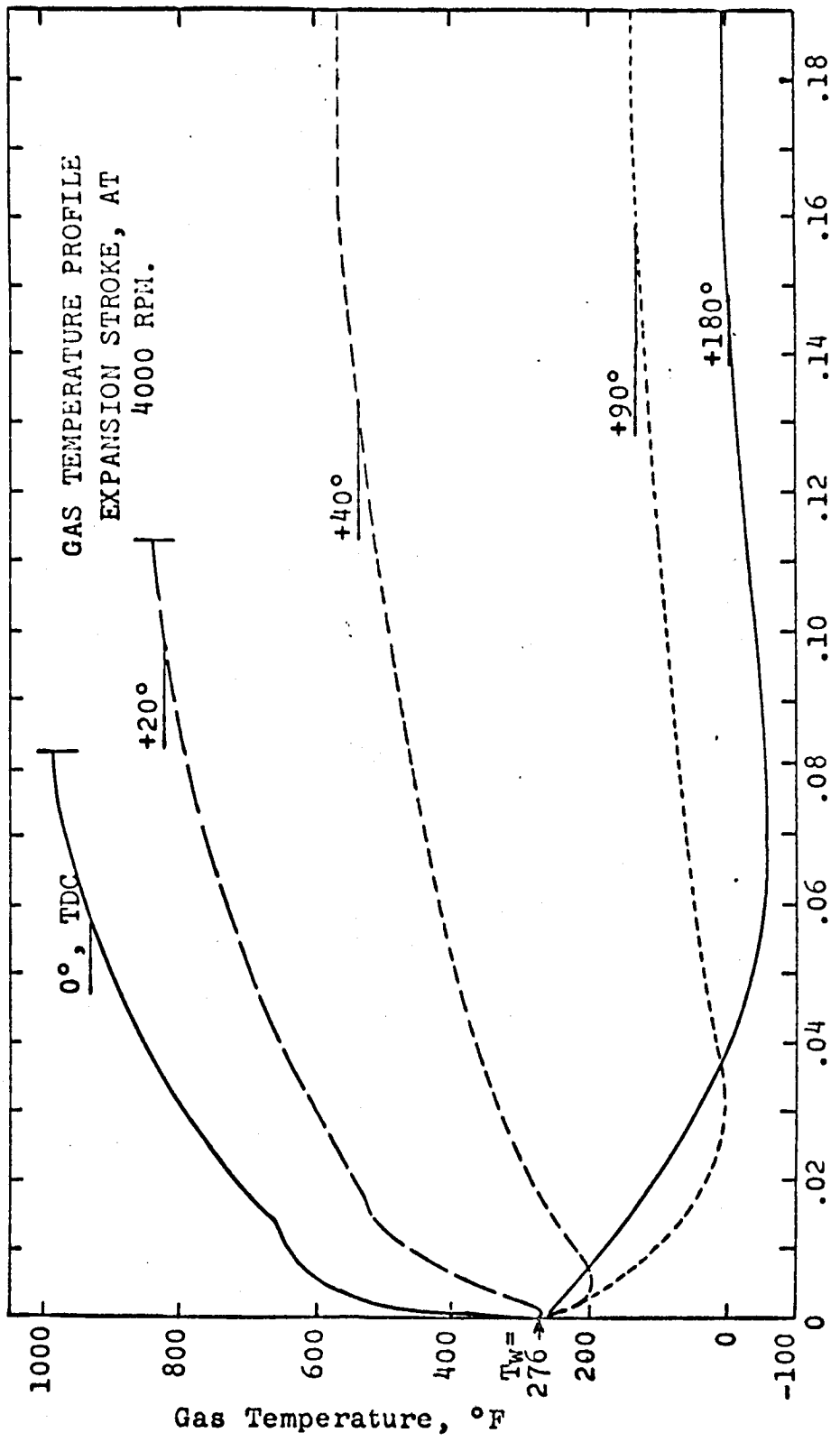
GAS TEMPERATURE PROFILE
EXPANSION STROKE, AT
4000 RPM.
0°, TDC
+20°
+40°
+90°
+180°
1000
800
600
400
T_w = 276 →
200
0
-100
Gas Temperature, °F
0
.02
.04
.06
.08
.10
.12
.14
.16
.18
DISTANCE INTO GAS FROM WALL SURFACE, Inches

Fig. 29

ature gradients seem to be within 2mm of the wall at BDC and 1mm at TDC. The traces for +20 and +40 crankangle degrees on the expansion stroke (Fig. 29) show clearly the "negative h" phenomenon: with a positive temperature potential from gas to wall, the heat flux is from wall to gas. The +20° trace corresponds to a zero or slightly negative value for h; a +60° trace (large heat transfer, nearly zero ΔT) would correspond to nearly infinite h.

Fig. 30 shows how the profile at 30° before TDC (chosen only because of its distinctive shape) changes with driving frequency. It is clear that the boundary layer thickness is much larger at low frequencies than at high frequencies.

Fig. 31 shows the behavior of the heat transfer coefficient calculated in the program from the ratio of the wall heat flux and the adiabatic plane to wall temperature difference. This coefficient is compared to information published by Overbye (33) which was generated in a motored CFR engine with four piston strokes per data cycle and which required a calculated gas temperature. It is interesting to note that in spite of the difference in engine cycles and in the orders of magnitude of the heat transfer coefficients, they pass to infinity (i.e., the gas - wall temperature difference passes to zero) at nearly the same times and have quite similar shapes. The vertical arrows on the abscissa indicate the infinity asymptotes. The dif-

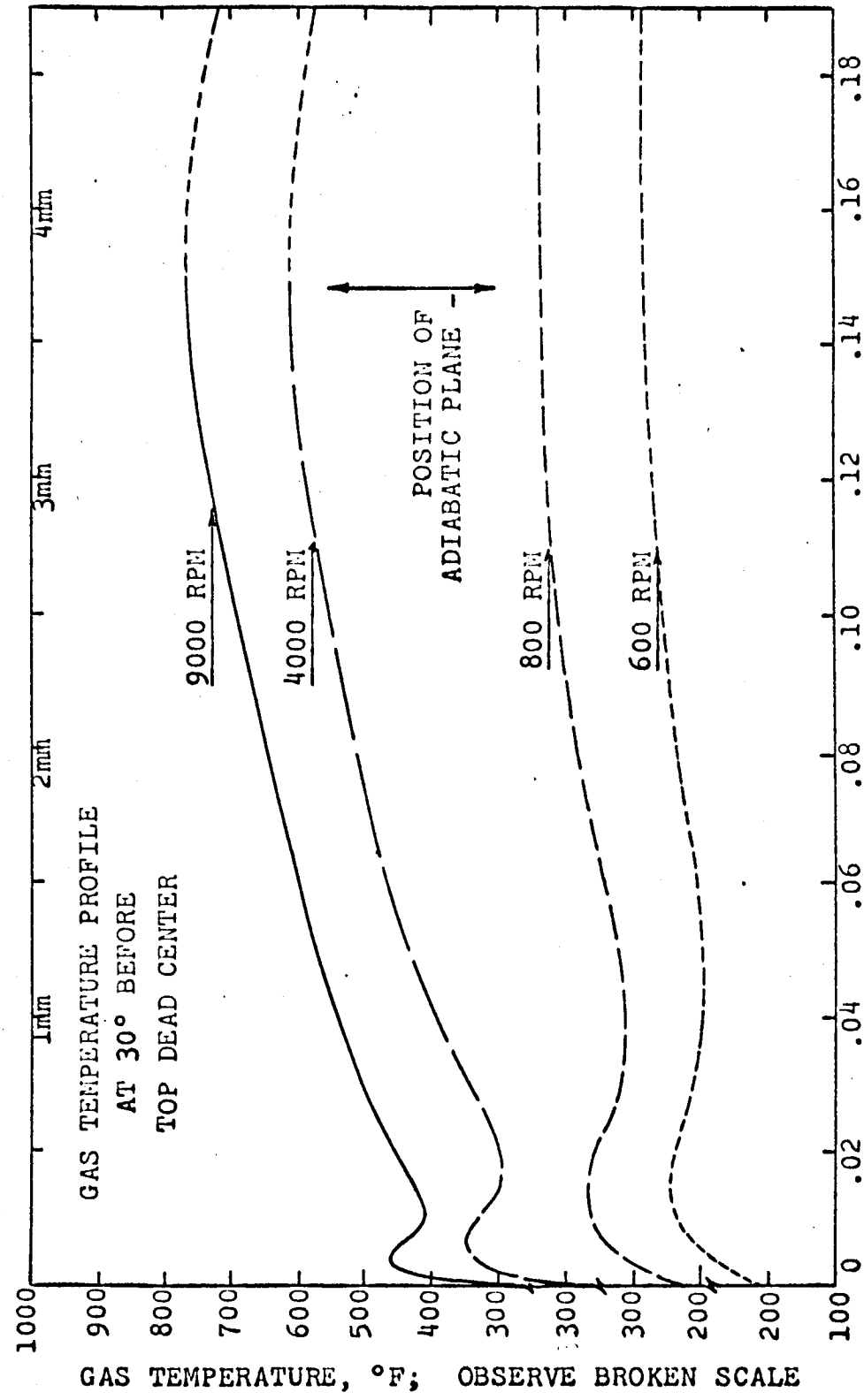
GAS TEMPERATURE PROFILE
AT 30° BEFORE
TOP DEAD CENTER
9000 RPM
4000 RPM
800 RPM
600 RPM
POSITION OF
ADIABATIC PLANE
1mm
2mm
3mm
4mm
1000
900
800
700
600
500
400
300
300
300
200
200
100
0
.02
.04
.06
.08
.10
.12
.14
.16
.18
GAS TEMPERATURE, °F; OBSERVE BROKEN SCALE
DISTANCE INTO THE GAS FROM THE WALL SURFACE, Inches

Fig. 30

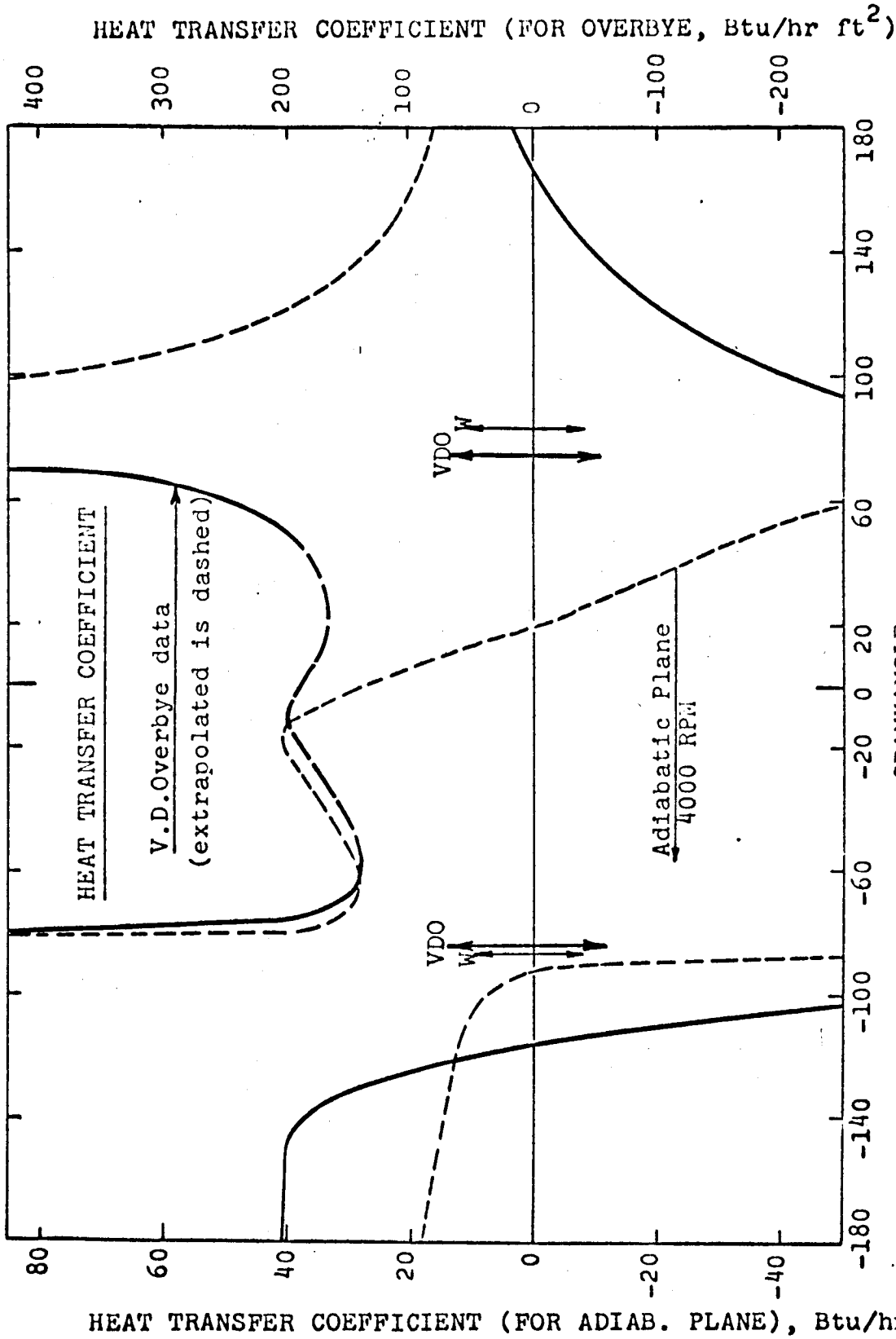
HEAT TRANSFER COEFFICIENT (FOR OVERBYE, Btu/hr ft²)
400
300
200
100
0
-100
-200
180
140
100
60
20
-20
-60
-100
-140
-180
CRANKANGLE
VDO
W
HEAT TRANSFER COEFFICIENT
V.D.Overbye data
(extrapolated is dashed)
Adiabatic Plane
4000 RPM
VDO
W
80
60
40
20
0
-20
-40
HEAT TRANSFER COEFFICIENT (FOR ADIAB. PLANE), Btu/hrft²

Fig. 31

ference in the sign of the histories after +100 crankangle degrees is due to the fact that in the Overbye data, the heat transfer was still from gas to wall at this stage, whereas the model predicts small negative heat transfer.

It is possible to calculate local fluid velocities from the rates of change of location of the laminae in the gas. When this was done, it was found that the velocity profiles from piston to wall were very close to linear for most portions of the calculated cycle. The nonlinearities occurred generally near the wall and were most obvious near TDC and BDC: where the adiabatic plane velocity changed sign precisely at -180° and 0°, the velocity at the center of the first lamina switched sign at -172° and +2° at all frequencies. In the larger portions of the compression and expansion strokes, however, the nonlinearity amounted to a few per cent of the velocity value calculated from the linear assumption.

A bulk-averaged gas temperature could be calculated at any instant in time by integrating the temperature profile in the gas with respect to distance. An easier, but equivalent, method is to use the perfect gas law:

$$T_{bulk} = \frac{P\, V_{total}}{mR} .$$

A comparison of the bulk gas temperature to the adiabatic plane temperature at 4000 rpm is presented in Fig. 32. The

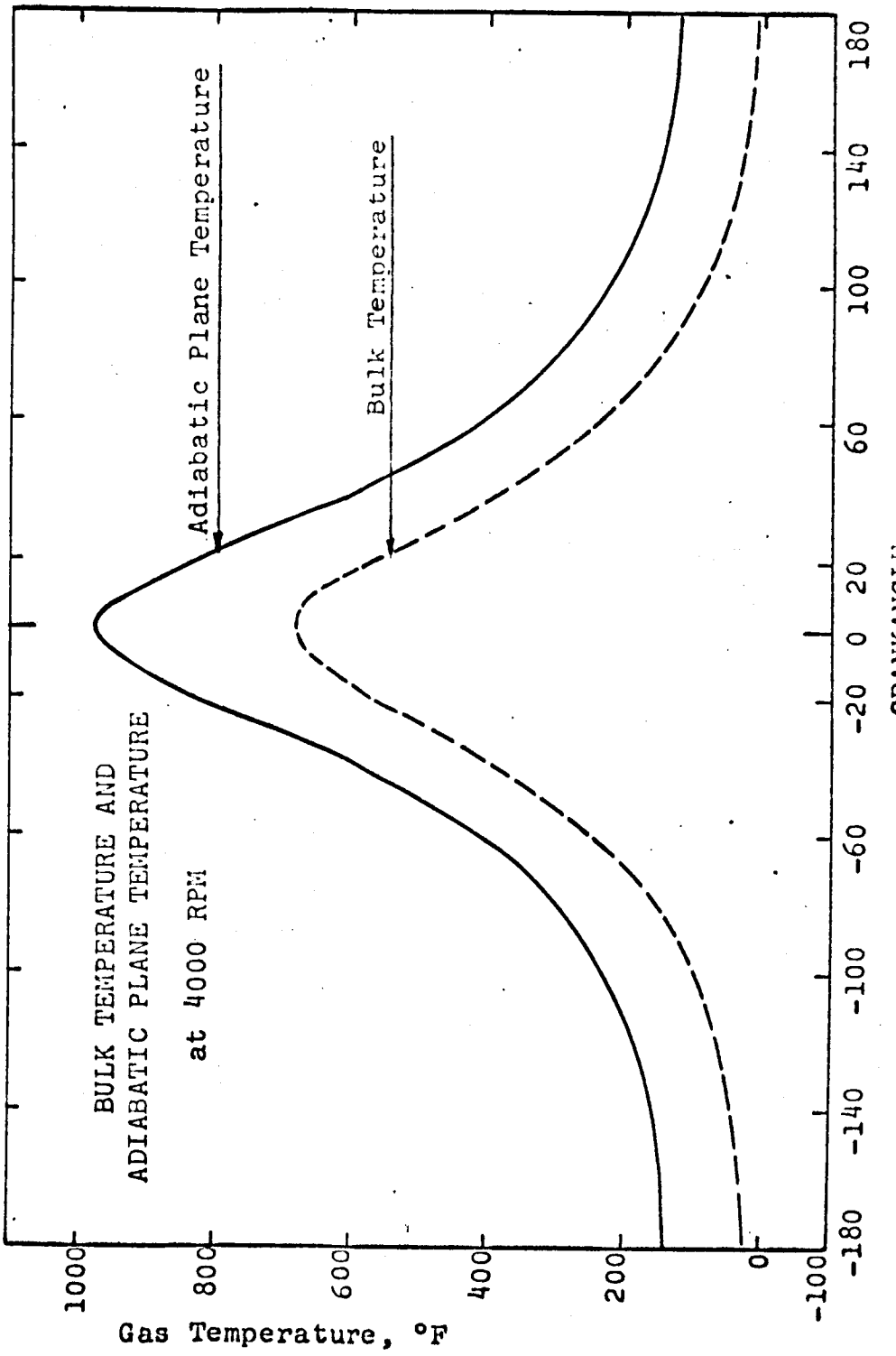
BULK TEMPERATURE AND
ADIABATIC PLANE TEMPERATURE
at 4000 RPM
Adiabatic Plane Temperature
Bulk Temperature
Gas Temperature, °F
1000
800
600
400
200
0
-100
-180
-140
-100
-60
-20
0
20
60
100
140
180
CRANKANGLE

Fig. 32

bulk temperature is seen to be consistently below the adiabatic plane temperature.

Since a heat transfer coefficient is generally applied to a bulk gas - wall temperature difference, a coefficient history can be calculated for the cycle from the relationship

$$h_{\text{adiabatic plane model}} = \dot{q}_{\text{wall}}/(T_{\text{bulk}} - T_{\text{wall}}).$$

For purposes of comparison, the Eichelberg coefficient can also be calculated from the driving frequency and the pressure and bulk gas temperature histories. These coefficients are compared in Fig. 33.

A comparison of the several approaches to wall heat transfer is presented in Fig. 34. The adiabatic plane model heat transfer is seen to agree quite well with the experimental heat flux with regard to phasing and shape. The Eichelberg heat transfer maximum is 12 degrees late and the negative heat transfer portion of the cycle is poorly simulated.

Finally, Fig. 35 shows the polytropic coefficient histories for the Nth volume (next to the adiabatic plane). These coefficients were calculated at time j from the data at time j-1 with the relationship:

$$n_N(j) = 1/[1-(\log[T_N(j)/T_N(j-1)]/\log[P(j)/P(j-1)])].$$

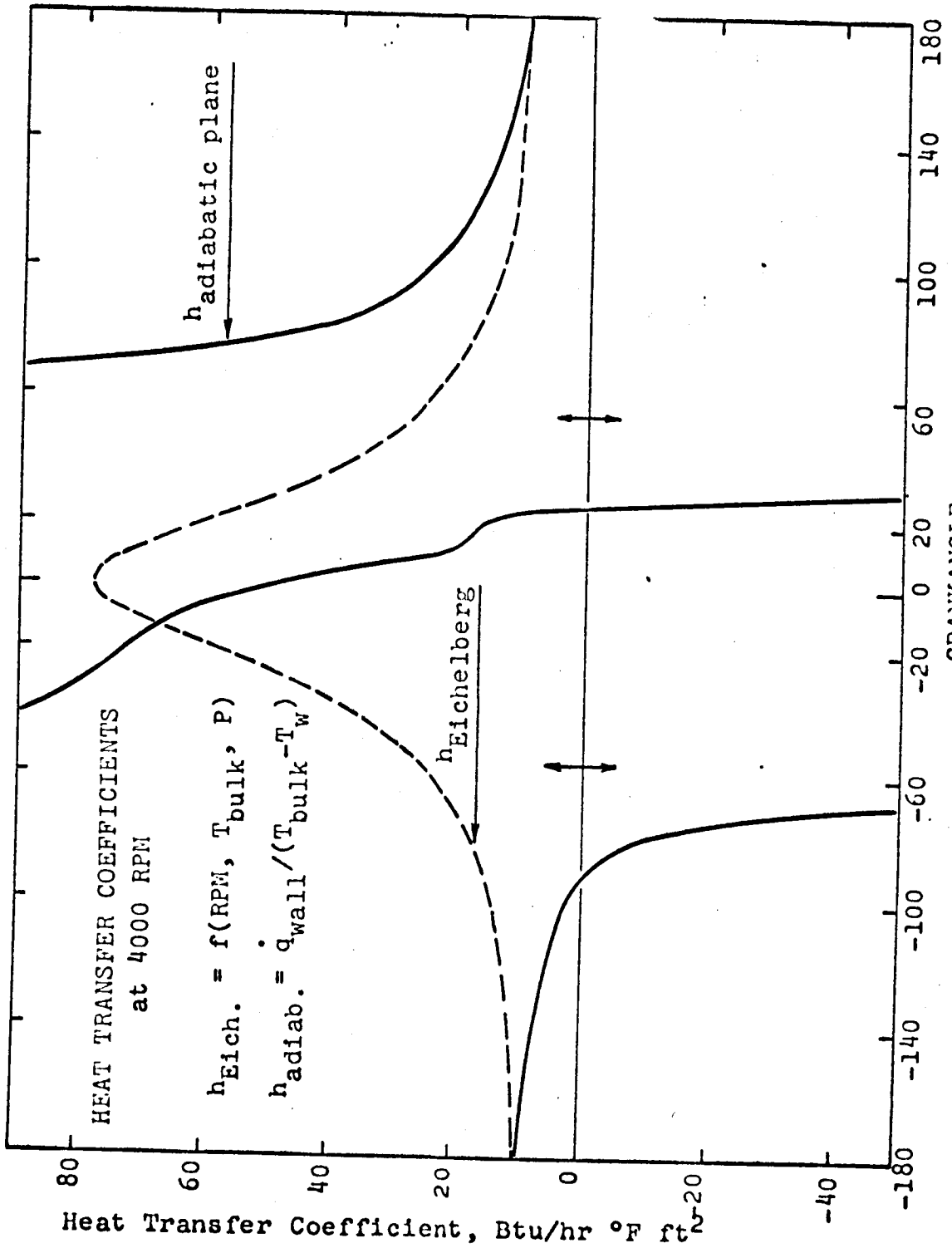
HEAT TRANSFER COEFFICIENTS
at 4000 RPM
$h_{Eich.} = f(RPM, T_{bulk}, P)$
$h_{adiab.} = \dot{q}_{wall}/(T_{bulk}-T_w)$
$h_{adiabatic\ plane}$
$h_{Eichelberg}$
Heat Transfer Coefficient, Btu/hr °F ft²
80
60
40
20
0
-20
-40
-180
-140
-100
-60
-20
0
20
60
100
140
180
CRANKANGLE

Fig. 33

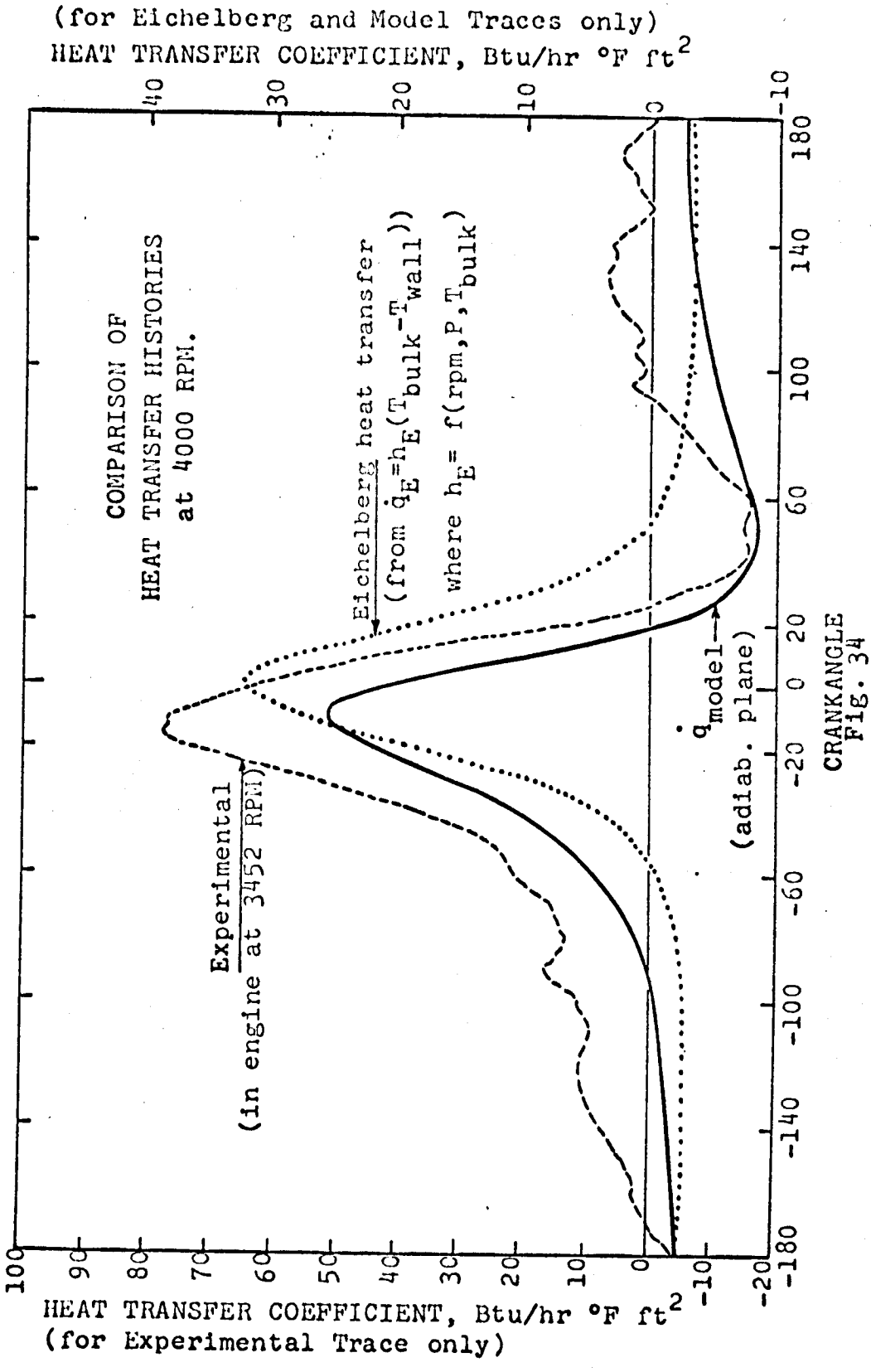
(for Eichelberg and Model Traces only)
HEAT TRANSFER COEFFICIENT, Btu/hr °F ft²
COMPARISON OF
HEAT TRANSFER HISTORIES
at 4000 RPM.
Eichelberg heat transfer
(from $\dot{q}_E = h_E(T_{bulk} - T_{wall})$)
where $h_E = f(rpm, P, T_{bulk})$
Experimental
(in engine at 3452 RPM)
$\dot{q}_{model}$
(adiab. plane)
CRANKANGLE
Fig. 34
HEAT TRANSFER COEFFICIENT, Btu/hr °F ft²
(for Experimental Trace only)

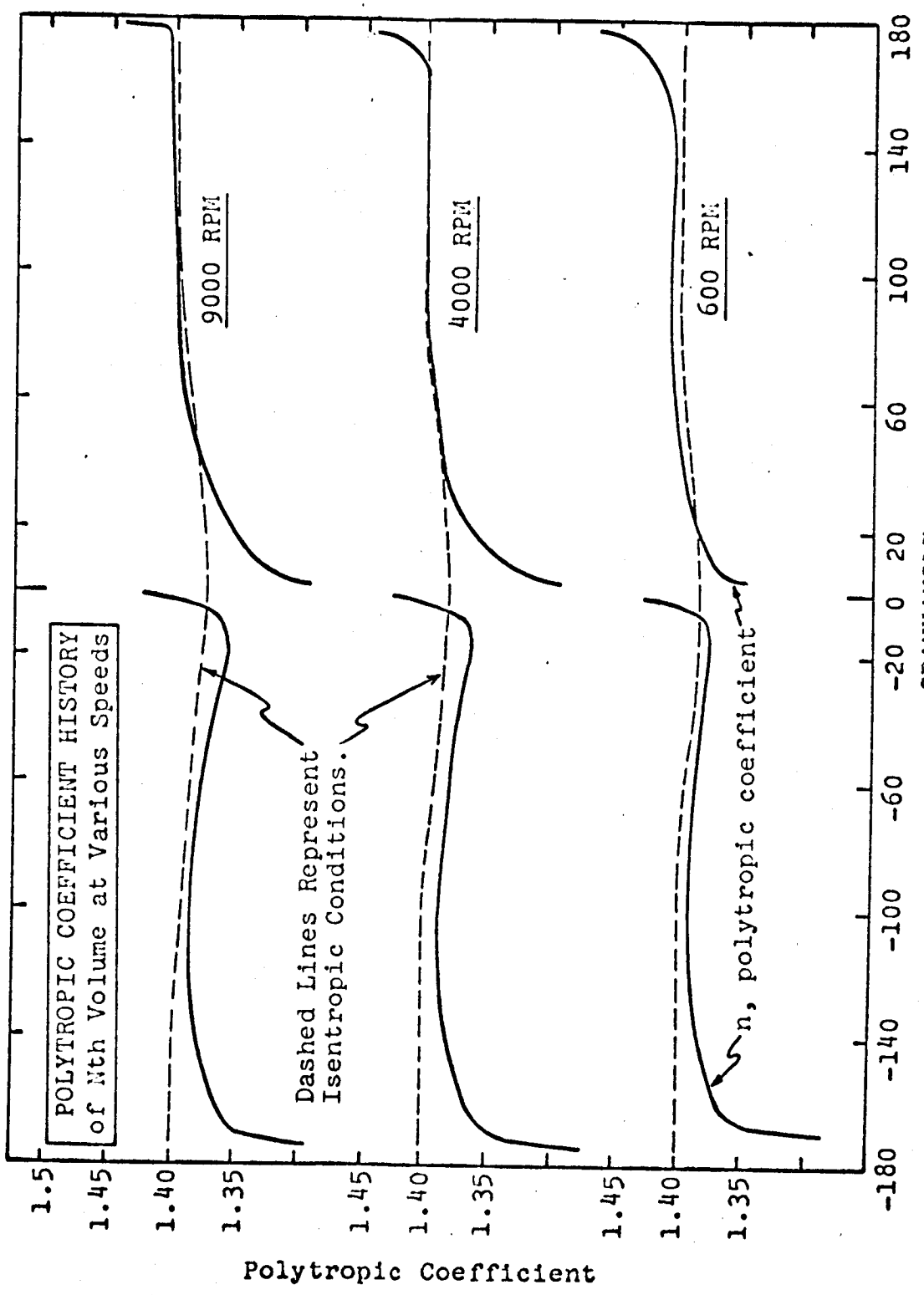
POLYTROPIC COEFFICIENT HISTORY
of Nth Volume at Various Speeds
9000 RPM
4000 RPM
600 RPM
Dashed Lines Represent
Isentropic Conditions.
n, polytropic coefficient
Polytropic Coefficient
1.5
1.45
1.40
1.35
-180
-140
-100
-60
-20
0
20
60
100
140
180
CRANKANGLE

Fig. 35

The coefficient for the Nth element is seen to be close to isentropic throughout the cycle for all speeds except near BDC and TDC (i.e., ±180°, 0°). The anomalous behavior at these points is probably due to the effect of the step nature of the calculation at the points of zero rate of change of the variables.

It was hoped that a generalized correlation could be developed for the prediction of accurate heat transfer histories from relatively simple engineering data: mean wall surface temperature, bulk gas history, and Eichelberg coefficient. Much effort was expended toward this goal. However, the variable histories did not have an easily expressed frequency dependence. The surface heat flux maximum and minimum occurred at the same crankangle position over the frequency range, but the crankangle times at which the difference ($T_{bulk} - T_{wall}$) passed through zero changed with frequency. As a consequence, the $\pm\infty$ asymptotes of the film coefficient were frequency-sensitive; the film coefficient could not be expressed as a simple function of frequency, wall temperature, and instantaneous bulk properties.

In conclusion, this model for the working fluid is preferred over the so-called secondary models, in that it proceeds from basic thermodynamic principles, is guided by a few simple assumptions, and contains little or no empirical data. It is interesting to note, however, that many of the empirical estimations used in earlier models agree

reasonably well with the calculated behavior of this model, and the output data (primarily the wall surface heat flux history shapes and phasing) of the Simulation Transient Model, the Variable h Resistive Model, and this Adiabatic Plane Model are in fairly good agreement.

The Adiabatic Plane Model output is in very close agreement with the high frequency experimental data with respect to phasing and the dependent variables' history shapes, although the variable amplitudes are slightly smaller, probably because of the influence of friction and makeup air in the experimental system. The program for the model, although presently rather expensive in terms of computation time, is very flexible. An interested investigator with sufficient time could modify it to:

1) study the effect of working fluid properties on heat transfer;
2) include time-dependent energy generation in the different laminae to simulate combustion or dissociation;
3) include the effects of viscous dissipation;
4) include time-dependent terms for gas - cylinder wall energy exchange and piston friction energy dissipation; and
5) compute the head surface temperature history from the surface heat flux history (as Fig. 27 , calculated in program with constant surface temperature);

insert time-dependent wall temperature as new boundary condition and rerun program. Comparison of wall heat flux histories would provide a measure of "feedback" from wall surface to gas.

IX. DISCUSSION OF RESULTS AND CONCLUSIONS

Experimental bulk gas temperature histories are given in Appendix A. As the driving frequency increases from 10 to 60 Hz, the crankangle location of the gas temperature maximum shifts from -2.5 to -1.5 crankangle degrees before top dead center, probably because of a phase lag introduced by the resistance wire (see Section VII. A.). The gas temperature swing increases from about 560°F to about 630°F. The histories remain approximately symmetric about the TDC ordinate line.

As the driving frequency increased from 10 Hz to nearly 60 Hz, the swing of the experimentally measured gas temperature increased from 560 to 630°F. By comparison, the Adiabatic Plane Model amplitudes increased from 625 to 850°F from 10 to 67 Hz. This amplitude difference can be attributed partially to an unknown and uncalculable attenuation of the resistance wire transducer due to thermal inertia and thermal resistance in the wire's own boundary layer, and partially to a slight mismatch of the Adiabatic Plane Model to the actual physical system (including, as previously noted, viscous energy dissipation and makeup and blowby air). None of these factors are very well understood quantitatively; however, small inaccuracies in the gas temperature amplitude have little effect on the qualitative side of the observations. The great difficulties in ob-

taining even a poor local gas temperature history were noted in a previous section.

Experimental bulk gas temperature ratios (maximum/minimum) ranged from 2.113 at 15.25 Hz to 2.188 at 57.53 Hz. Adiabatic Plane Model gas temperature ratios (bulk averaged gas temperature) were 2.350 at 13.3 Hz and 2.380 at 66.7 Hz; these ratios are somewhat higher than the experimental ratios because the model minimum temperature was somewhat low (because the mass in the tabulated example was guessed lower than the experimental mass--hence the compression process of the equilibrium cycle began at a low gas temperature and pressure).

Gas pressure histories are also found in Appendix A. The history shape, amplitude, and location of maximum are essentially independent of driving frequency: the amplitude remains at about 360 or 365 psi, and the maximum occurs at -2.5 crankangle degrees before TDC over the frequency range 10 to 60 Hz.

The gas pressure histories predicted by the Adiabatic Plane Model are almost identical to their experimental counterparts; the history shapes are much alike and the maxima occur at a few tenths of a crankangle degree before TDC. The amplitudes predicted by the model are low with respect to the experimental amplitudes because the mass assumed in the tabulated example is low. A later computer run of the

model with a higher system mass (or, equivalently, a more reasonable gas pressure at BDC of the equilibrium cycle) predicted gas pressure amplitudes close to the experimental values.

The Adiabatic Plane Model pressure ratios (maximum/minimum) were in the range of 24 to 25 on all runs. The experimental ratios ranged from 23.9 at 15.25 Hz to 30.5 at 57.53 Hz. The latter were subject to perhaps 10% scatter, however, because of resolution problems: an error of 1% in the minimum pressure (say 3.7 psi at 14 psi) causes a large change in the pressure ratio (from 26.9 to 33.4). Pressure ratio is not, therefore, the best of parameters by which to describe these pressure histories; pressure swing might be better.

The experimental surface temperature histories can be found in Appendix A. Fig. 13 is a summary of surface temperature and surface heat flux histories, and with Fig. A1 for a lower frequency constitutes the best illustration for the following discussion. The data of Fig. A1 were not included in the summary figure, because gas properties were not measured during this run; the runs of Fig. 13 represent complete data sets. Fig. 14 shows the locus of the surface temperature maxima with driving frequency, and will also be helpful.

At low frequencies, the predominate characteristic of the

experimental surface temperature history is seen in essence in Fig. A1: the history is relatively smooth and nearly sinusoidal, peaking at +55 crankangle degrees at 9.65 Hz. As driving frequency decreases, the so-called "hump" shifts closer to the gas temperature maximum (near TDC, or zero crankangle degrees); no experimental recordings were made at less than 9.65 Hz, but at frequencies less than, say, 1 Hz, the gas temperature and wall surface temperature histories should be nearly in phase. As the frequency increases to 15 or 16 Hz, the peak shifts later in time (to +66 degrees at 15.25 Hz, for example). Above this frequency, the late "hump" degenerates in amplitude and a second peak begins to emerge at TDC (refer to Fig. 14). At frequencies greater than about 25 Hz the "central" peak predominates. Above 33 Hz, the late peak is hardly discernible and the surface temperature histories are somewhat peaked and nearly symmetric about the TDC ordinate line.

These trends are reflected in the experimental heat flux histories of Fig. 13 (with Fig. A1 for 9.65 Hz). At very low frequencies the heat flux histories are also roughly sinusoidal, leading the surface temperature by some 20 or 25 crankangle degrees. As the frequency increases the two heat flux "humps" separate, the late hump growing smaller, the central peak growing and leading the surface temperature maximum by about 17 degrees. At 57.53 Hz, the late hump in heat flux is quite small. The high frequency ex-

perimental heat flux histories are very much like those predicted by the Adiabatic Plane Model in Fig. 27.

This is not the first occasion on which this type of behavior in surface temperature or surface heat flux has been observed. T. LeFeuvre (80), working at the University of Wisconsin, used a surface thermocouple to measure instantaneous head surface temperatures in a diesel engine under both motored and fired conditions. The single-cylinder research diesel engine had a compression ratio of 15:1 and a swirl ratio of about 2 (i.e., the working fluid swirls, or rotates, twice inside the compression chamber during one revolution of the crankshaft. Since this was a four-stroke cycle device, two revolutions of the crankshaft represent one cycle of the system). Under certain conditions LeFeuvre obtained surface temperature histories with two maxima remarkably like those previously presented (at about 16 to 20 Hz). Fig. 36 is from an oscillograph record of LeFeuvre's observations. Most of the "hash," or high frequency signal, on the temperature trace is probably aerodynamic in origin, since it was closely reproducible from cycle to cycle (particularly in the motored case), and probably represented regular patterns of air motion.

A.Chu (81) reported unpublished work done at Cummins Diesel Company. Investigators used a computer program to simulate the thermodynamic state of a 17:1 compression ratio motored diesel engine with low gas swirl. Unsmoothed

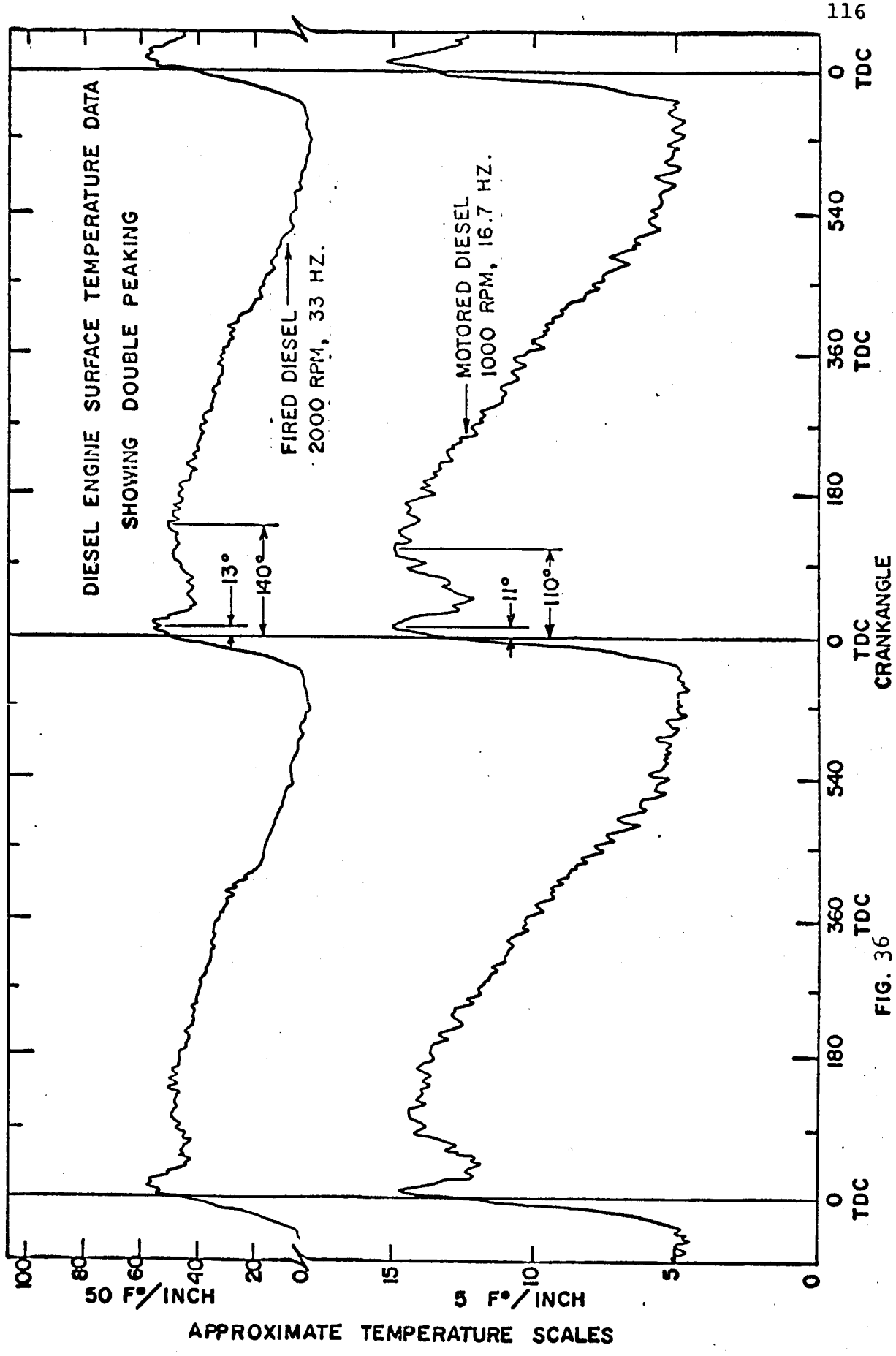
DIESEL ENGINE SURFACE TEMPERATURE DATA
SHOWING DOUBLE PEAKING
FIRED DIESEL
2000 RPM, 33 HZ.
13°
140°
MOTORED DIESEL
1000 RPM, 16.7 HZ.
11°
110°
0 TDC
180
360 TDC
540
0 TDC CRANKANGLE
100
80
60
40
20
0
50 F°/INCH
15
10
5
0
5 F°/INCH
APPROXIMATE TEMPERATURE SCALES

FIG. 36

experimental gas pressure histories were used to compute bulk gas temperature histories; the Annand heat transfer coefficient was used to represent the thermal resistance, but other details of the model used for the boundary layer were not specified. At 1500 rpm (25 Hz) the computed head heat flux history had a double peak, one at about zero crankangle degrees, the other quite late in the cycle. By 2100 rpm (35 Hz) the history had resolved to the expected peak at about TDC. No further information was available on these observations. Chu also reported encountering an experimentally measured head temperature history showing the double humping phenomenon.

It is difficult, if not impossible, to construct a single theoretical model predicting both the high frequency and the low frequency experimental behavior of the thermal boundary layer. Some modelling can be done, however, if the regions are considered separately.

In the experimental observations at frequencies greater than about 25 Hz (see Fig. 14), the central peak is the strong feature of the surface temperature history; peaking at about zero crankangle degrees (i.e., the top dead center position of the piston), the surface temperature lags the gas temperature by only two or three degrees. The surface heat transfer histories associated with these surface temperature histories led the surface temperature by about six crankangle degrees and had the characteristic shape described

in Fig. 14. The Adiabatic Plane Model did a good job in predicting the high frequency heat transfer in that the shape and the phasing of the wall surface flux histories were quite close to their experimental counterparts.

The low frequency surface temperature observations are more troublesome to understand. The RC model for the gas-wall interface, which is explained in detail in the author's thesis, assumes that the thermal boundary layer is relatively thick (four millimeters on the average) and that pressure work exerts no influence in the boundary layer. This model will account for the low frequency (up to about 20 Hz) surface temperature and heat flux histories. However, as this model does not represent a smooth transition from a theoretical treatment of the energy equation to a mathematical representation of the energy fluxes in the boundary layer, and is a rather after-the-fact construction, it is not presented in this report.

The significance of the transition region (i.e., 18 to 30 Hz), in which the surface temperature history has two maxima, is unknown. It suffices to say that other investigators have observed this phenomenon and have offered no explanation for it.

Finally, at this point we can summarize the important thoughts scattered in various places in this text on the relationship of surface heat transfer response to the gas

pressure and temperature driving functions. The lag or lead of surface heat transfer at the surface of a fuel droplet with respect to variations of pressure and/or temperature with time is a crucial factor in determining whether increased vaporization of the droplet will support or oppose the amplitude of the variations. The magnitude of this lag or lead is dependent upon, among other things, the properties of the gas and the wall, and the harmonic distribution of the pressure and temperature oscillations.

We can focus our thoughts by "constructing" a gas in the one-dimensional space between a plane wall surface and a bulk gas "driver" which is undergoing large periodic excursions in pressure and temperature. If we begin by hypothesizing a gas with no heat capacity and an invariant pressure, but only a thermal conductivity (which can be thought of as indicating only a thermal resistance between wall and driver gas), the driving potential for heat transfer $[T_{gas}(t) - T_{wall}(t)]$ and the conductivity of the gas (or the reciprocal resistance) will maximize at approximately the same time as the "driver" temperature. As a consequence, the surface heat transfer will be almost exactly in phase with the temperature and pressure of the driving gas. The obvious analog is a resistive electrical circuit. The comparable model in this work is the Variable h Resistive Model, and as expected, the heat transfer peaks right in phase with the gas temperature (and with the gas-to-wall temperature dif-

ference) at about -1 crankangle degree.

If, still keeping the pressure constant, we add to the gas a finite heat capacity, the heat flux and temperature variations of the surface are delayed with respect to the temperature variations of the bulk gas driver: when the driving temperature is rising, the capacity causes the interface gas to act as an energy absorber, decreasing the energy flux to the surface. When the temperature falls, the interface gas releases the energy. The net result is a lag, or delay in the peaking of the surface temperature and heat flux with respect to the driving gas temperature. The RC Model in this work examined this phenomenon by varying the mean value and the amplitude of the heat capacity of the interface gas while keeping the mean value and the amplitude of the thermal conductivity the same. As an example, in a computer run at 915 rpm (15.25 Hz) with a Nu_δ of 15 and a mean boundary layer thickness of 4.6 mm, the heat flux peaked at 40 degrees <u>after</u> TDC (or 42 degrees <u>after</u> the bulk gas temperature). When the heat capacity was decreased to zero, the heat flux shifted and became exactly in phase with the bulk gas temperature again.

When the pressure of the interface gas is forced to vary with time (and essentially in phase with the bulk gas temperature), the pressure work in the interface gas leads the bulk gas temperature and pressure variations. The phase of the heat transfer with respect to the bulk gas tempera-

ture variations is then determined by the relative magnitudes of the pressure work and the capacitive energy storage. In the experimental measurements with air, the heat flux peaked at about 8.5 crankangle degrees before TDC (about six degrees before the bulk gas temperature and pressure). In the Simulation Transient Model, the heat flux peaked at about 6 to 10 degrees before TDC. In the Adiabatic Plane representation, the heat transfer led the bulk gas temperature and pressure by 9 or 10 crankangle degrees. These phase relationships are illustrated in the sketch below, which is not to scale.

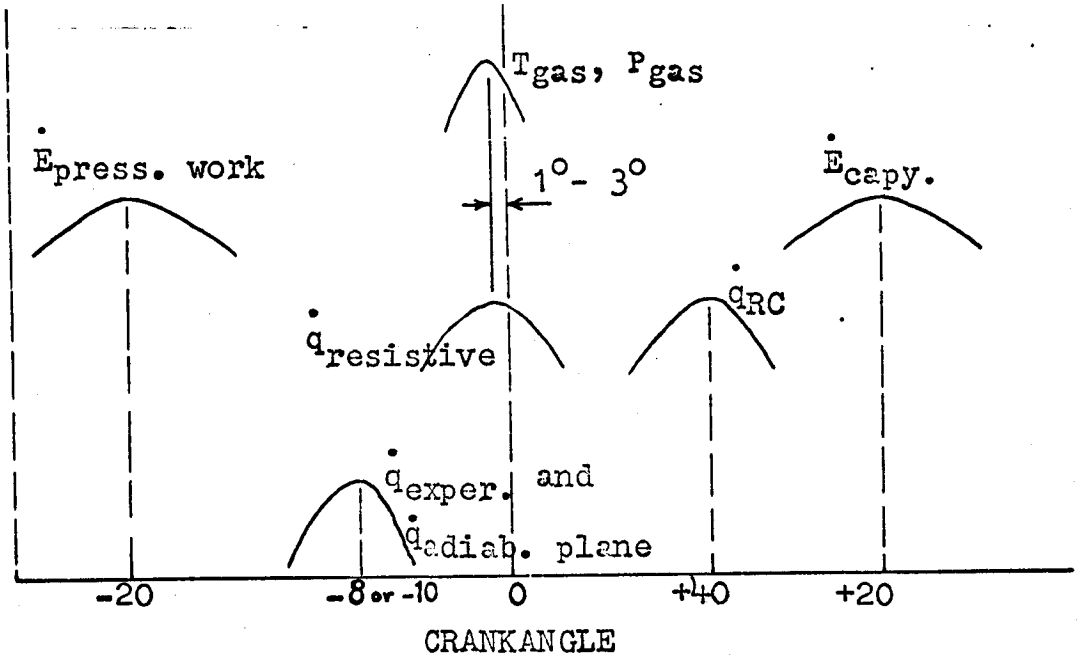

Thus, the "leading" effect of pressure work slightly more than offsets the "lagging" effect of gas capacity. It is apparent that pressure work is an important factor in de-

termining the phase relationship of the heat transfer to the "bulk gas" oscillations.

In summary, the following statements can be made from the experimental and theoretical observations:

1) Above about 30 Hz (to about 60 Hz experimentally and to at least 150 Hz analytically) the wall surface temperature lags the bulk gas temperature by only 2 or 3 crankangle degrees (.03 to .05 radians) and the gas pressure by 1 or 2 degrees (.02 to .03 radians).
2) The surface heat transfer rate leads the surface temperature by about 10 crankangle degrees.
3) The surface temperature history shape or amplitude do not change appreciably above 30 Hz.
4) The amplitude of the heat flux history increases regularly with frequency, from 52,400 Btu/hr ft^2 at 25.21 Hz to 93,900 Btu/hr ft^2 at 57.53 Hz.
5) For frequencies above about 30 Hz, a simple resistance model of the boundary layer (with a time-varying resistance based on a "reasonable" internal heat transfer coefficient) gives a satisfactory first order prediction of the thermal response of the wall to a gas-side temperature disturbance. The Adiabatic Plane Model, which does not require such an assumed coefficient, does an even better job.

6) For frequencies below about 20 Hz, the RC Model can predict the phase lag of the surface temperature with respect to the gas temperature.

7) The heat transfer coefficient h, calculated from the ratio of $q_{surface}$ and $(T_{gas} - T_{wall})$, assumes negative, zero, and infinite values, and as such is of questionable utility in accurately describing the instantaneous surface heat flux.

8) Among the models developed, the Adiabatic Plane Model, based almost entirely on fundamental thermodynamics, provides the best qualitative model for unsteady heat transfer between a plane surface of a solid and a gas experiencing pressure and temperature fluctuations.

APPENDIX A

GRAPHS OF EXPERIMENTAL DATA

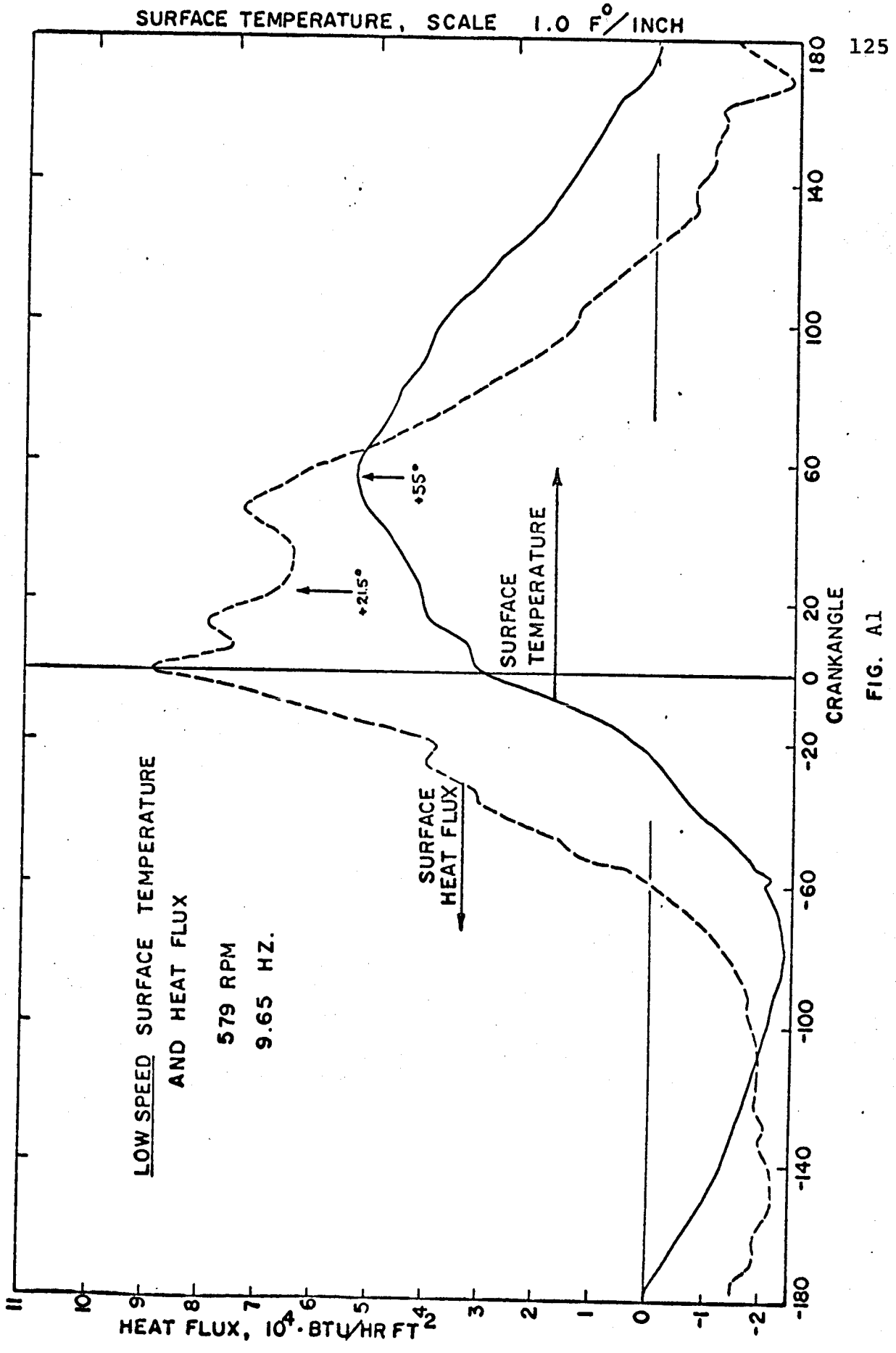
SURFACE TEMPERATURE, SCALE 1.0 F°/INCH
LOW SPEED SURFACE TEMPERATURE AND HEAT FLUX
579 RPM
9.65 HZ.
+21.5°
+55°
SURFACE TEMPERATURE
SURFACE HEAT FLUX
HEAT FLUX, 10^4 · BTU/HR FT^2
CRANKANGLE
180
140
100
60
20
0
-20
-60
-100
-140
-180
11
10
9
8
7
6
5
4
3
2
1
0
-1
-2

FIG. A1

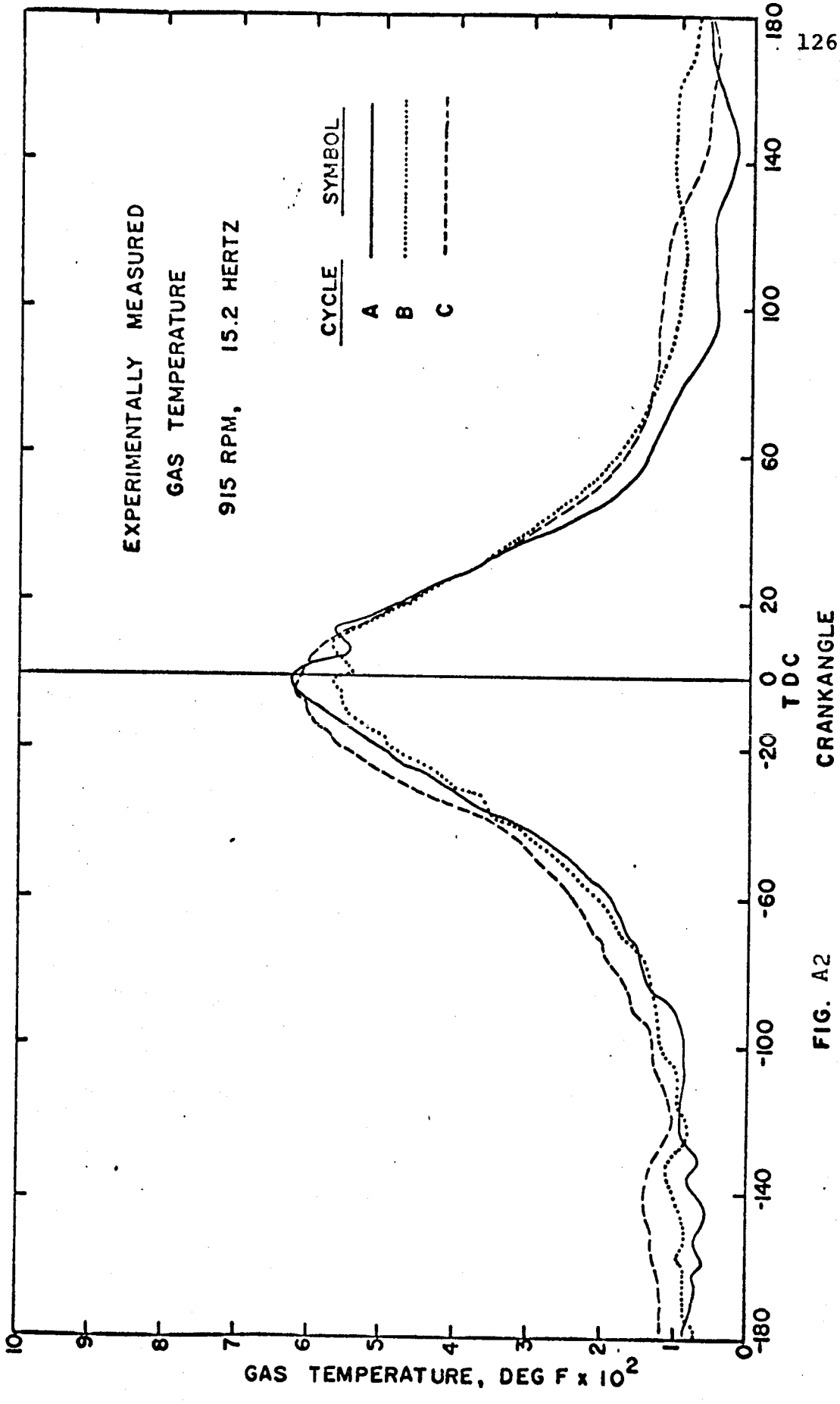
EXPERIMENTALLY MEASURED
GAS TEMPERATURE
915 RPM, 15.2 HERTZ
CYCLE SYMBOL
A
B
C
GAS TEMPERATURE, DEG F x 10²
CRANKANGLE
TDC
0
-20
-60
-100
-140
-180
20
60
100
140
180
1
2
3
4
5
6
7
8
9
10

FIG. A2

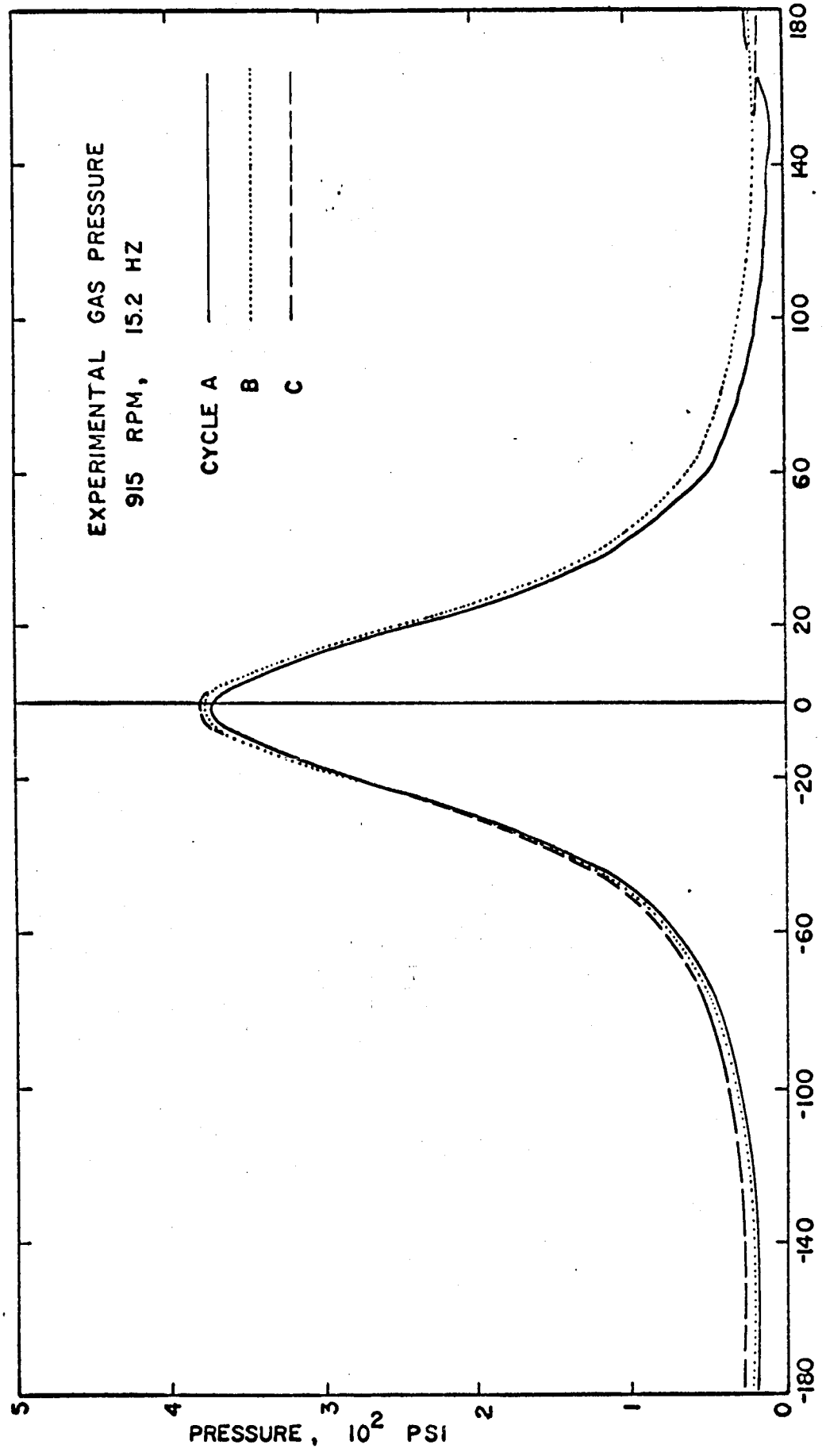
EXPERIMENTAL GAS PRESSURE
915 RPM, 15.2 HZ
CYCLE A
B
C
PRESSURE, 10^2 PSI
CRANKANGLE
5
4
3
2
1
0
180
140
100
60
20
0
-20
-60
-100
-140
-180

FIG. A3

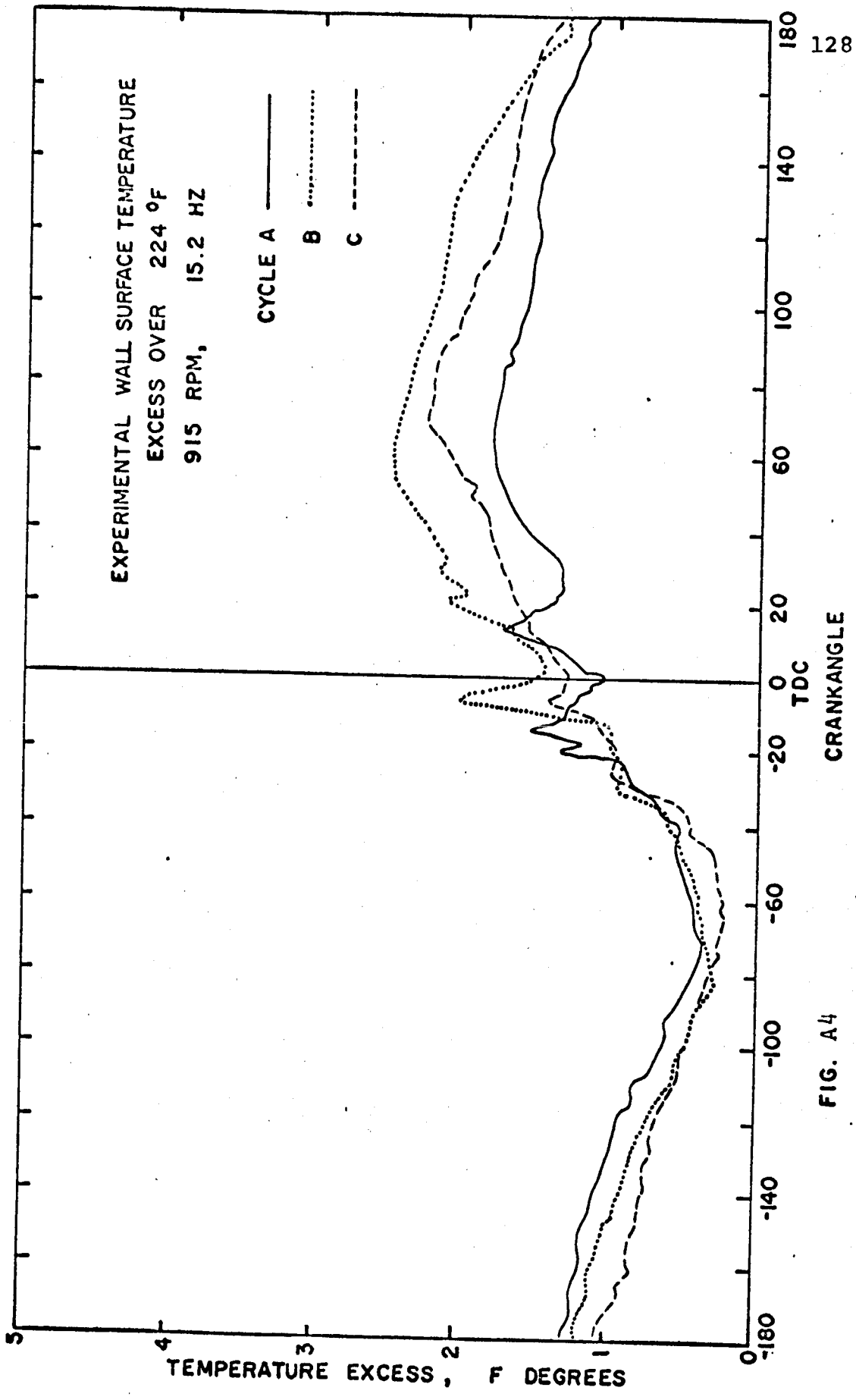
EXPERIMENTAL WALL SURFACE TEMPERATURE
EXCESS OVER 224 °F
915 RPM, 15.2 HZ
CYCLE A
B
C
TEMPERATURE EXCESS, F DEGREES
CRANKANGLE
TDC
180
140
100
60
20
-20
-60
-100
-140
-180
0
1
2
3
4
5

FIG. A4

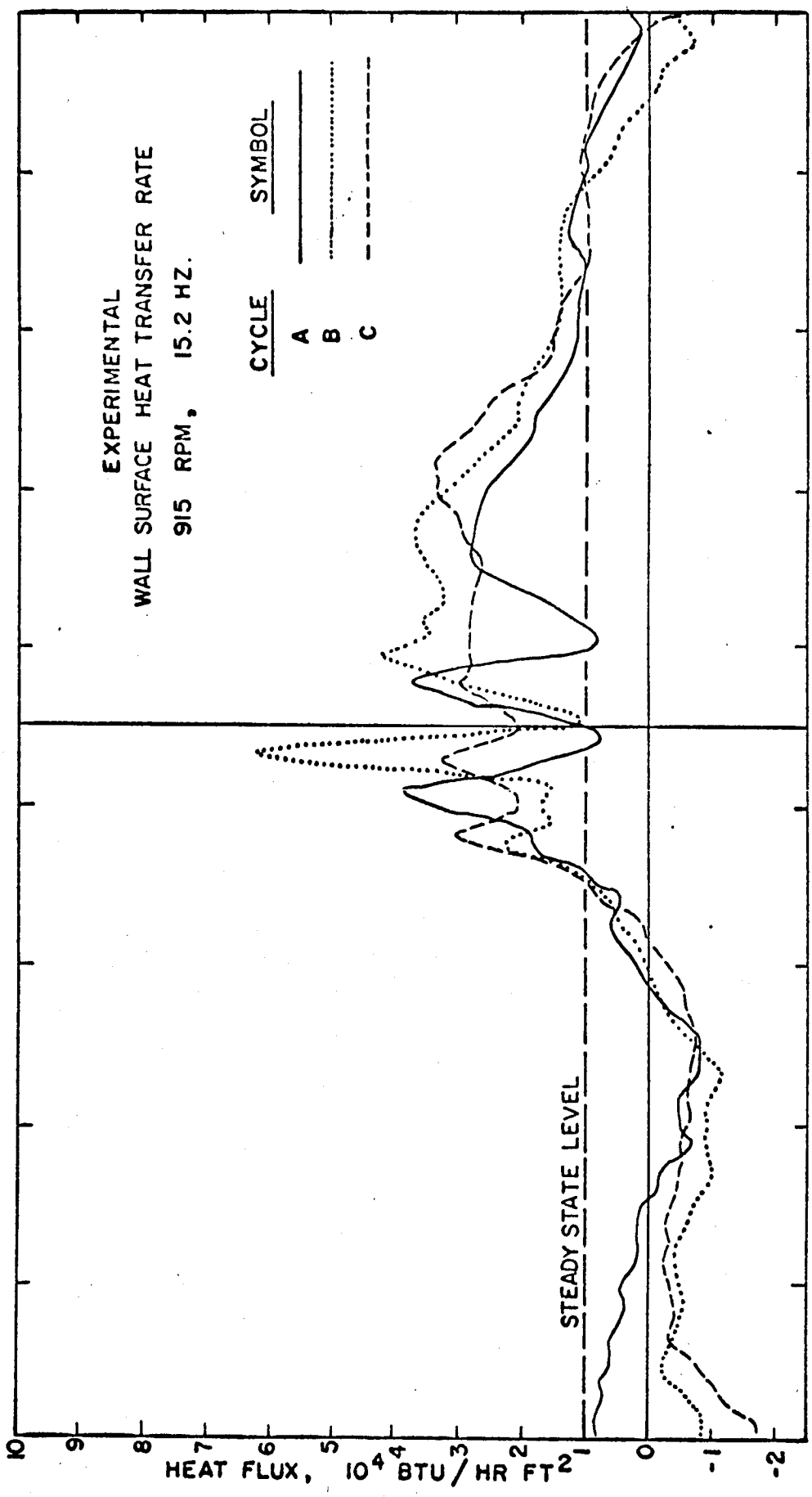
EXPERIMENTAL
WALL SURFACE HEAT TRANSFER RATE
915 RPM, 15.2 HZ.
CYCLE SYMBOL
A
B
C
STEADY STATE LEVEL
HEAT FLUX, 10^4 BTU/HR FT^2
CRANKANGLE
10
9
8
7
6
5
4
3
2
1
0
-1
-2
180
140
100
60
20
0
-20
-60
-100
-140
-180

FIG. A5

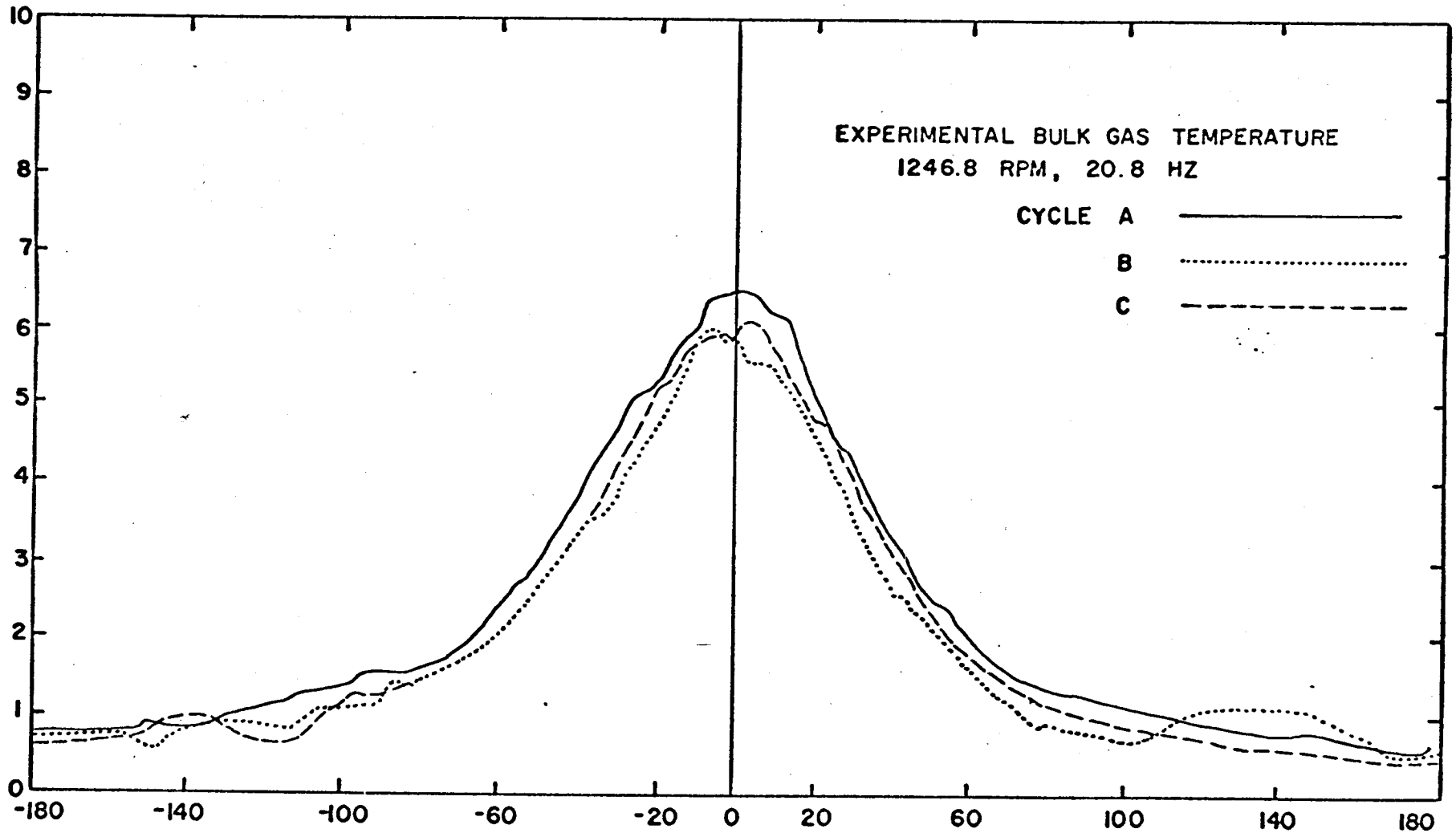
EXPERIMENTAL BULK GAS TEMPERATURE
1246.8 RPM, 20.8 HZ
CYCLE A
B
C
10
9
8
7
6
5
4
3
2
1
0
-180
-140
-100
-60
-20
0
20
60
100
140
180
CRANKANGLE, T.D.C. = 0

FIG. A6

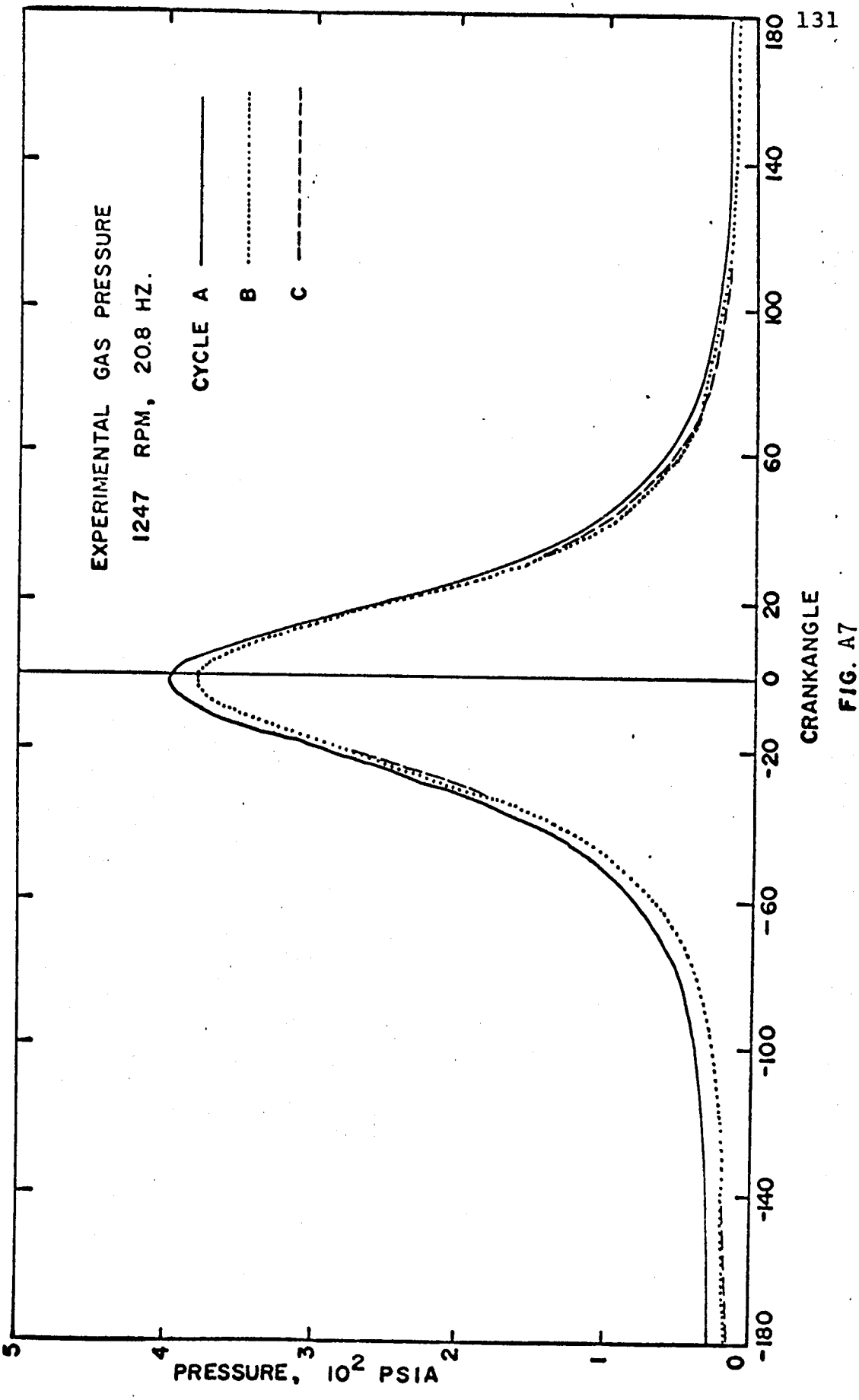
EXPERIMENTAL GAS PRESSURE
1247 RPM, 20.8 HZ.
CYCLE A
B
C
PRESSURE, 10^2 PSIA
CRANKANGLE
5
4
3
2
1
0
180
140
100
60
20
0
-20
-60
-100
-140
-180

FIG. A7

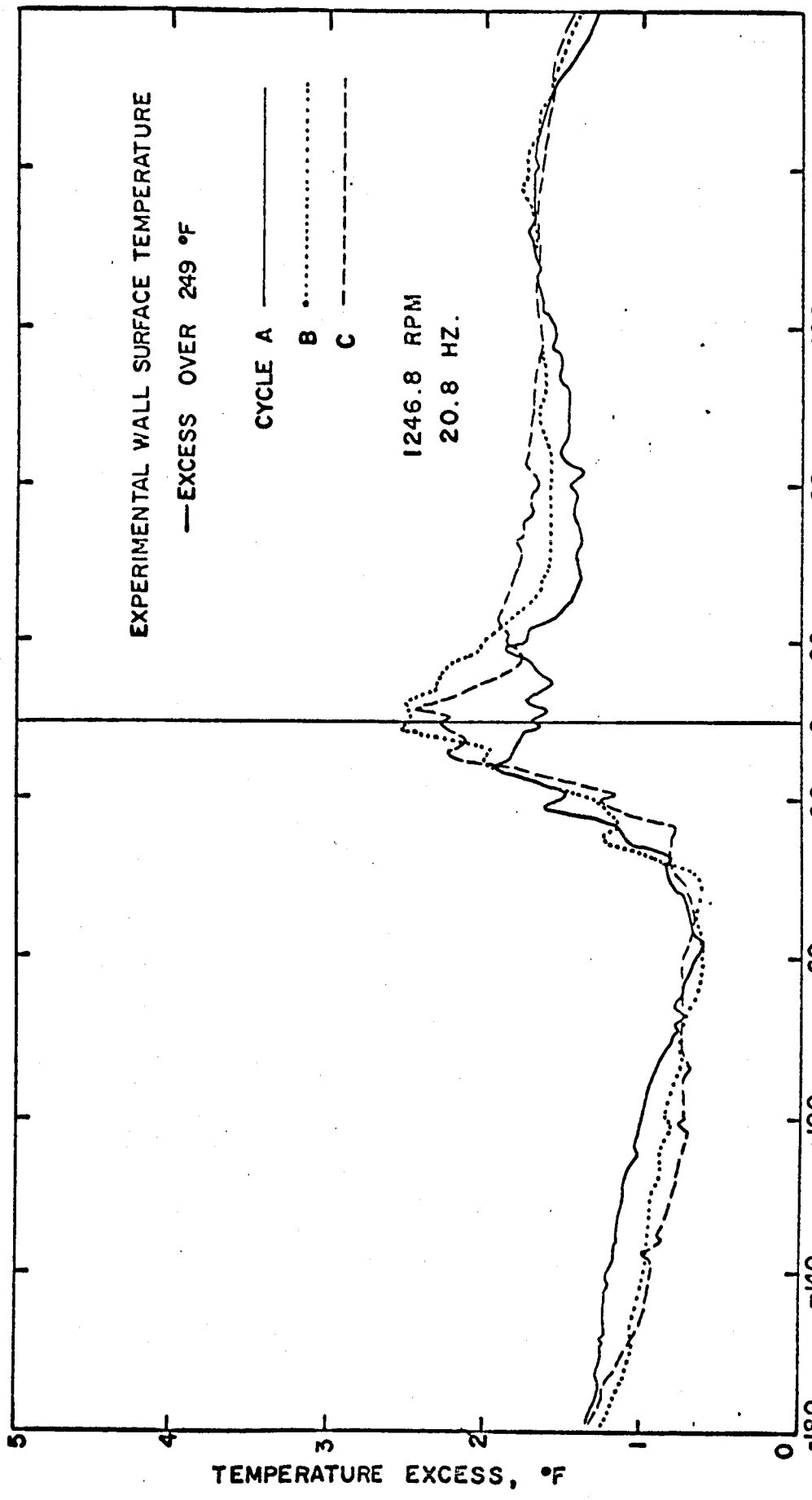
EXPERIMENTAL WALL SURFACE TEMPERATURE
—EXCESS OVER 249 °F
CYCLE A
B
C
1246.8 RPM
20.8 HZ.
TEMPERATURE EXCESS, °F
CRANKANGLE
0
1
2
3
4
5
-180
-140
-100
-60
-20
0
20
60
100
140
180

FIG. A8

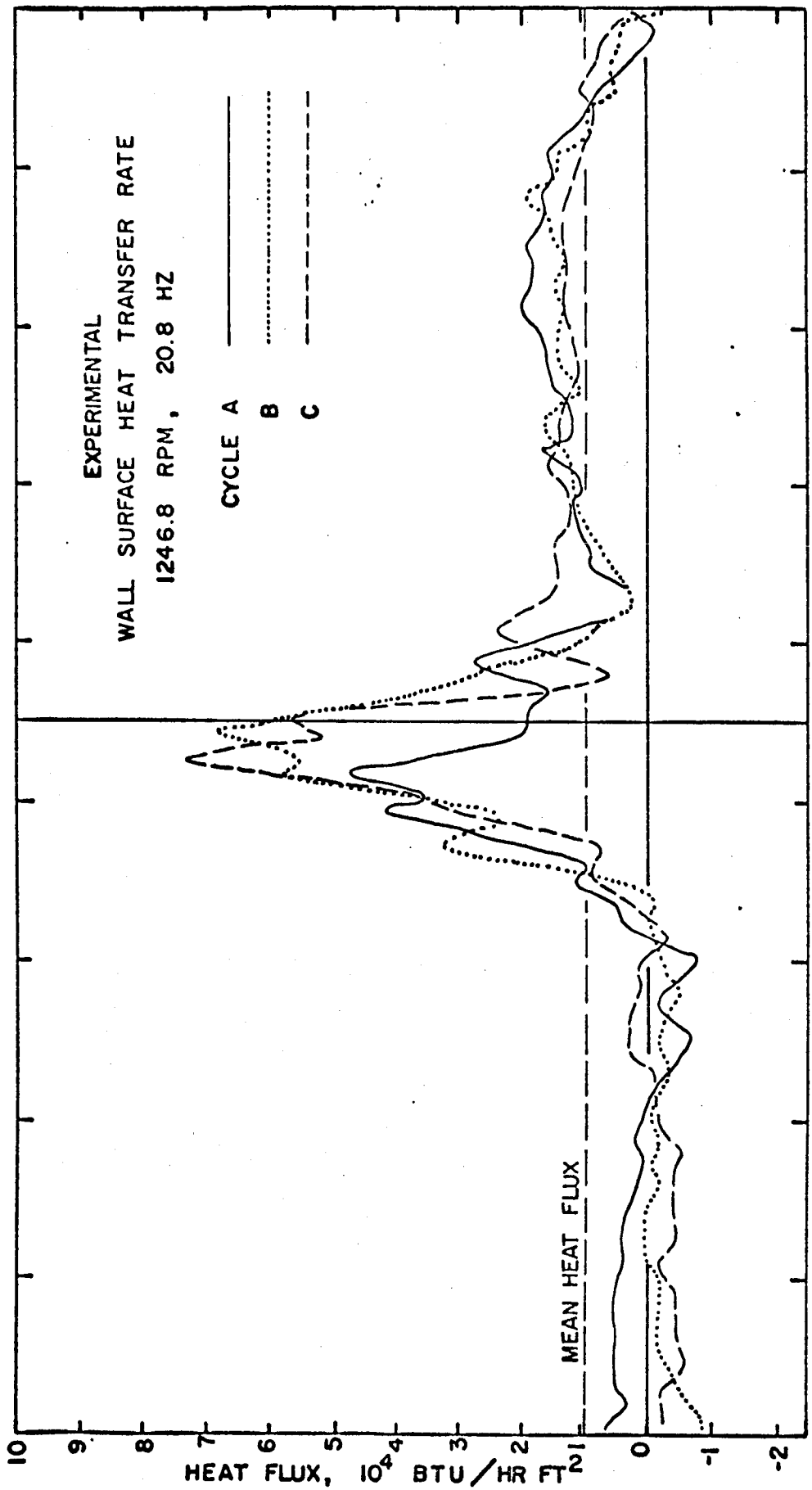
EXPERIMENTAL
WALL SURFACE HEAT TRANSFER RATE
1246.8 RPM, 20.8 HZ
CYCLE A
B
C
MEAN HEAT FLUX
HEAT FLUX, 10^4 BTU/HR FT^2
CRANKANGLE
10
9
8
7
6
5
4
3
2
1
0
-1
-2
180
140
100
60
20
0
-20
-60
-100
-140
-180

FIG. A9

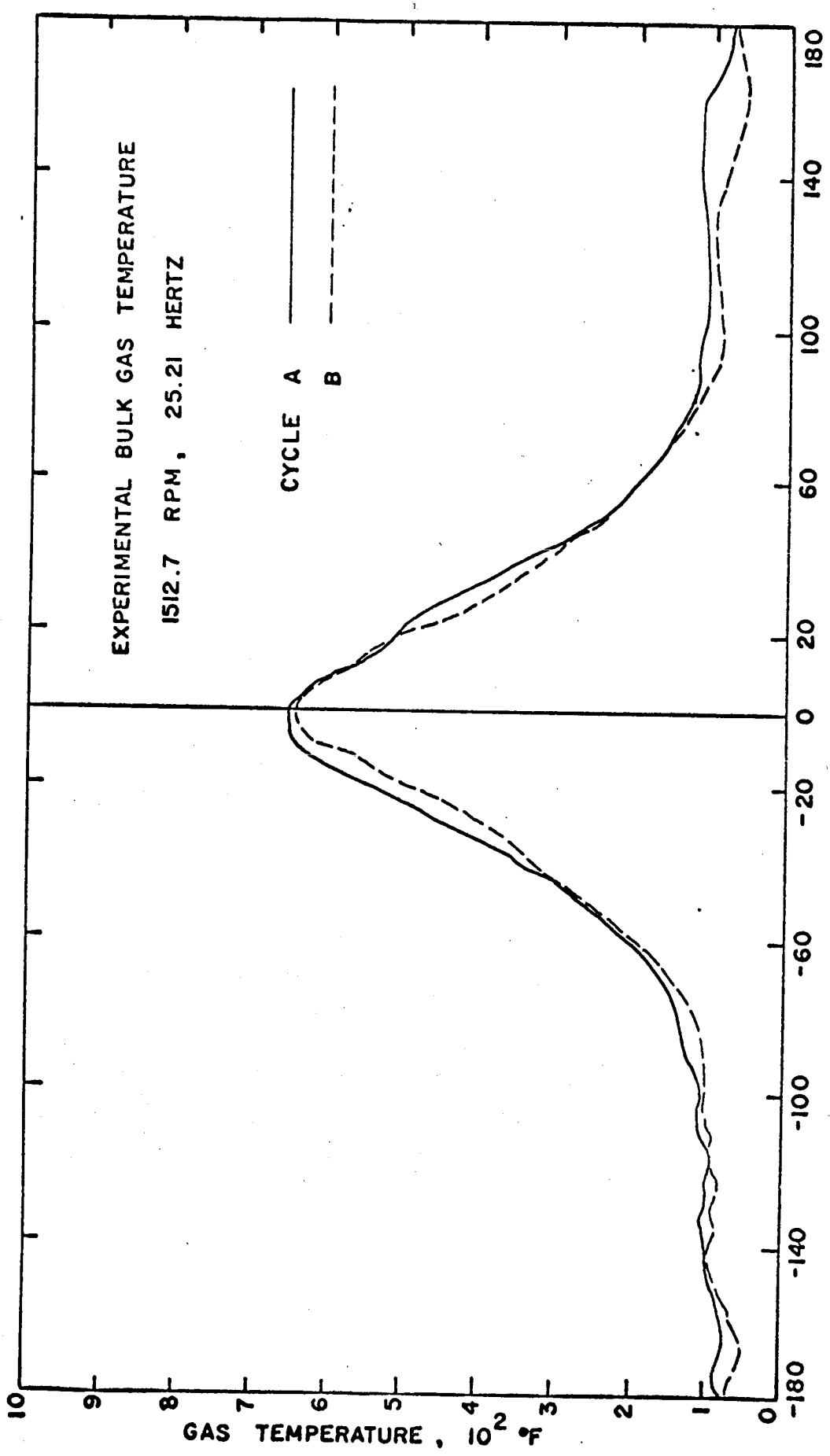
EXPERIMENTAL BULK GAS TEMPERATURE
1512.7 RPM, 25.21 HERTZ
CYCLE A
B
GAS TEMPERATURE, 10^2 °F
CRANKANGLE
10
9
8
7
6
5
4
3
2
1
0
-180
-140
-100
-60
-20
0
20
60
100
140
180

FIG. A10

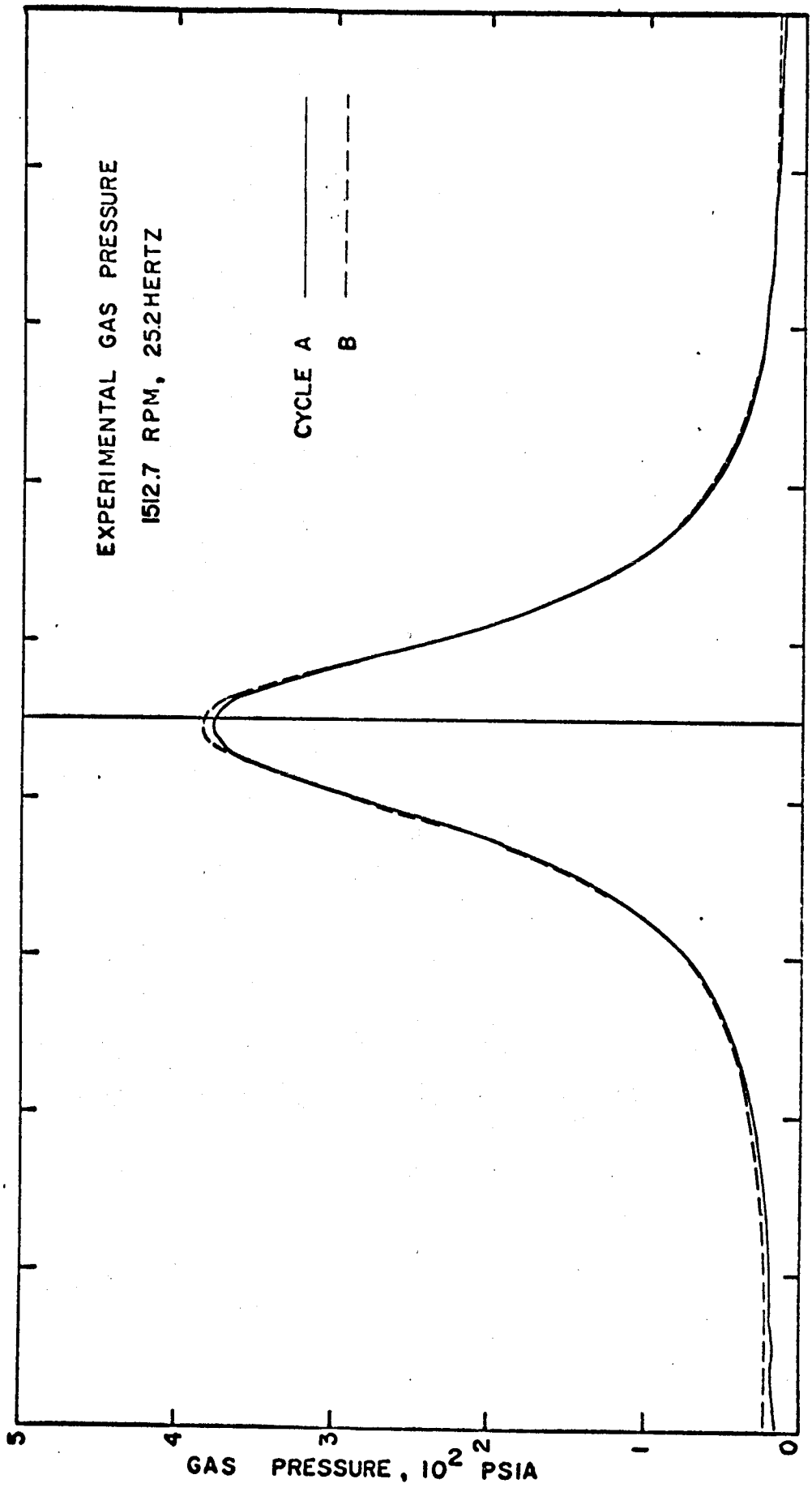
EXPERIMENTAL GAS PRESSURE
1512.7 RPM, 25.2HERTZ
CYCLE A
B
GAS PRESSURE, 10^2 PSIA
CRANKANGLE
5
4
3
2
1
0
-180
-140
-100
-60
-20
0
20
60
100
140
180

FIG. A11

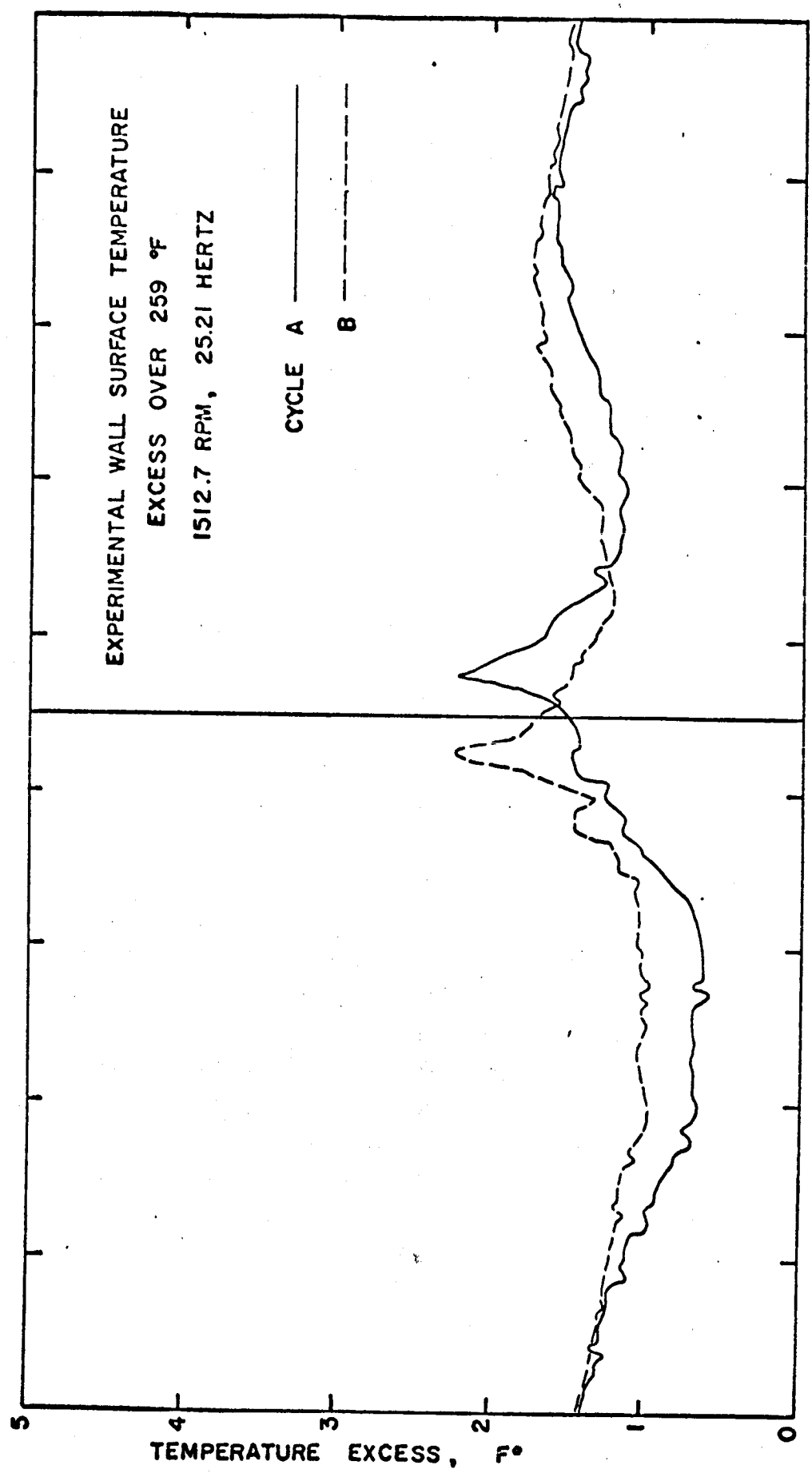
EXPERIMENTAL WALL SURFACE TEMPERATURE
EXCESS OVER 259 °F
1512.7 RPM, 25.21 HERTZ
CYCLE A
B
TEMPERATURE EXCESS, F°
CRANKANGLE
5
4
3
2
1
0
180
140
100
60
20
0
-20
-60
-100
-140
-180

FIG. A12

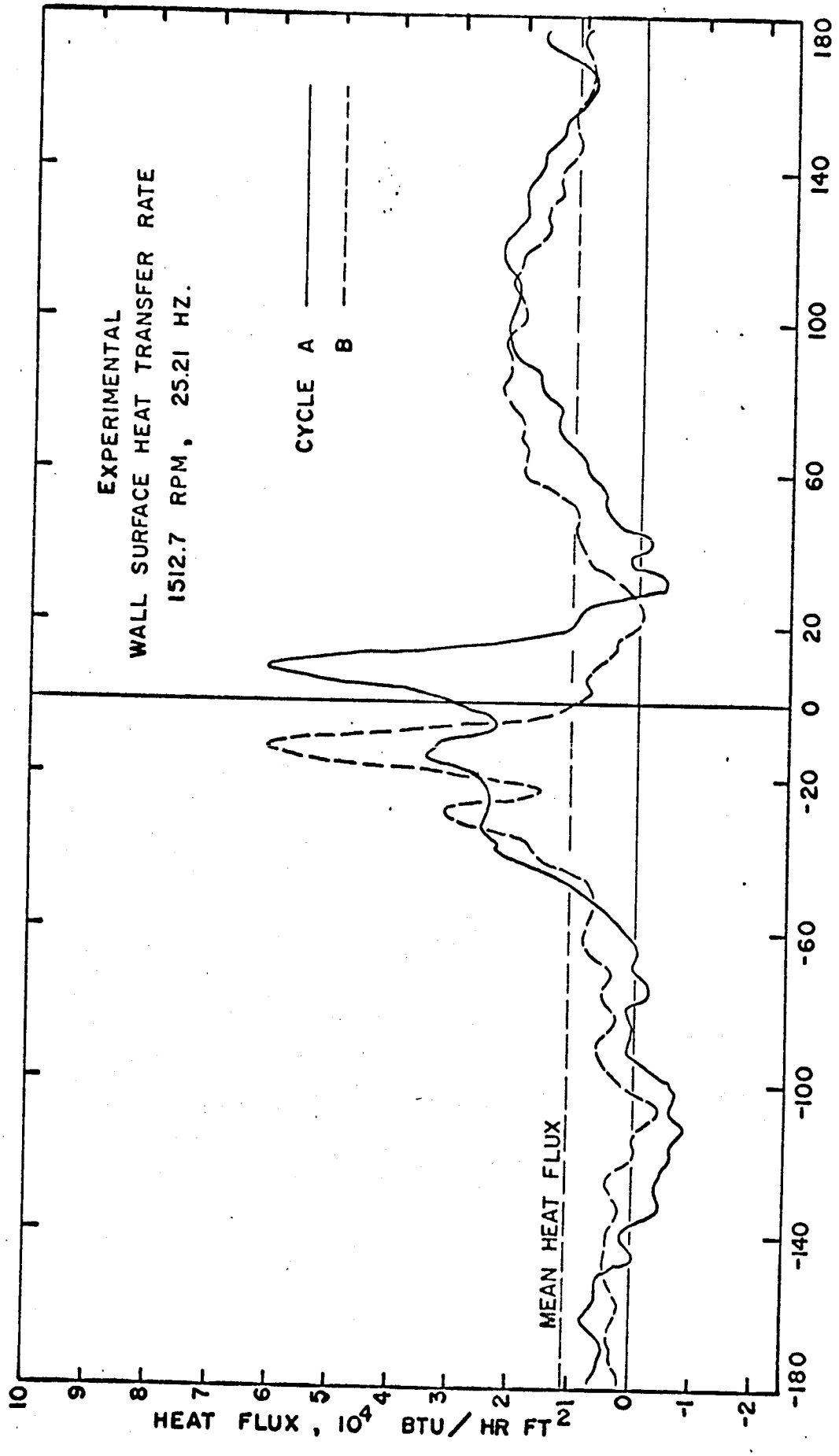
EXPERIMENTAL
WALL SURFACE HEAT TRANSFER RATE
1512.7 RPM, 25.21 HZ.
CYCLE A
B
MEAN HEAT FLUX
HEAT FLUX, 10^4 BTU/HR FT^2
CRANKANGLE
10
9
8
7
6
5
4
3
2
1
0
-1
-2
180
140
100
60
20
0
-20
-60
-100
-140
-180

FIG. A13

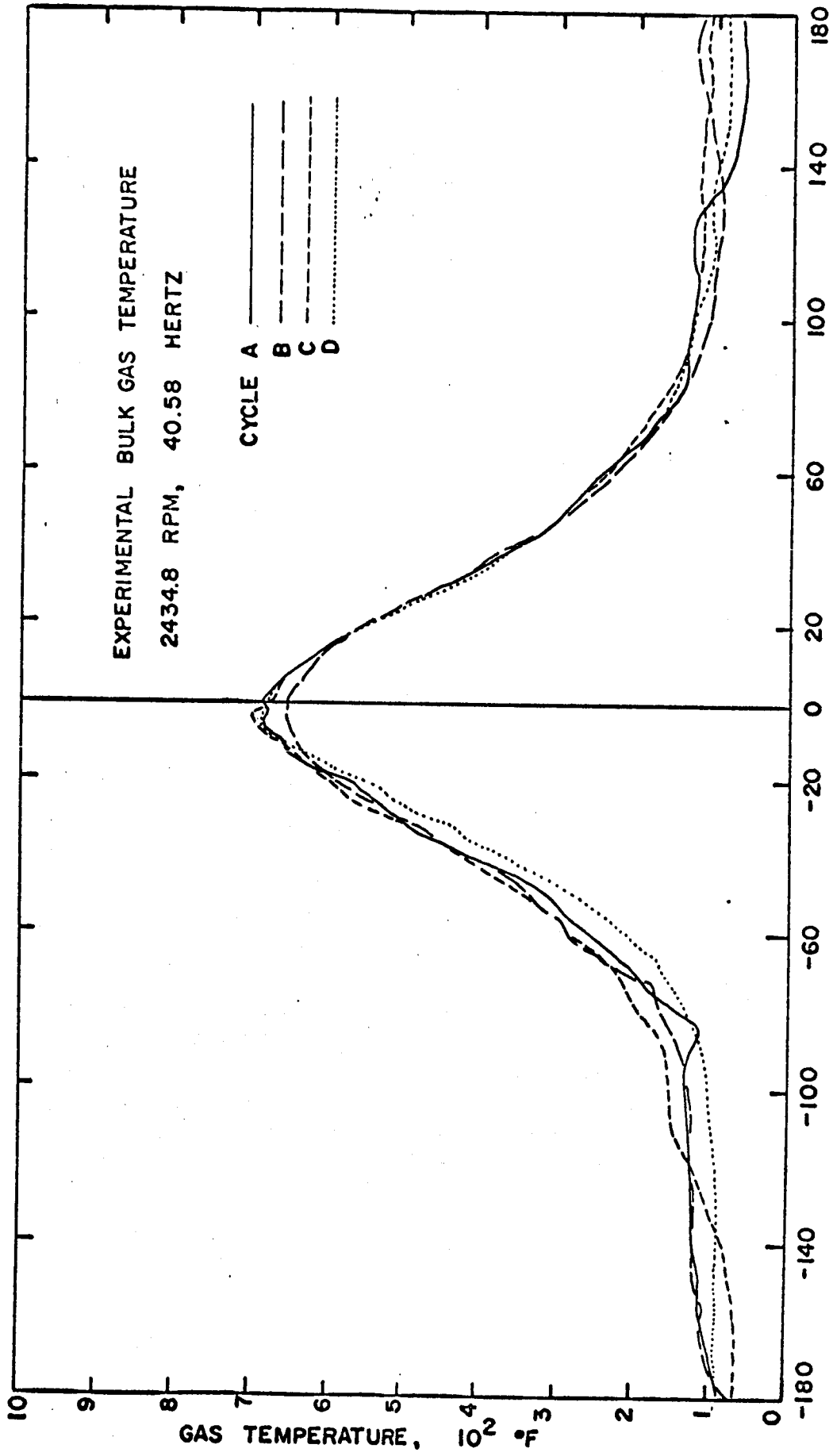
EXPERIMENTAL BULK GAS TEMPERATURE
2434.8 RPM, 40.58 HERTZ
CYCLE A
B
C
D
GAS TEMPERATURE, 10^2 °F
CRANKANGLE
10
9
8
7
6
5
4
3
2
1
0
-180
-140
-100
-60
-20
0
20
60
100
140
180

FIG. A14

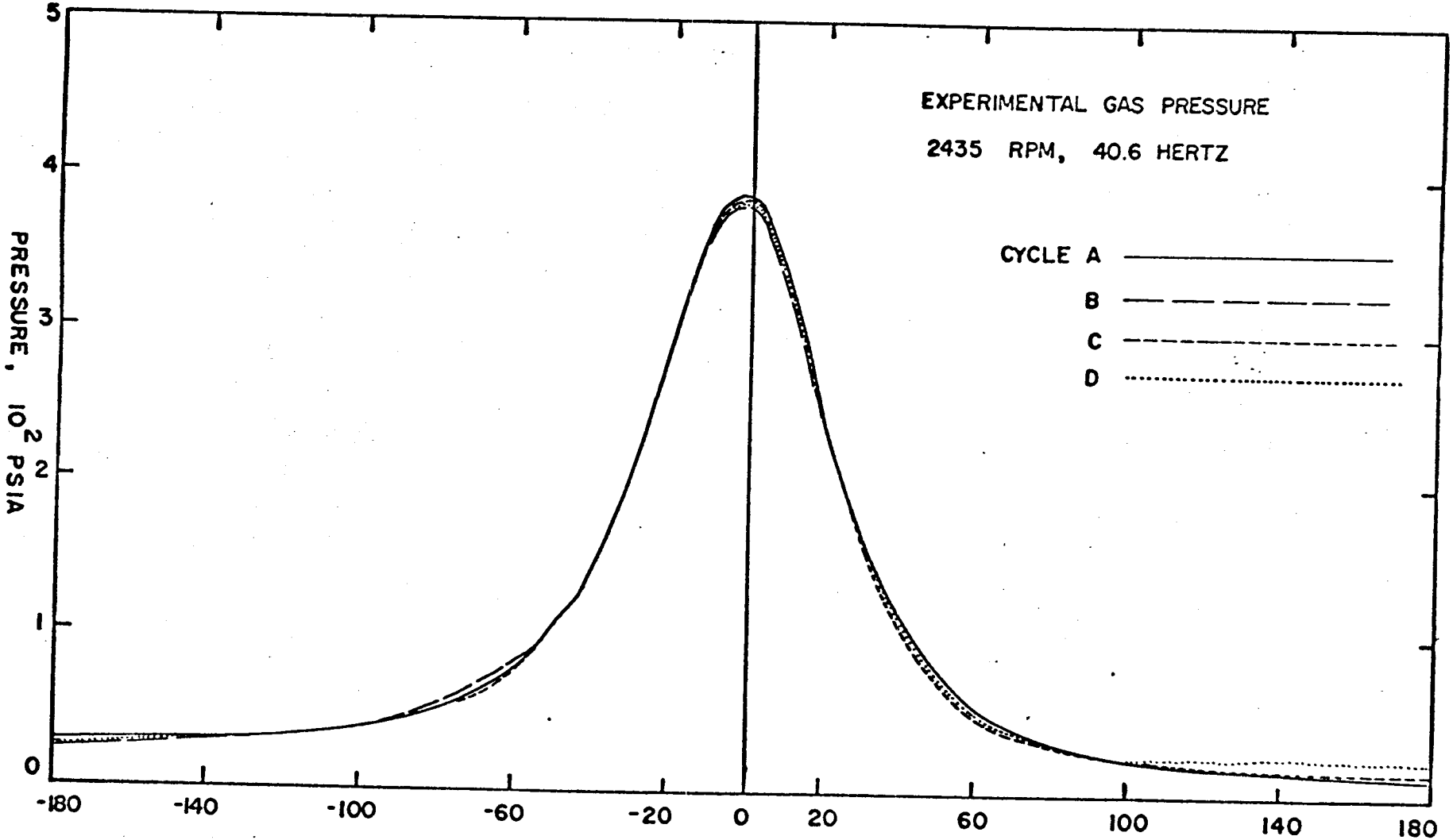
EXPERIMENTAL GAS PRESSURE
2435 RPM, 40.6 HERTZ
CYCLE A
B
C
D
PRESSURE, 10^2 PSIA
0
1
2
3
4
5
-180
-140
-100
-60
-20
0
20
60
100
140
180
CRANKANGLE

FIG. A15

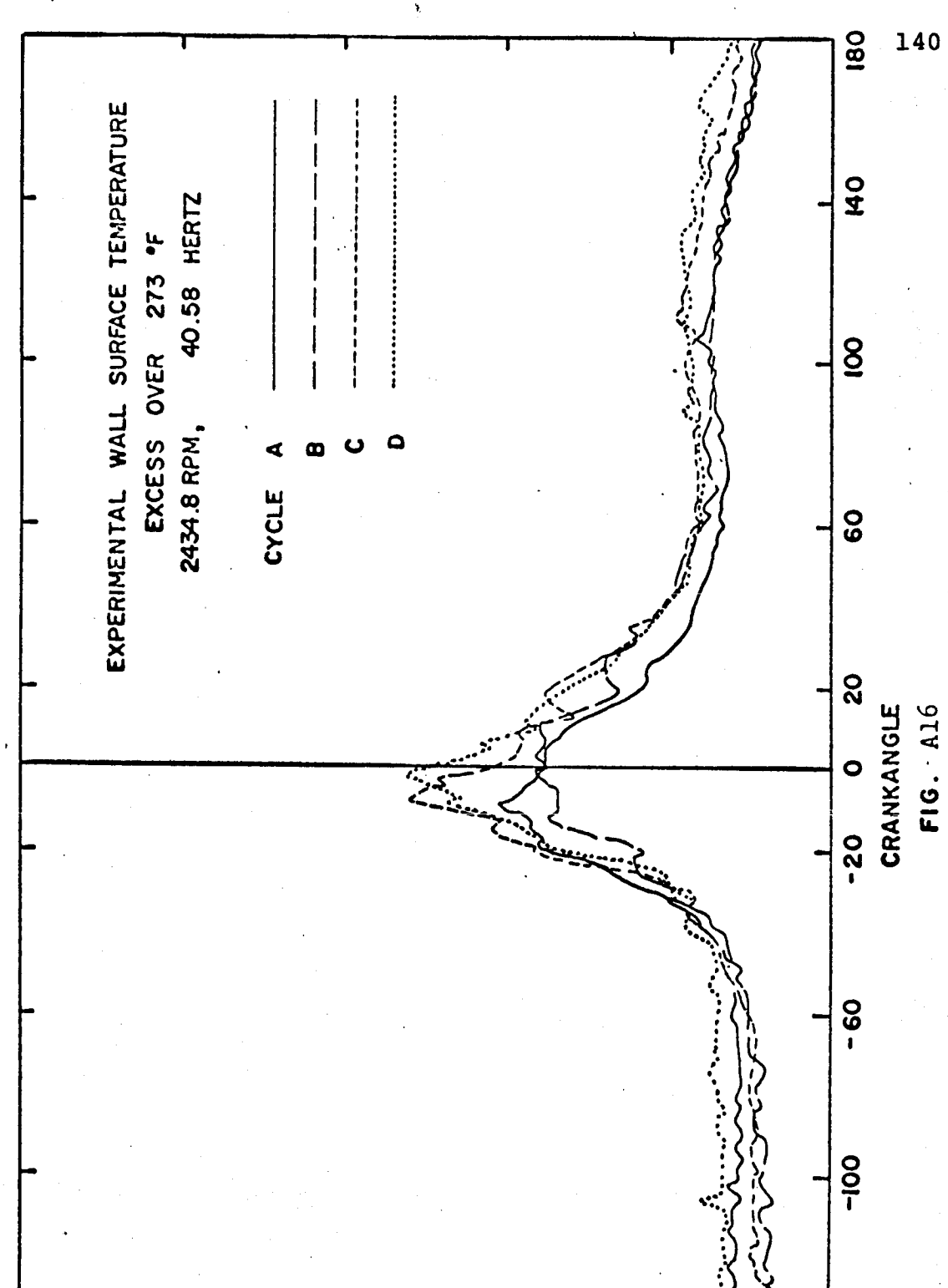
EXPERIMENTAL WALL SURFACE TEMPERATURE
EXCESS OVER 273 °F
2434.8 RPM, 40.58 HERTZ
CYCLE A
B
C
D
TEMPERATURE EXCESS, F°
CRANKANGLE
5
4
3
2
1
0
-180
-140
-100
-60
-20
0
20
60
100
140
180

FIG. A16

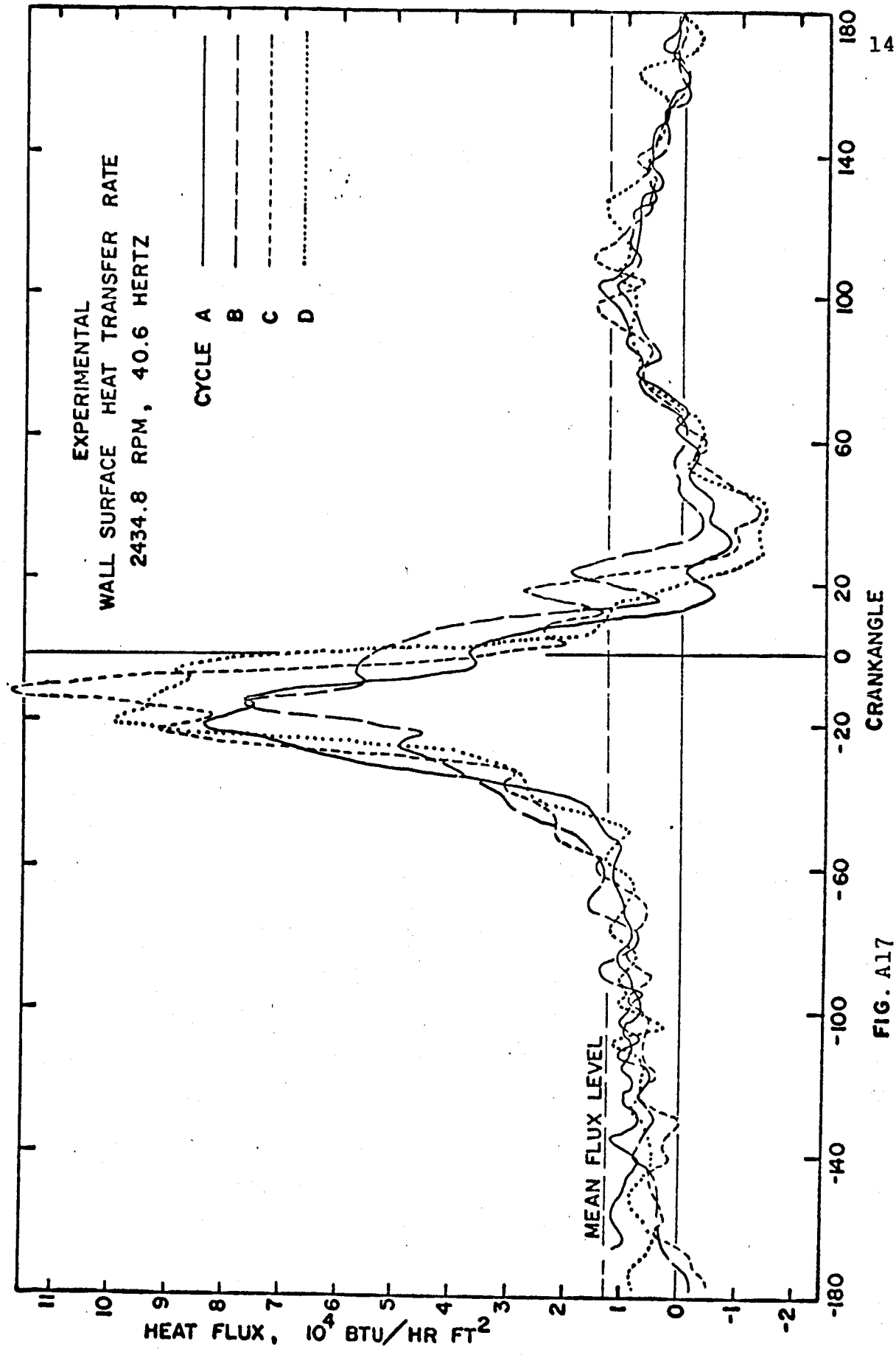
EXPERIMENTAL
WALL SURFACE HEAT TRANSFER RATE
2434.8 RPM, 40.6 HERTZ
CYCLE A
B
C
D
MEAN FLUX LEVEL
HEAT FLUX, 10^4 BTU/HR FT^2
CRANKANGLE
11
10
9
8
7
6
5
4
3
2
1
0
-1
-2
180
140
100
60
20
0
-20
-60
-100
-140
-180

FIG. A17

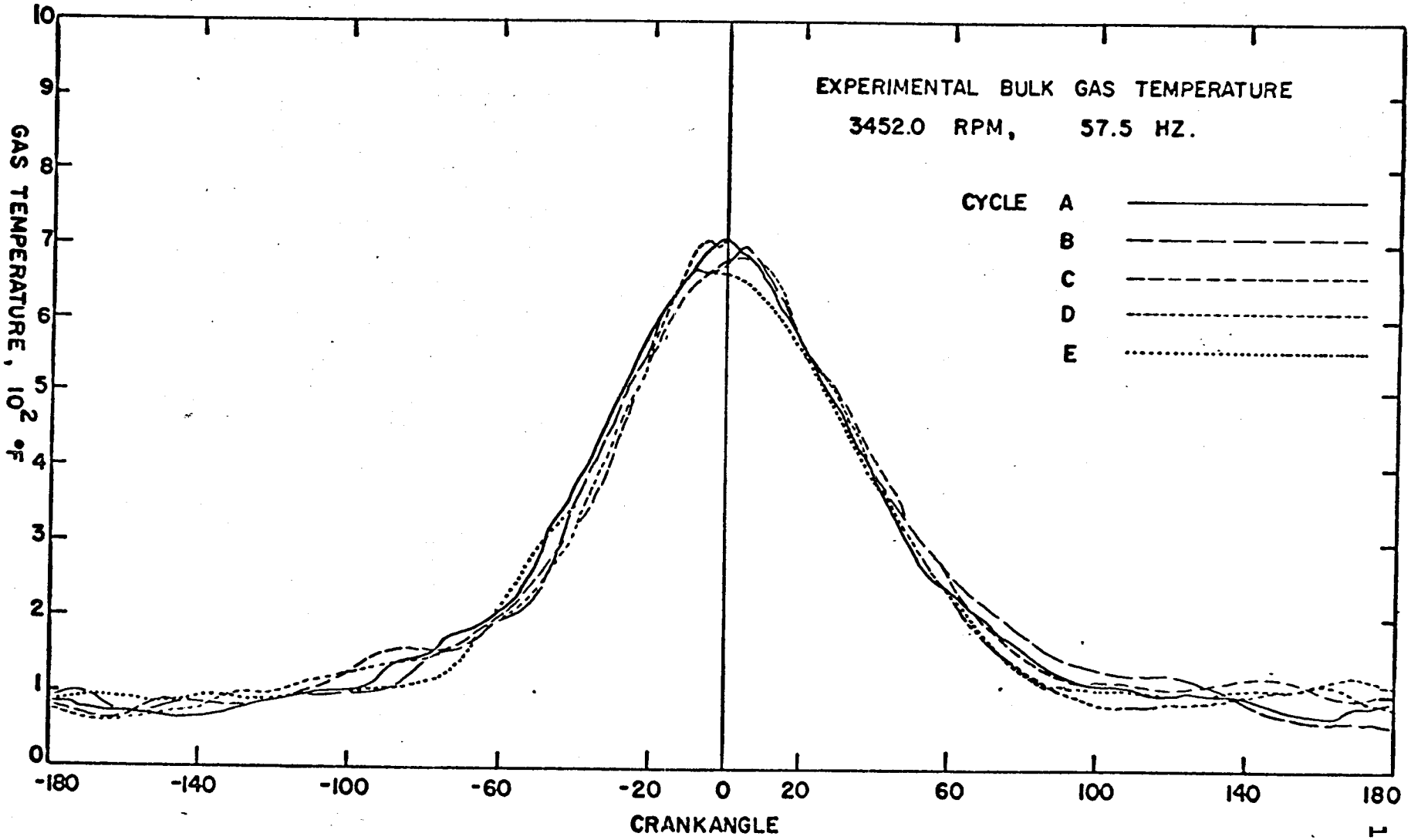
EXPERIMENTAL BULK GAS TEMPERATURE
3452.0 RPM, 57.5 HZ.
CYCLE A
B
C
D
E
GAS TEMPERATURE, 10^2 °F
0
1
2
3
4
5
6
7
8
9
10
-180
-140
-100
-60
-20
0
20
60
100
140
180
CRANKANGLE

FIG. A18

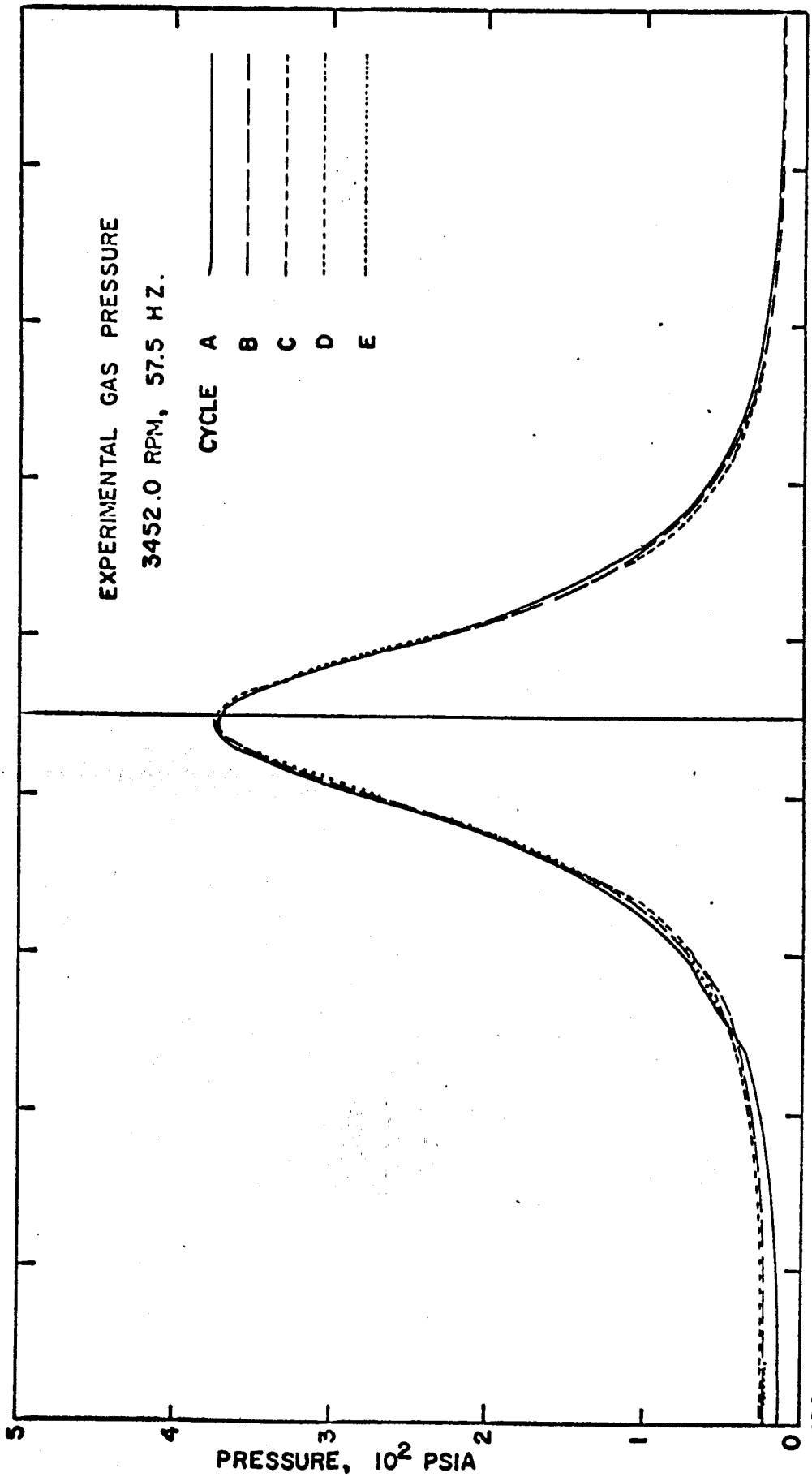
EXPERIMENTAL GAS PRESSURE
3452.0 RPM, 57.5 HZ.
CYCLE A
B
C
D
E
PRESSURE, 10^2 PSIA
0
1
2
3
4
5
-180
-140
-100
-60
-20
0
20
60
100
140
180
CRANKANGLE

FIG. A19

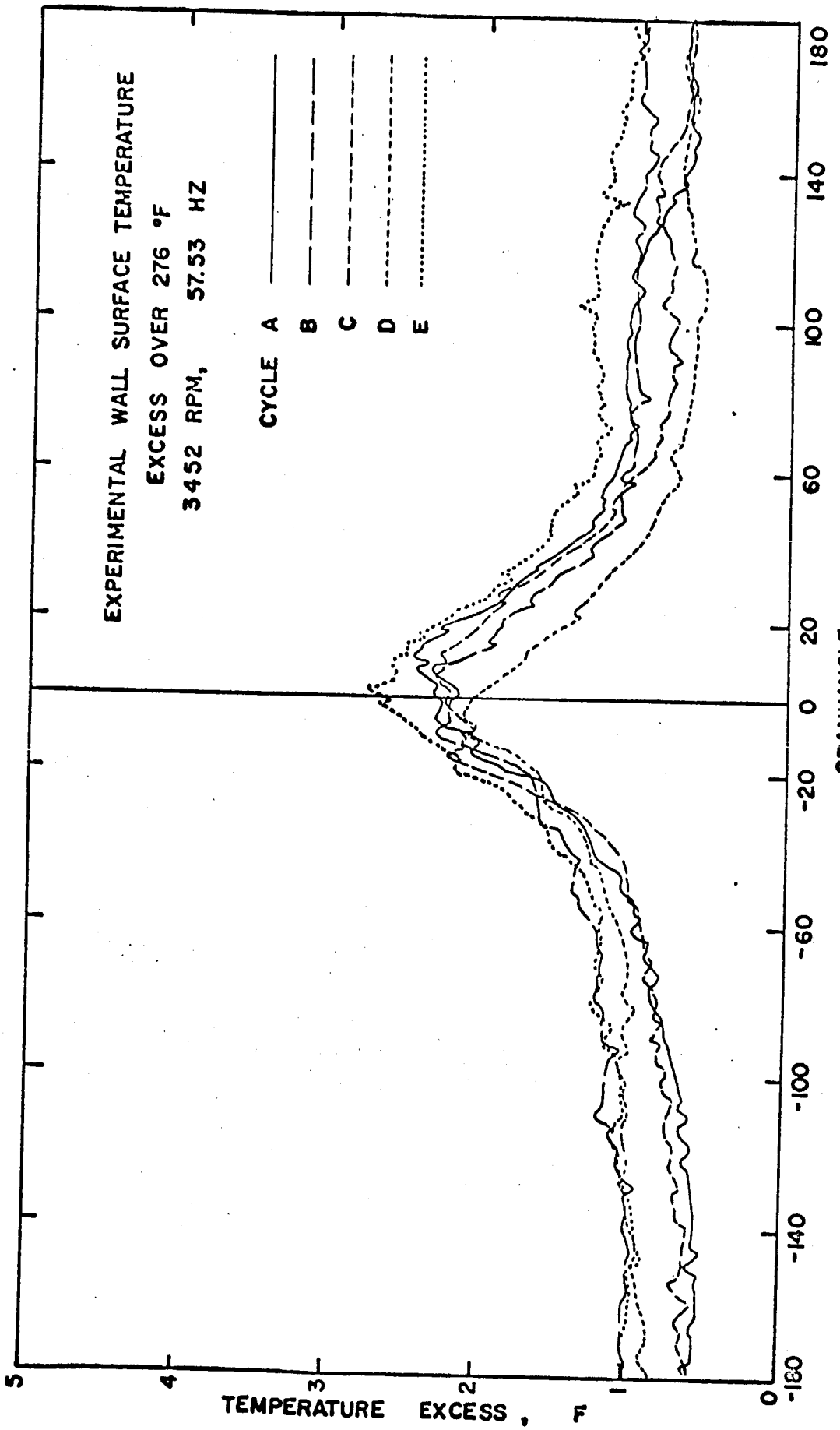
EXPERIMENTAL WALL SURFACE TEMPERATURE
EXCESS OVER 276 °F
3452 RPM, 57.53 HZ
CYCLE A
B
C
D
E
TEMPERATURE EXCESS, F
CRANKANGLE
5
4
3
2
1
0
-180
-140
-100
-60
-20
0
20
60
100
140
180

FIG. A20

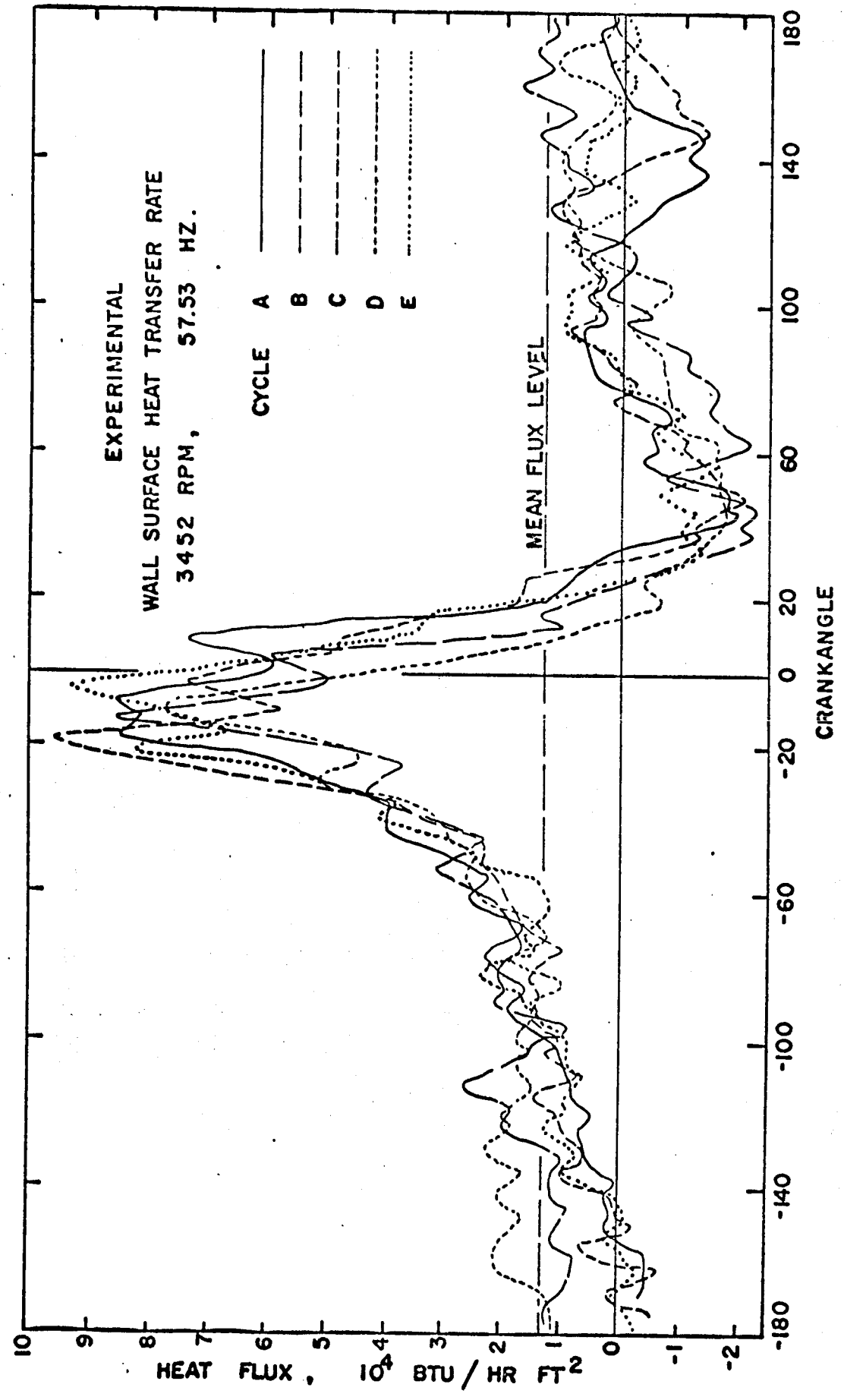
EXPERIMENTAL
WALL SURFACE HEAT TRANSFER RATE
3452 RPM, 57.53 HZ.
CYCLE A
B
C
D
E
MEAN FLUX LEVEL
HEAT FLUX, 10^4 BTU / HR FT^2
CRANKANGLE
10
9
8
7
6
5
4
3
2
1
0
-1
-2
180
140
100
60
20
0
-20
-60
-100
-140
-180

FIG. A21

BIBLIOGRAPHY

1. Shine, A. J., "The Effect of Transverse Vibrations on the Heat-Transfer Rate from a Heated Vertical Plate", M. S. Thesis, Air Institute of Technology, Wright Patterson A. F. B., 1957.

2. Lord Rayleigh, "On the Circulation of Air Observed in Kundt's Tube, and on Some Allied Acoustical Problems", Philosophical Transactions of the Royal Society of London, Vol. 175, Part I (1884).

3. Andrade, E. N. da C., "On the Circulations Caused by the Vibrations of Air in a Tube", Roy. Soc. Proceedings A, Vol. 134, 1931-1932, pages 445-470.

4. Hwu, C. K., "The Effect of Vibration on Forced Convective Heat Transfer", Ph. D. Thesis, University of Cincinnati, 1959, University Microfilms, Inc., Ann Arbor, Mich., Mic 59-6067.

5. Fand, R. M., Kaye, J., "The Influence of Sound on Free Convection from a Horizontal Cylinder", Journal of Heat Transfer, Vol. 83, May 1961, page 133.

6. Harrison, W. B., Boteler, C. W., Jackson, T. W., Lowi, A., and Thomas, F. A., "Heat Transfer from Vibrating Air Columns", Final Report, Project A 183, December, 1955, Engineering Experiment Station, Georgia Institute of Technology, N.A.C.A. N 49857.

7. Kubanskii, P. N., "Currents Around a Heated Solid in a Standing Acoustic Wave", Trans. USSR Academy of Science, Vol. 82, 1952, page 585.

8. Ibid., "Effects of Acoustic Vibrations of Finite Amplitude on the Boundary Layer", Zhurnal Technika Fizika, Vol. 22, 1952, page 593.

9. Boucher, M. G., "Ultrasonics Boosts Heatless Drying", Chemical Engineering, Sept. 21, 1959, page 151.

10. Jackson, T. W., Purdy, K. R., Oliver, C. C., "The Effects of Resonant Acoustic Vibrations on the Nusselt Numbers for a Constant Temperature Horizontal Tube", paper for Second International Heat Transfer Conference, Aug. 28 - Sept. 1, 1961.

11. Purdy, K. R., Jackson, T. W., Gorton, C. W., "Viscous Fluid Flow Under the Influence of a Resonant Acoustic Field", American Society of Mechanical Engineers Paper No. 62-WA-116, 1962.

12. Eastwood, I., Jackson, T. W., Oliver, C. C., Purdy, K. R., "Heat Transfer Threshold Values for Resonant Acoustic Vibrations in a Horizontal Isothermal Tube", Aeronautical Research Laboratories, Office of Aerospace Research, United States Air Force, ARL 62-326, April, 1962.

13. Westervelt, P. J., "Effect of Sound Waves on Heat Transfer", Acoustical Society of America Journal, Vol. 32, No. 3, August, 1960, page 214.

14. Illingworth, C. R., "The Effects of a Sound Wave on the Compressible Boundary Layer on a Flat Plate", Journal of Fluid Mechanics, Vol. 3, Part 5 (1958), page 471.

15. Lemlich, R., Hwu, C. K., "The Effect of Acoustical Vibration on Forced Convective Heat Transfer", A. I. Ch. E. Journal, Vol. 7, No. 1, March 1961, page 102.

16. Goluba, R. W., et al, "Oscillatory Combustion in Rockets", Third Semiannual Report, June 1 - Nov. 30, 1965, N. A. S. A. CR - 71895.

17. Crocco, L., "Heat Transfer in Oscillating Flow", June 30, 1963, Aeronautical Engineering Report No. 483-e, Department of the Navy, Office of Naval Research, Contract USN-Nonr 1858(29).

18. Blackshear, P. L., "Study of Screeching Combustion in a 6" Simulated Afterburner", NACA TN 3567.

19. Barrère, M., "Low Frequency Combustion Instability in Bi-Propellant Rocket Motors - Experimental Study", Jet Propulsion, Jan., 1956, page 9.

20. Cheng, Sin-I., "Low Frequency Combustion Stability of Liquid Rocket Motor with Different Nozzles", Jet Propulsion, April, 1955, page 163.

21. Marble, F. E., "Servo-Stabilization of Low Frequency Oscillations in a Liquid Bipropellant Rocket Motor", American Rocket Society Journal, March-April, 1953, page 63.

22. Kaskan, W. E., et. al., "High Frequency Oscillations of a Flame Held by a Bluff Body", ASME Transactions, Vol. 77, No. 6, Aug. 1955, page 885.

23. Truman, J. C., et. al., "Why Do High-Thrust Engines Screech?", Aviation Age, Vol. 23, No. 5, May 1955, pages 136-143.

24. Rogers, D. E., "Mechanism for High Frequency Oscillation in Ramjet Combustors and Afterburners", Jet Propulsion, June 1956, page 457.

25. Berman, K., "Rocket Motor Instability Studies", Jet Propulsion, October 1955, page 513.

26. Cheng, Sin-I., "High Frequency Instability in Solid Propellant Rockets, Part 1 and Part 2", American Rocket Society Journal, Jan., Feb. 1954, page 27.

27. Ibid., "High Frequency Combustion Instability in Liquid Propellant Rocket with Concentrated Combustion and Time Lag", Jet Propulsion, Feb. 1956, page 87.

28. Crocco, L., Cheng, Sin-I., "High Frequency Combustion Instability in Rocket Motor with Concentrated Combustion", American Rocket Society Journal, Sept., Oct. 1953, page 301.

29. Priem, R. J., "Application of Similarity Parameters for Correlating High Frequency Instability Behavior of Liquid Propellant Combustors", ARS Propulsion, Combustion, and Liquid Rocket Conference, April 26-28, 1961, Palm Beach, Florida.

30. Chu, B. T., "Pressure Waves Generated by the Addition of Heat in a Gaseous Medium", NACA TN 3411.

31. Blackshear, P. L., "Driving Standing Waves by Heat Addition", NACA TN 2772.

32. Schalla, R. L., "Examination of Pressure Oscillations Induced by Changes in the Burning Rate of Flames", NASA TN D-764.

33. Overbye, V. D., "Variation of Instantaneous Wall Temperature, Heat Transfer, and Heat Transfer Coefficients in a Spark-Ignition Engine", Ph. D. Thesis, University of Wisconsin, 1960.

34. Pless, L. G., "The Effect of Selected Operating Variables on Instantaneous Combustion-Chamber Surface Temperature", M. S. Thesis, University of Wisconsin, 1956.

35. Bennethum, J. E., "Heat Transfer and Combustion Chamber Deposits in a Spark Ignition Engine", Ph. D. Thesis, University of Wisconsin, 1960.

36. Overbye, V. D., "Instrumentation and Analysis for Instantaneous Heat Transfer in Internal-Combustion Engines", M. S. Thesis, University of Wisconsin, 1959.

37. Bendersky, D., "A Special Thermocouple for Measuring Transient Temperatures", Mechanical Engineering, Vol. 75, 1953, page 117.

38. Buchman, A. S., "Noise Control in Low Level Data Systems", Electromechanical Design, Sept. 1962, page 64.

39. Coker, E. G., and Scoble, W. A., "Cyclic Changes of Temperature in a Gas-Engine Cylinder", Proceedings of Institution of Civil Engineers, Vol. 196, 1913-1914, Part II, pages 1-74.

40. Schultz, B. H., "Measuring Rapidly Fluctuating Gas Temperatures", Phillips Review, Oct. 1951, Vol. 13, No. 4, page 104.

41. Semenov, E. W., "Studies of Turbulent Gas Flow in Piston Engines", reprinted in "Combustion in Turbulent Flow", L. N. Khitrin, Editor; translated 1959.

42. Hershey, A. E., and Paton, R. F., "Flame Temperatures in an Internal Combustion Engine Measured by Spectral Line Reversal Method", University of Illinois Engineering Experiment Station Bulletin 262, Urbana, Ill., 1933.

43. Rassweiler, G. G. M., Withrow, L., "Flame Temperatures Vary with Knock and Combustion Chamber Position", Trans. Soc. Automotive Engineers, 36, 125-133.

44. Beck, N. J., Chen, S. K., "Temperature Measurement from Iodine Absorbtion Spectrum", Fifth Symposium (International) on Combustion, Reinhold Publ. Co., New York, 1955.

45. Agnew, W. G., "End Gas Temperature Measurement by a Two-Wavelength Infrared Radiation Method", Society

of Automotive Engineers Preprint, summer meeting, Chicago, Illinois, June 5, 1960.

46. Taylor, C. F., and Livengood, J. C., Unpublished Summary Report, Sloan Automotive Laboratory, M. I. T., Oct. 1958. See also Livengood and Taylor, "Measurement of Gas Temperature in an Engine by the Velocity of Sound Method", S. A. E. Trans., Vol. 66, 1958, 683-699.

47. Burrows, M. C., "The Measurement of Unburned Gas Temperatures in an Engine by an Infrared Radiation Pyrometer", University of Wisconsin Engineering Experiment Station Reprint No. 512.

48. Ghandi, B. K., "Gas Temperature Measurements in Internal Combustion Engines", Temperature - Its Measurement and Control in Science and Industry, Vol. 3, Part 2, 1962, Reinhold Publ. Co., New York.

49. King, L. V., "On the Convection of Heat from Small Cylinders in a Stream of Fluid", Phil. Trans. Roy. Soc. Ser. A, Vol. 214, Nov. 13, 1914, page 373.

50. Lowell, H. H., and Patton, N., "Response of Homogeneous and Two-Material Laminated Cylinders to Sinusoidal Environmental Temperature Changes, with Applications to Hot Wire Anemometry and Thermocouple Pyrometry", NACA TN 3514, Sept. 1955.

51. Wienke, H. J., "A Resistance Thermometer for Engine Compression Temperatures", University of Wisconsin Engineering Experiment Station Reprint No. 617, Madison, Wisconsin.

52. Tsao, K. C., Myers, P. S., Uyehara, O. A., "Gas Temperatures During Compression in Motored and Fired Diesel Engines", SAE Trans., Vol. 70, 1962, pages 136-145.

53. Grant, H. P., and Kronauer, R., "Fundamentals of Hot Wire Anemometry", Symposium on Measurement in Unsteady Flow, published by A.S.M.E., 345 E. 47th St., New York 17, N.Y. (1962).

54. Weske, J. R., "Measurement of Arithmetic Mean Velocities in a Pulsating Flow of High Velocity by the Hot Wire Method", NACA TN 990.

55. Aftalion, S., "The Determination of Rapidly Changing Exhaust-Gas Temperatures in Internal Combustion Engines", Sulzer Technical Review, Vol. 40, No. 2, pages 67-74.

56. Hunt, M. H., "Design and Use of Fine Wire Thermocouples for Research", U. S. Naval Ordnance Test Station Report, Navord Report 5828, China Lake, Calif., 1959.

57. Meyer, W. E., and de Carolis, J. J., "Compression Temperatures in Diesel Engines Under Starting Conditions", S.A.E. Trans., Vol. 70, 1962, page 163.

58. Thermosystems Incorporated, "Applications of the Heat Flux System in Low Temperature Gases and Liquids", Technical Bulletin #4, Thermo-Systems, Inc., 2418 E. Hennepin Ave., Minneapolis 13, Minn.

59. Hinze, J. O., Turbulence, An Introduction to Its Mechanism and Theory, McGraw-Hill Book Co., Inc., New York (1959).

60. Lowell, H. H., "Design and Applications of Hot-Wire Anemometers for Steady-State Measurements at Transonic and Supersonic Air Speeds" NASA TN 2117, July 1950.

61. Otis, D. R., Private communication, University of Wisconsin, Dec. 1966.

62. Pfriem, H., "Zur Messung Veränderlicher Temperaturen von Gasen und Flüssigkeiten", Forschung 7 (1936) pages 85-92.

63. Rounthwaite, C., "Double Wire Method of Resistance Thermometry in Gaseous Explosions", Fuel, London, April 1955, pages 59-70.

64. McAdams, W. H., Heat Transmission, 3rd Edition, 1954, McGraw-Hill Book Co., Inc., New York, N. Y.

65. Morgan, G. A., Private communications of June 20, 1966, July 13, 1966, Dept. of Mechanical Engineering, University of Adelaide, Adelaide, South Australia.

66. Ebersol, G., "The Radiant and Convective Components of Diesel Engine Heat Transfer", SAE International Summer Meeting, June 10, 1963, Paper No. 701C.

67. Schneider, P. J., Conduction Heat Transfer, Addison-Wesley Publishing Co., Inc., Reading, Mass. (1957).

68. Hamming, R. W., Numerical Methods for Scientists and Engineers, McGraw-Hill Book Co., Inc., New York, N. Y. (1962), page 297.

69. Kudryavtsev, Unsteady Heat Transfer, American Elsevier Publ. Co., Inc., 52 Vanderbilt Ave., New York, N. Y., 10017 ($7.50).

70. Binder, R. C., Fluid Mechanics, Prentice-Hall, Inc., Engelwood Cliffs, N. J., 1955, page 150.

71. Hobson, E. W., Waermeleitung, Mathematischer Teil, in Encyklopaedie der Mathematischen Wissenschaften, Vol. 5, Part 1, Art. 4, B. G. Teubner, Berlin, 1903.

72. Jakob, M., Heat Transfer, Vol. I, John Wiley and Sons, Inc., New York, N. Y. (1949).

73. Shamah, E., M. S. Thesis (title unknown), Dept. of Mechanical Engineering, University of Wisconsin, 1968.

74. Smith, G. D., Numerical Solution of Partial Differential Equations, Oxford University Press, New York, 1965, page 6.

75. Dusinberre, G. M., Heat Transfer Calculations by Finite Differences, International Textbook Company, Scranton, Penn., 1961, page 24.

76. Bird, R. B., Stewart, W. E., Lightfoot, E. N., Transport Phenomena, John Wiley and Sons, New York, 1960, page 322, Eqn. 10.1 - 19J.

77. Kreith, F., Principles of Heat Transfer, International Textbook Company, Scranton, Penn. (1958).

78. Geidt, W. H., Principles of Engineering Heat Transfer, D. Van Nostrand Co., Inc., Princeton, N. J., 1957, page 149.

79. Kays, W. M., Convective Heat and Mass Transfer, McGraw-Hill Book Co., Inc., New York, N. Y., 1966, page 211.

80. LeFeuvre, T., Personal communication, June, 1967.

81. Chu, A., Personal communication, July 21, 1967.

III. PRESSURE RECORDING CIRCUITRY AND NOTES

The piezoelectric Kistler 601H pressure pickup generated a charge of 1.078 picocoulombs per psi of applied pressure. This change in charge was converted to a voltage signal by a Kistler #1713 charge amplifier in short time constant operation, and further amplified by an Astrodata direct coupled amplifier. The signal was displayed on one channel of the four-channel Tektronix 565 oscilloscope. Provision was made for injecting a 1000 Hz square wave of 1.0 volt amplitude into a calibration input jack on the Kistler charge amplifier. By this means a simulated 100 psi square wave could be superimposed upon the pressure trace to aid in pressure signal calibration.

The 601H transducer produced smooth, trouble-free signals through all test phases. Very little cycle-to-cycle variation was noted in the high-pressure (say $-90° \leq$ crankangle $\leq +90°$) half of the cycle. In the low pressure (up to perhaps 80 degrees to either side of bottom dead center) portions of the cycle, some cyclic variation was noted, perhaps inside an "envelope" of about 20 psi. The 601H transducer does introduce an erroneous pressure indication when the transducer surface is stressed by cyclic temperature changes. With a proportionality constant of about 3 psi/F°*,

*Unpublished data of J. Alyea, Department of Mechanical Engineering, University of Wisconsin

a surface temperature swing of 2 F° will induce a false pressure reduction of 6 psi, a 1.7% error compared to the 340 psi pressure swing. Having no precise information of the phasing of this small error, it was ignored throughout the tests.

Fig. 4 is a block diagram of the pressure signal circuitry.

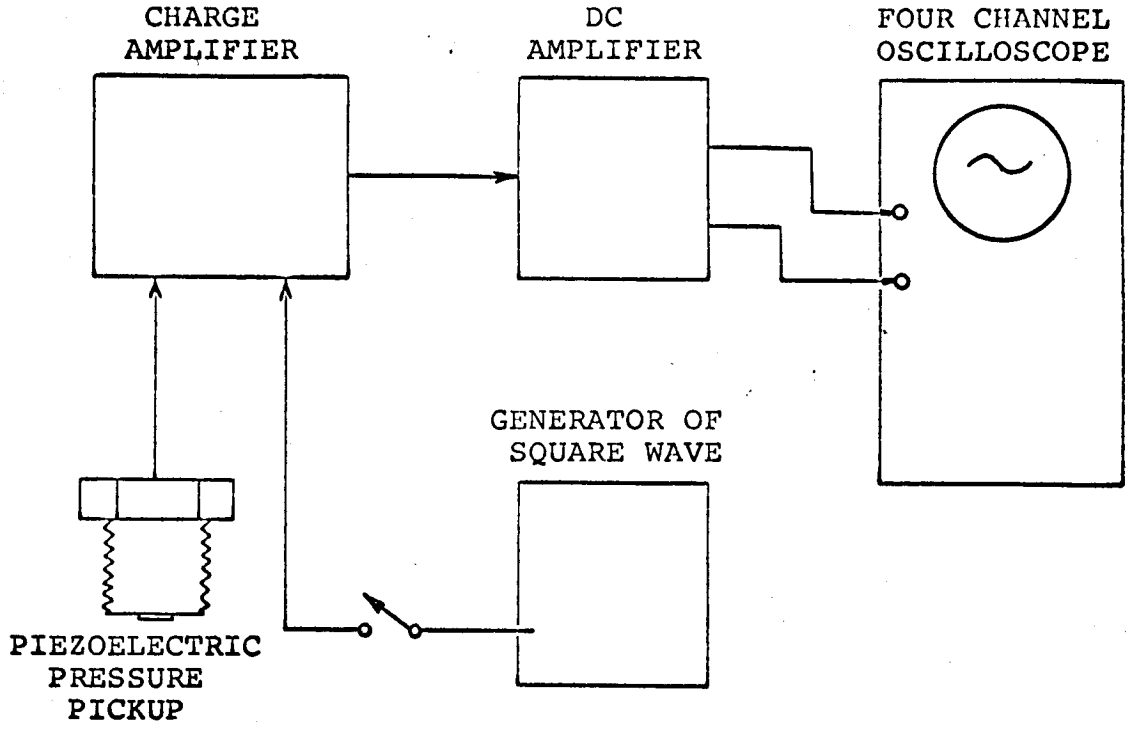

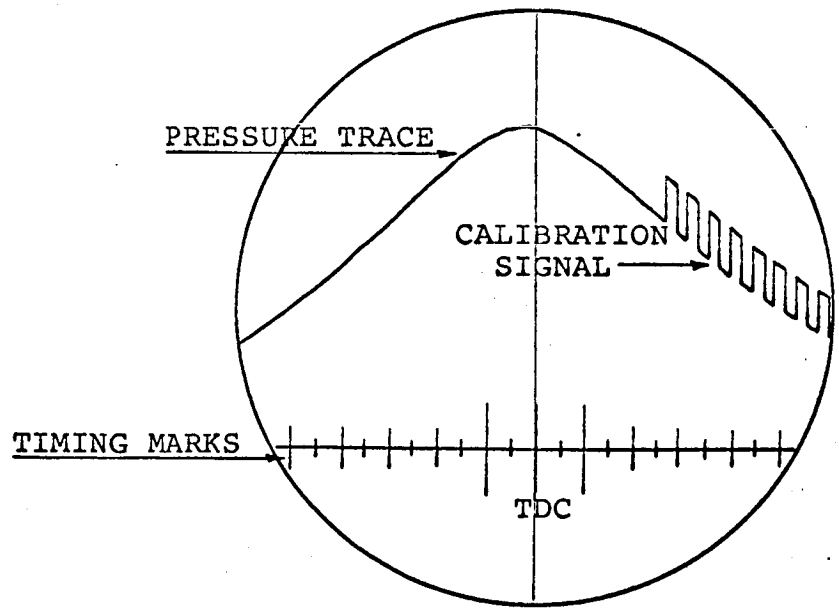

Fig. 4 Pressure Display Circuitry and Traces

IV. SURFACE TEMPERATURE CIRCUITRY AND NOTES

There are two popular varieties of surface thermocouples in the United States: those manufactured by Nanmac Corporation*, of Indian Head, Maryland, and those available from Heat Technology Laboratory*, of Huntsville, Maryland. The Nanmac thermocouples have a wider range of application than the second variety. The active surface can be eroded by combusting gases or rubbing friction. For a variety of reasons, however, the product of the second manufacturer was chosen.

The surface thermocouples used in this study were the same type as were used by Pless (34), Bennethum (35), and Overbye (36) in recording surface temperatures in spark- and compression-ignition engine combustion chambers. Developed by Bendersky (37) in the early 1950's, the instrument is little changed from the original in design. Iron-constantan and iron-nickel metal combinations were obtained and mounted in a cast iron head for all major tests. For some preliminary studies in which a variety of head materials were used, an aluminum-nickel surface thermocouple was the transducer.

The thermocouple construction was as follows: a nickel (or constantan) wire has its surface oxidized; this nickel

*See List of Manufacturers and Addresses

oxide is an electrical insulator. The iron is drawn down on the nickel wire by a wire-drawing die. After metallurgically grinding and polishing the end of the resulting concentric cylinders, a one-micron-thick layer of constantan is plated on the end. Thus the thermocouple junction is located at the washer-shaped constantan-iron interface. Originally, nickel was used as the plating material, but since the one-micron plating is at essentially the same instantaneous temperature throughout, the law of intermediate metals does not require the plating and wire materials to be common; a better bonding substance was chosen in the constantan. The cylinder of iron is finally given a UNC 2-56 thread.

Fig. 5 shows a thermocouple as it was mounted in the head, and Fig. 6 gives, in block form, the circuit in which it was the signal source. The gas-metal interface temperature is seen in the voltage between ground (G) and the oxided nickel wire (N1) with its cold junction, and is indicated by $E_{interior}$. The head exterior temperature (a constant when the system is in equilibrium) is seen in the voltage between ground (G) and a nickel wire (N2) held between the head and an iron mounting nut, with its cold junction, the voltage indicated by the symbol $E_{exterior}$.

Since the interior temperature signal must be displayed at high gain for good resolution, and since this signal contains a large dc component (the swing of 2 F° superimposed

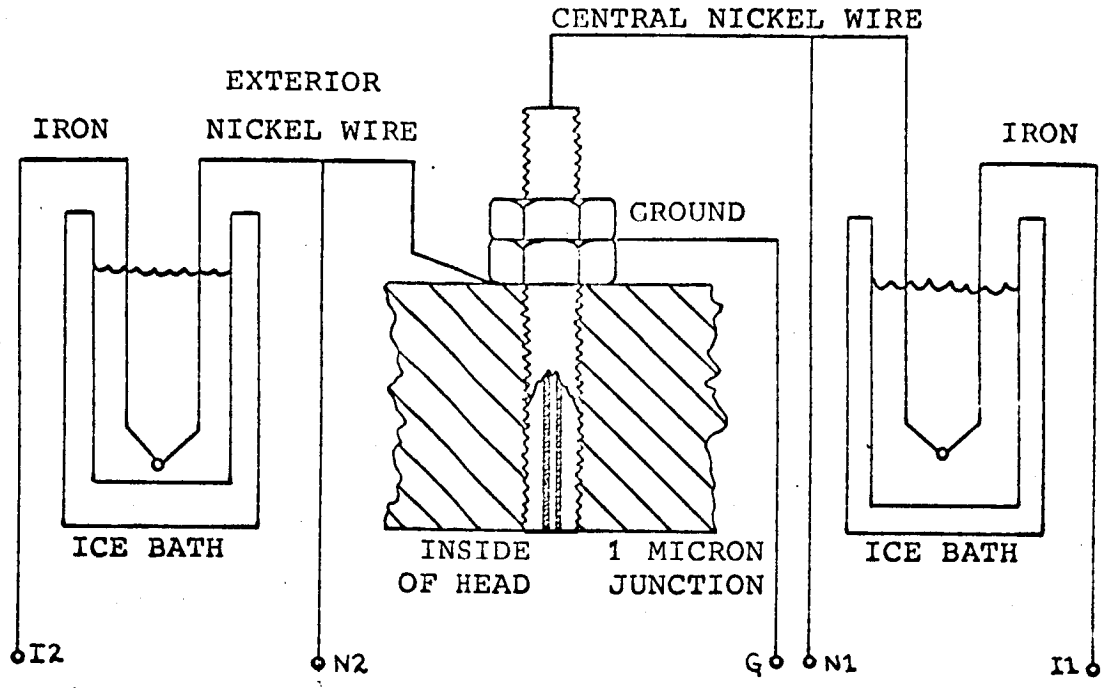

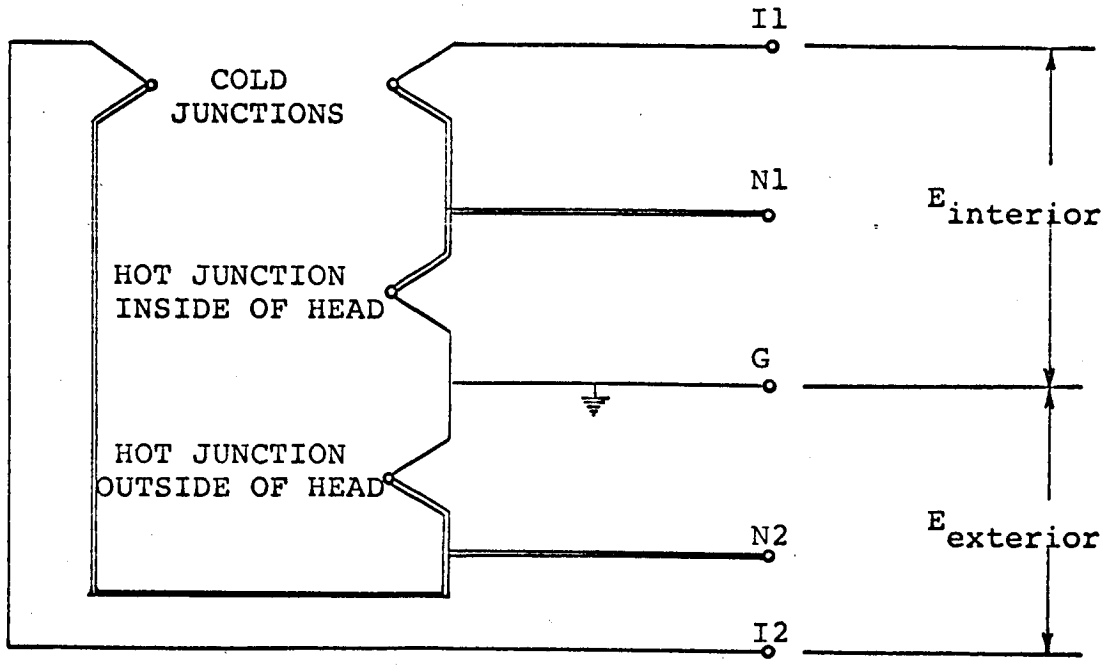

Fig. 5 Thermocouple Construction and Hookup

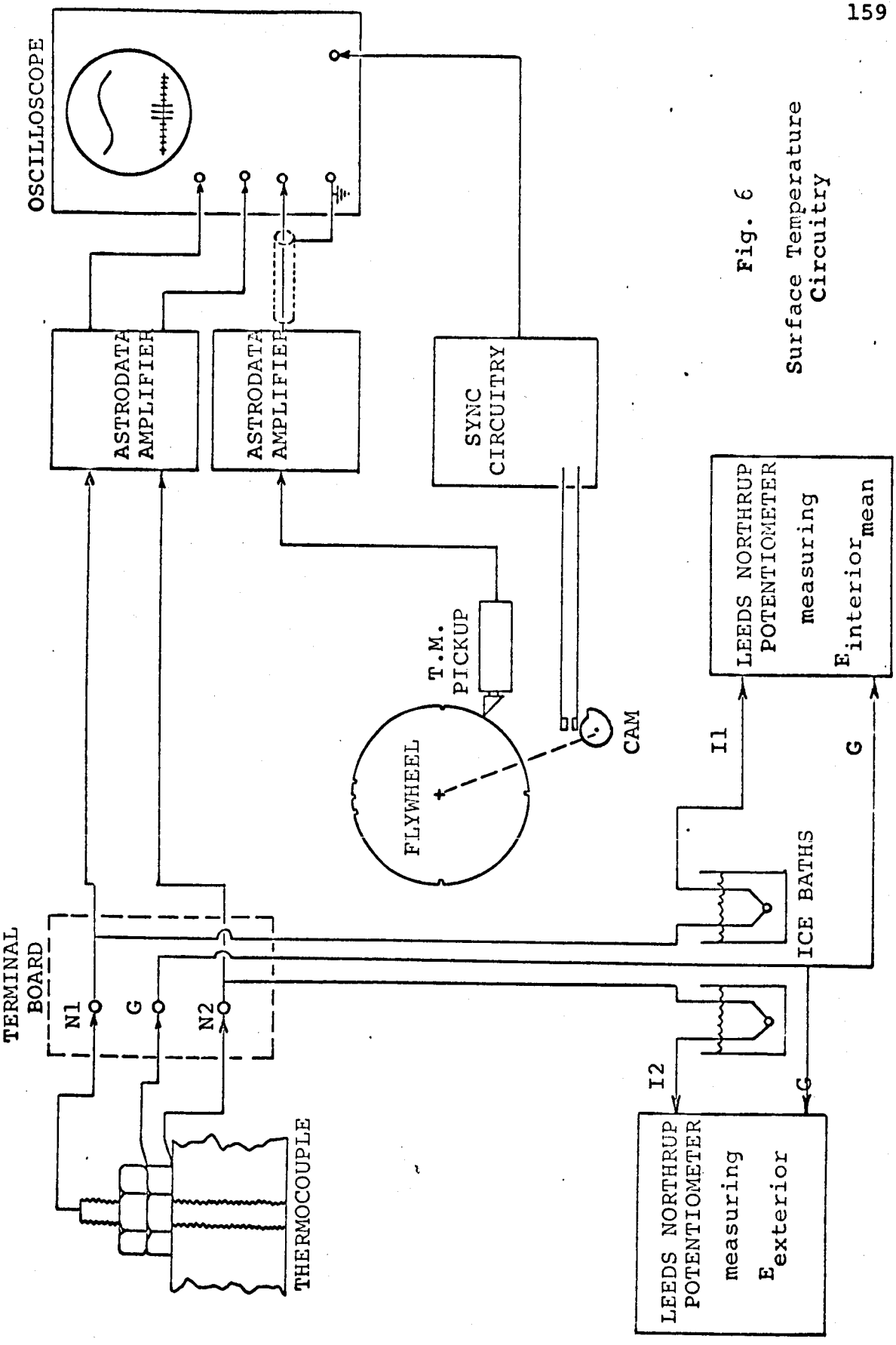

Fig. 6

Surface Temperature Circuitry

upon a 200 F° surface-to-ice bath difference), it is much more convenient to display the voltage corresponding to the temperature difference through the head ($E_{interior} - E_{exterior}$). An indication of equilibrium is given when this displayed voltage difference ceases to increase. The voltage (N1 - N2) is the same as voltage (I1 - I2) since the only difference between them is two iron-nickel junctions at 32°F connected in opposition; the former signal is the one displayed. Because even at equilibrium the surface temperature (with a swing of perhaps 2 F° per engine cycle) appears to "hunt" or drift up and down by a degree or two in a periodic fashion at a fraction (like one-tenth) of the system fundamental, photographic records are made with a blocking capacitor feeding only the ac signal to the oscilloscope.

The voltage difference is amplified 3000 times by an Astrodata d.c. amplifier and displayed at 100 millivolts/centimeter on one channel of the oscilloscope. Because one side of the transducer is electrically grounded (by its design), 60 Hz (and higher harmonic) noise causes great trouble in this type of work, and efforts must be made to minimize it. All connections must be shielded; cables must be coaxial and shields must be grounded as close to a central point as possible to avoid ground loops. D.c. amplifiers must have differential inputs and outputs, and input and output grounds should be independent from each other

and from the case. The oscilloscope should be operated in differential mode. A. S. Buchman (38) presents a good discussion of this kind of noise abatement technique. Data were taken when the local electromagnetic noise level was low, with all nearby fluorescent lamps and unshielded transformers turned off. Batteries were used for all possible power supplies (as opposed to ripple-containing rectified power supplies). The very high frequency noise level (contributed primarily by the oscilloscope amplifiers) and the 60 Hz noise level were held below approximately 0.18 F° and 0.12 F° equivalent temperature signal, respectively.

Some of the surface thermocouples used in this study were originally purchased in the late 1950's and were used by Overbye (33) in a fired spark-ignition engine. They were recalibrated and cleaned with denatured alcohol. At speeds in excess of 1800 rpm (30 Hz) some of these older thermocouples occasionally gave an output which was clearly not a temperature response. This extraneous signal was clearly recognizable by its appearance: a high amplitude, high frequency harmonic signal superimposed in "packets" of 10 or 20 crankangle degrees length upon the temperature signal. High speed drum camera films showed these extraneous signals to be of 3000 Hz frequency. The portions of the cycle in which these signals appeared remained the same from cycle to cycle. No mechanism for this anomalous signal is proposed, except perhaps vibration of a partially

detached one-micron film. No traces containing this type of signal were used or analyzed. Surface thermocouples sometimes degenerate to this type of signal before they break up when used in a fired engine.

V. GAS TEMPERATURE MEASUREMENT

HISTORICAL SURVEY

Probably the greatest problem in contemporary engine (or compressor) instrumentation is the accurate measurement of gas temperature at a point. An instrument must be small enough not to influence the flow about it materially, rugged enough to withstand high gas velocity and temperature and pressure extremes, and sensitive enough to detect changes in gas temperature at relatively high frequency (the 50th harmonic at 3600 rpm is at 3000 Hz). The alternative to this set of requirements is a computational method: assume constant mass, polytropic processes at fixed polytropic coefficient, and a perfect gas whose properties are time functions only. A new analytical tool is the thermodynamic simulation program, made possible by the advent of large-core-storage, high-speed digital computers. A program of this sort is discussed later. However, in general, a mass of experimental data is given more credence than an analytical conclusion in a flow system of this order of complexity.

Historically, many investigators have measured temperatures in operating and motored engines. Some of the earliest methods suggested and tried involved the use of either resistance thermometers or thermocouples. Coker and Scoble (39) used thermocouples made of flattened platinum-alloy

wires 500 micro-inches thick (12.7μ). Burstall used resistance thermometers made of 38 to 64 micron platinum to obtain temperatures in an operating gas engine. Schultz (40) used 2 micron flattened platinum wires in measuring fluctuating gas temperatures. The slow response rate, oxidation of the wires, and early wire breakage left much to be desired. Thermocouples rugged enough to withstand engine turbulence proved to be too large for rapid temperature response.

The work of Semenov (41) represents one of the most successful attempts to measure instantaneous local gas temperatures and velocities in a motored piston engine with small-wire instrumentation. This work was done in the Soviet Union prior to 1959 and was translated into English in 1963. Semenov's interest was primarily in gas turbulence; his three basic objectives were:

1) to study the variation of turbulence parameters throughout the motored cycle,

2) to study the nature of the gas flow during the intake and compression processes, and

3) to study the effect of certain operating variables on the level and the frequency distribution of the turbulence.

Measurements were made in a single cylinder CFR (variable compression ratio) engine with a cylindrical compression chamber (with large overhead intake and exhaust valves) at low speeds (from 10 to 20 Hz) and at moderate compression

ratios (4 to 9.5).

Although Semenov's major objective was velocity and turbulence level measurements, local gas temperatures were measured in the course of his work. A constant temperature hot-wire anemometer (see next major section for description of this type of transducer) was designed; it consisted of an 11 micron diameter tungsten filament for instantaneous gas velocity and turbulence measurement, and a long (about one inch) 11 micron diameter tungsten filament heated by a "weak current" for temperature compensation purposes. Since the constant temperature anemometer is sensitive to both velocity and temperature changes, the latter filament tries to follow the gas temperature; the temperature compensation in the anemometer is electronic rather than computational. In order to locate the compensation wire so that it sees a gas temperature history similar to that experienced by the velocity sensor, a gas temperature survey was made throughout the chamber around the cycle with an uncompensated 8 micron resistance thermometer at a 15 Hz driving frequency and 6:1 compression ratio.

A number of interesting observations were made by Semenov which may find application in the present work. It must be emphasized, however, that because of the intake and exhaust processes, the gas velocity and turbulence levels in the Semenov investigation probably were considerably greater

than those encountered in this work. Velocity measurements were made between the exhaust and intake valves; the valves represented some 48% of the head area. The observations of Semenov include:

1) Immediately after closing the intake valve on the compression stroke, the mean gas velocity dropped from about 8 meters/sec. to about 1.5 meters/sec. in 45 crankangle degrees. The "directional" gas flow quickly ceased and only turbulent eddies remained.

2) Sharp velocity gradients were found only within about 3 millimeters of the wall; this may be an estimate of the viscous boundary layer thickness.

3) Measurements with the 8 micron resistance thermometer indicated that the thermal boundary layer was from 1.5 to 2 millimeters in thickness (at 15 Hz) and that the gas temperature beyond this penetration was spatially uniform (but time-varying). This tends to confirm a model incorporating a "bulk gas" and a thin boundary layer.

In the 1920's a trend toward using radiation techniques started. Hershey and Paton (42) of the University of Illinois measured temperatures using the Spectral Line Reversal Method. Rassweiler and Withrow of General Motors

(43) used a similar technique. More recently, the temperatures in the unburned gas of an engine were measured by other optical methods. The absorption of radiation by iodine vapor was used in one technique (44) by Beck and Chen, and Agnew (45) described a unit which operated by comparing the relative amounts of infrared radiation emitted in two wavelength bands.

Another method of measuring fluctuating gas temperature in a cylinder-piston-compression chamber is to measure the time interval it takes for a high frequency sonic pulse to travel the bore of the cylinder. The computed speed of sound is then related to the mean temperature of a perfect gas. This method has been developed by C. F. Taylor (46) of Sloan Laboratory, Massachusetts Institute of Technology. Still another is the infrared null method, used at the University of Wisconsin by Burrows (47) to measure end gas temperatures in a spark ignition engine and gas temperatures up to and during injection in compression-ignition engines. Radiation from a blackbody held at an elevated, fixed, and known temperature is passed through filters and sapphire windows across the bore of a compression/combustion chamber and allowed to fall on a lead sulphide sensor. When the gas is at the blackbody temperature, the gas will emit exactly as much radiation to the sensor as it absorbs from the blackbody, and the sensor will see the same radiation it would see from the blackbody alone.

There are other optical methods; however, all of these are subject to a "long path length" error. The path length includes two boundary layers at reduced temperatures, with temperature gradients as great as 6000 F°/inch, and a mass of "core" gas which may or may not be homogeneous. How the "long path length" instrument weights these different density and temperature regions is not known, and this adds uncertainties to data interpretation. Some pyrometers approximate the mass average, and some the "free stream" temperature, and in the absence of an understanding of the flow processes and heat transfer, a rational decision is difficult. Ghandhi (48) gives an interesting discussion and summary of these matters.

A truly "local" gas temperature measurement was needed for this study, and under restrictions in frequency and gas behavior, the small-wire transducer can approach this standard and give at least a good qualitative, if not a quantitative, understanding of the gas temperature behavior.

SMALL WIRE INSTRUMENTS

There are four general categories of instruments employed in the study of fluid properties which use a small diameter wire as the transducer: the thermocouple, the constant temperature anemometer, the constant current anemometer, and the resistance thermometer. The principal differences between these four categories are the magnitude of the wire

current and the philosophy applied to the output signal. It is instructive to consider all four categories briefly to understand the heat transfer principles involved.

SMALL WIRE THERMOCOUPLE

The small wire thermocouple can be used to measure transient gas temperatures if the fluctuation frequency is relatively low. A thermocouple constructed of 0.001 inch diameter wire will have about a 7 millisecond response time (to 63.2% of a step change) in a high velocity gas flow. Thermocouples of this sort are available from Heat Technology Laboratories*. Omega Engineering, Inc.* makes a 0.0005 inch thermocouple; thermocouples as small as 0.001 inch can be built using resistance welding or spot welding joining techniques. However, the frequency response of these instruments limits their applicability to speeds less than 100 or 150 rpm (about 2 Hz); they would clearly be unsuitable for this investigation.

CONSTANT TEMPERATURE AND CONSTANT CURRENT ANEMOMETERS

The constant current anemometer uses a resistance wire in a bridge circuit with a high impedance dc power supply to insure a constant probe current during small changes in probe resistance. The wire is heated with a dc current of

*See List of Manufacturers and Addresses

from 30 to 300 milliamps; when the heated wire is cooled by a fluid stream, its electrical resistance decreases with its temperature. The energy dissipation and fluid velocity are related by the famous law derived and verified by L. V. King (49) of McGill University in 1914:

$$I^2R = (R - R_o)\ (A + B\ \sqrt{Re}) \qquad (4)$$

where A and B are functions of the gas properties and wire dimensions, Re is the Reynolds Number associated with the wire, I the current, R the hot wire resistance, and R_o the room temperature wire resistance. King's Law was subsequently found to be correct for wide ranges in Re and accurate for ordinary wires in the velocity range 0 to 200 ft/sec. The use of this instrument for time-varying velocity requires electronic compensation and essentially constant fluid temperature.

The constant temperature anemometer uses the same basic circuitry as the constant current device, except that the bridge unbalance signal is passed to a control amplifier which automatically adjusts the heating current in the wire (still on the order of hundreds of milliamps) to restore the bridge to balance. Thus, as long as the amplifier is able to bring the bridge near balance, the resistance is maintained constant, and the current in the hot wire is a direct measure of the stream velocity at any time (when interpreted by King's Law).

RESISTANCE THERMOMETER

The resistance thermometer also consists of a fine wire immersed in a gas (although the wire must be finer and the gas cleaner than in the previous devices), a bridge, a power supply (constant current source), a calibration methodology, d.c. amplifiers, and a display device. As the temperature of the gaseous medium changes, the fine wire tries to remain in thermal equilibrium with the gas; as its temperature changes, its resistance changes in a well known fashion. The resistance changes cause a change in bridge unbalance (the bridge never need be in exact balance), and this voltage is amplified, displayed, and recorded. Since the wire is very small, its thermal inertia is small. It is insensitive to gas velocity except insofar as greater gas velocities increase the convective heat transfer to the wire, enabling it to remain in closer thermal equilibrium with the gas. The electrical current through the wire must be so small as to make the energy dissipation through I^2R losses negligible. It is in this respect, the power dissipation in the wire being negligible and the device being insensitive to King's Law, that the resistance thermometer differs from the hot wire anemometer. The wire is not "hot" as viewed by its environment.

Circuitry

A simplified circuit diagram for the resistance thermometer

is presented in Fig. 7. The bridge, whose unbalance is displayed and recorded, is an equal-arm constant-current bridge.

As the input impedance of the amplifiers and oscilloscope is on the order of 100 megohms, negligible current flows in the output circuit. The nominal wire resistance and dummy arm resistance are about 10 ohms, while the upper arms are 47,000 ohms each; all resistors are 1% low-noise film resistors, and all pots are wirewound. The dummy and transducer arm currents are fixed by the 47K arms and the bridge voltage, and are held constant at a maximum of 0.491 ma (compared to hundreds of ma for an anemometer). Since wire resistance varies linearly with temperature in the range 0°F to 800°F, it is apparent that a change in bridge unbalance is very closely proportional to a change in wire temperature. With proper scaling, calibration, and amplification, the displayed signal may be taken for wire temperature. If the wire is small enough for the highest important harmonic of the gas temperature fluctuation, the displayed signal can be taken as gas temperature.

During calibration and set-up, switching transients in the probe current were thought responsible for a rash of wire failures. A ten-turn 300K ohm rheostat was installed in series with the power supply and bridge; bridge voltage could be continuously varied from 1.8 to 22.4 volts, and all subsequent switching was done at the lowest voltage.

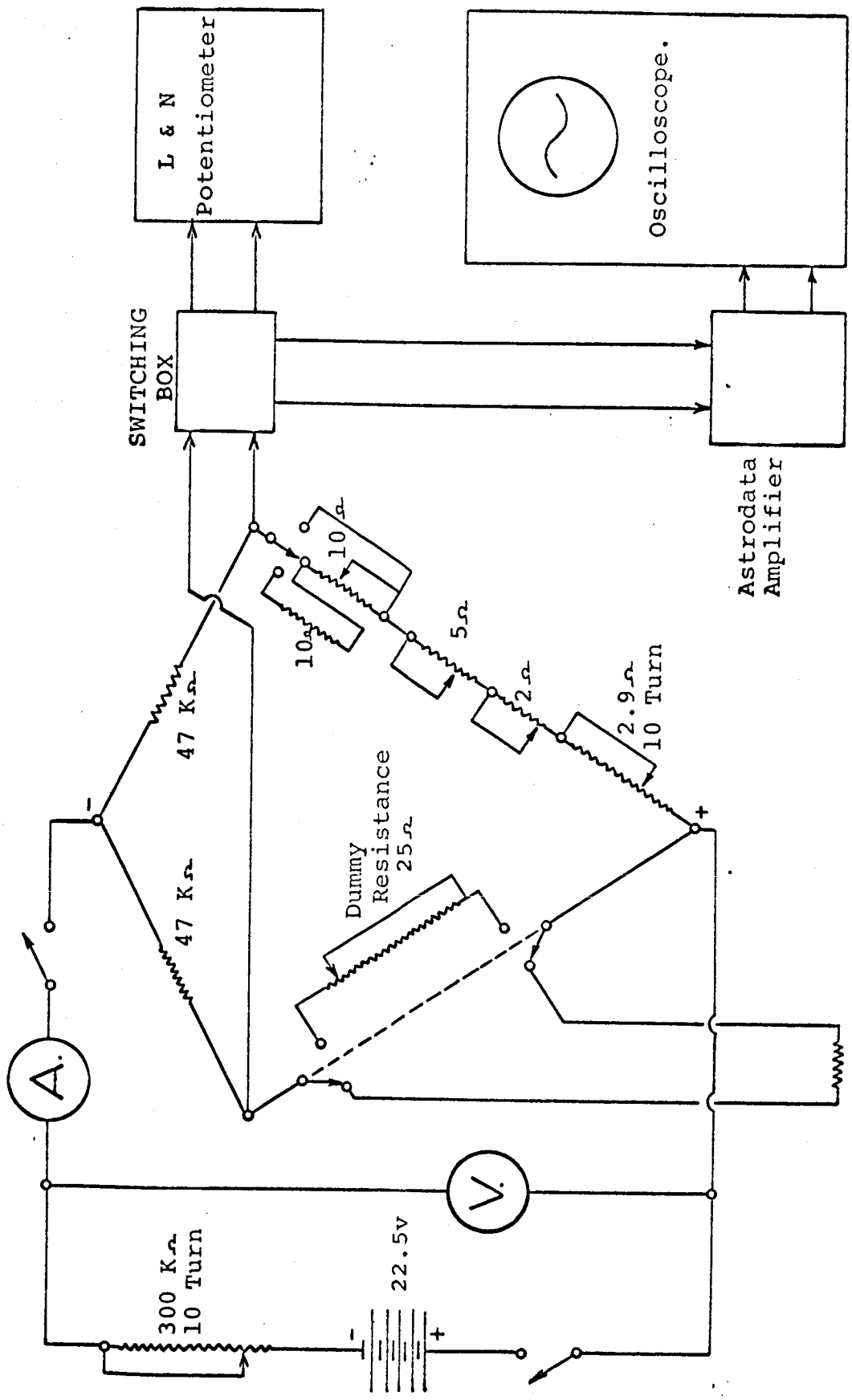

Fig. 7 Resistance Thermometer Circuitry

All data were taken with full 22.4 volt bridge voltage. Problems with switching transients were also noted by small-wire experimenters in England, and essentially the same solution was employed.

Fabrication

Small diameter resistance wires have been used by experimenters in "homemade" resistance thermometers for the study of low frequency transients in gas temperature for over 90 years. The major drawback to using this type of instrument has been its fragility, since extremely small wires must be used to provide a high enough frequency response. In very recent years, very small wire hot wire anemometer probes have been available commercially, but they are generally designed for use in the study of fluctuating fluid velocities at constant temperature. No other experimenters are known to have applied these probes to the study of fluctuating gas temperatures.

Since anemometer probes are available in wire diameters in many steps from five microns (one micron = 10^{-6} meters) to less than one micron, in tungsten, platinum, or platinum/10% rhodium, and in various probe styles, they seem to be natural transducers for the study of changing gas temperatures at a point. However, there are a number of distinct disadvantages and limitations to their use in this application:

1) The environment must be clean and free from oil droplets, dust, or condensed phases.

2) Local velocities may not exceed a few hundred ft/sec. (see Appendix B), the mean temperature should not exceed about 300°F, and peak temperatures should not exceed about 800°F.

3) Initial cost is in excess of $50 per probe, with a $20 average for wire replacement.

4) It is difficult to seal the probe bodies against compression pressures above 200 psi.

5) Wire length is short and electrical resistance is very low, making the design of a satisfactory bridge difficult.

To counter these difficulties, it is sometimes necessary to design a custom resistance wire mounting to the system specifications.

The custom wire mountings initially used in this project were constructed on a half-inch thick, one-inch diameter cast iron instrument plug with a 1-14 UNF thread. Fig. 8 shows two views of such a plug with a centrally located 2-56 UNC threaded hole for a surface thermocouple. The resistance wire used is Wollaston process wire; this wire is supplied as a one mil (25.4 micron) silver wire with a one to five micron core wire of platinum/10% rhodium. The silver sheath is etched away after mounting, leaving the precious metal core as the active resistive element. Two 20 gage constantan wires were used with a 3/8 to 5/8 inch spacing as wire supports. Constantan was used because it has low thermal conductivity and heat capacity while retaining high electrical conductivity.

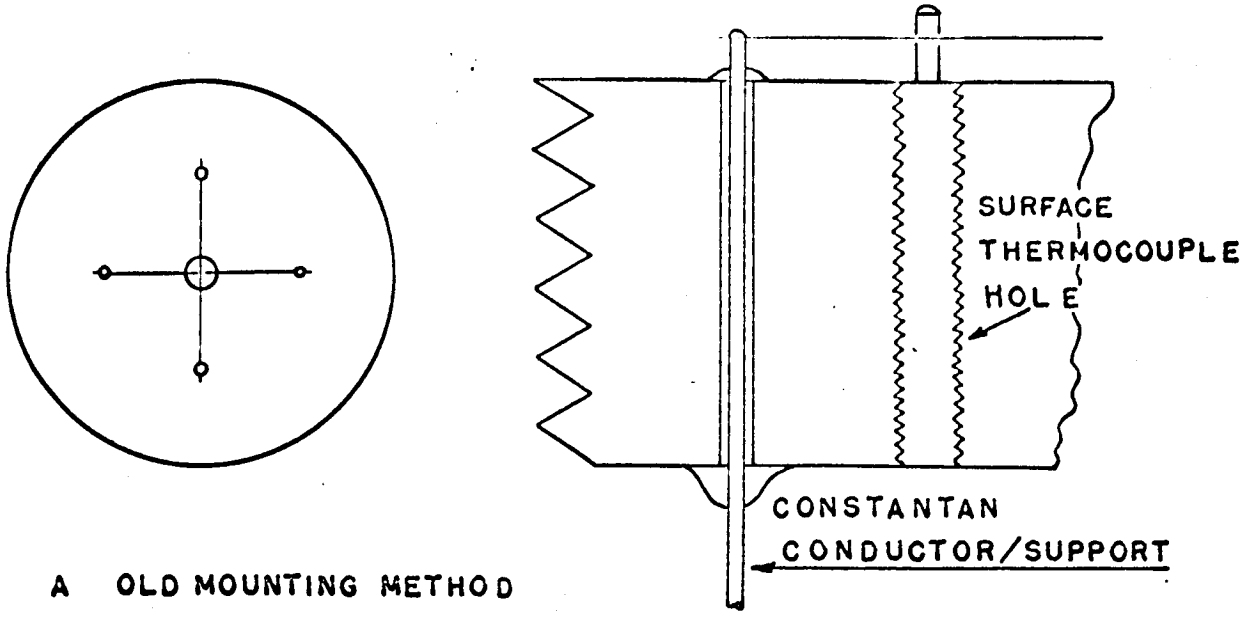

A OLD MOUNTING METHOD

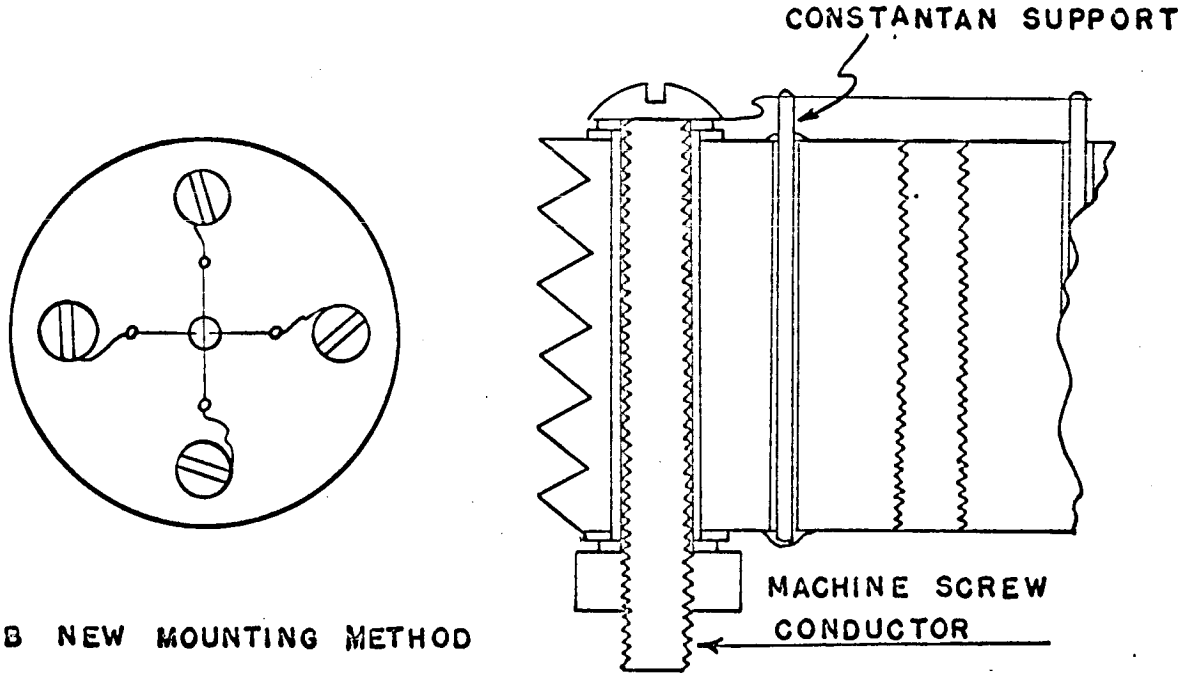

B NEW MOUNTING METHOD

FIG. 8 HAND-MADE INSTRUMENT PLUGS

The most difficult problem in probe construction is making a rigid, electrically conductive, low heat capacity connection of resistance wire to supports. If the resistance wire diameter is less than .0005 inches (12 microns), it is practically impossible to solder, spotweld, or otherwise effect a satisfactory metallic bond of wire to constantan support because the wire is easily melted. Cold solder joints tend to soften under high compression temperatures, and flux flows along and coats the wire. Silver solder joints were attempted using the smallest torch commercially available*, with a butane-oxygen flame 1/2 millimeter by 1 millimeter; the wires melt or deform at the conditions required to melt the solder. In recent years, micromanipulative and microwelding equipment capable of handling wires as small as one micron has become available. This equipment is used by commercial suppliers of hot wire anemometer probes; it is, however, very expensive and requires a talented and patient operator.

Silver-impregnated epoxy resin* (designed for use in printed circuit board repair) was used for a time by the author to hold the wires to the supports, but the epoxy resistivity is quite high, and the epoxy joint constituted a very high resistance (about 400 ohms) in series with the active length of wire (3 or 4 ohms). As this series resistance was temperature-sensitive and the silver impregnation des-

*See List of Manufacturers and Addresses

troyed most of the bonding power of the epoxy, the resistance thermometer performance was erratic; this bonding method was therefore discarded.

The best solution for the mounting problem was later corroborated by a private communication with G. J. Schott, associate of B. H. Schultz*, dean of resistance thermometer experimenters. Fig. 8B shows the construction of an instrument plug incorporating the solution. The wire is stretched and suspended, with its silver sheath intact, over the plug and its constantan support posts. The assembly is held on a special jig on the stage of a Leitz stereoscopic microscope. The wire is lowered until it is stretched across the centers of the constantan post tops and is placed under moderate tension. This is done because the core wire is kinked slightly inside the silver sheath. Using fine dental tools and a 50x gain on the microscope, insulating household two-component epoxy is daubed onto the wire-support junctions and allowed to dry and harden for 24 hours. The wire excess outside of the active length between the support posts is wrapped around two 2-56 brass machine screws which serve as electrical

*Schultz was a brilliant physicist and experimentalist employed by Phillips in Holland. According to G. J. Schott, Schultz straightened his wires and reduced their diameters by rolling them between glass slides separated at one end by a gramophone needle. The wires were used in Stirling cycle devices using air and light gases as working fluids.

terminals. Thus the constantan posts serve only as mechanical supports and to define the active length, and the machine screws carry the electrical signal. Wire slack is allowed between support post and screw, and the screw is tightened down and sealed with nonconductive epoxy. After this seal dries, the etching operation can commence.

As mentioned earlier, the wire is mounted in the form of a small platinum/10% rhodium core inside a silver sheath. The silver is etched away with a drop of dilute nitric acid: a 40% H_2O / 60% HNO_3 mixture worked best and provided an etching time of 25 to 35 seconds. During the entire mounting and etching operation, the central surface thermocouple was replaced with a steel 2-56 machine screw. As the etching mixture also attacks constantan, cast iron, and epoxy, it is necessary to protect these surfaces with a non-etchable coating. Schultz used nail polish. The author used paraffin, which was applied with a small, heated, hollow brass tube to the support posts, epoxy joint, and in a circular "wall" which defined and concentrated the etching droplet. One or two drops of etch mixture are applied with an eye-dropper; the etching action is watched through the stereo microscope. A skin of paraffin forms on the etch droplet and will grip the wire and tear it from the supports when the etchant is drained away. This skin is dissolved by adding 1/2 drop of xylene to the nitric acid mixture at the end of the etching period. The fluid is

then quickly removed with a 25 gage hypodermic needle. The surface is flushed with two or three drops of distilled water and the protective paraffin is dissolved with drops of xylene. Residual paraffin is removed with curved dental tools; this is a very delicate step.

Using this technique, over a dozen probes were constructed with wires from 1/8 inch to 5/8 inch long and penetration depths of 1 to 5 millimeters. Several multiple mounts were made with wires parallel or crossing at different penetration depths. One plug was constructed in which the penetration depth could be continuously varied from near zero to 5 millimeters.

Platinum Plating Technique

A possible alternative to the fragile small wire was a platinum-plated quartz wire. According to a monumental work by H. H. Lowell and N. Patton (50), under certain conditions of frequency and geometry a solid cylinder of insulating material with a thin metallic coating will have a frequency response superior to a solid metal wire of the same size.

Quartz fibers of .0004 inch (9 micron) diameter were obtained from the General Electric Company*. These filaments have a tensile strength in excess of 500,000 psi and could

*See List of Manufacturers and Addresses

be mounted by silver soldering at 1100°C.

A plating solution was obtained* which contained organic gold and platinum compounds in a solution of volatile oils. When fired at 1022°F, the solution will coat a fuzed quartz fiber with a 97% pure conductive film 0.000005 inches (0.1 micron) thick with a resistivity of 35 micro-ohms/centimeter.

Preparations were underway to attempt the difficult mounting and firing operations when it was discovered that a manufacturer of anemometer probes had the capability of constructing probes in which the wire was replaced by a 25.4 micron hollow glass tube with the fired precious metal coating 0.5 microns thick. As this size tube would significantly disturb the flow patterns and hold a large boundary layer, inquiry was made whether the firm** could construct a probe with a 10 micron or smaller tube. After lengthy consultation, it was determined that the number of fired coatings required to produce a reasonable thickness of metal increased inversely as the square of the diameter and became unreasonable at 20 microns and smaller.

The basic principle of this type of system is that at high enough frequencies the core becomes thermally dissociated from the coating and remains at constant temperature; the

*See List of Manufacturers and Addresses

**ThermoSystems, Inc.: see List of Manufacturers and Addresses

thin conductive coating follows the environment temperature. At lower frequencies the entire laminated cylinder responds as a solid wire (i.e., very slowly). The Lowell reference (50) previously mentioned indicated that for the geometries commercially available, the core material would not dissociate itself thermally below 100 cps (6000 rpm); for these reasons the coated quartz fiber probe was not used.

Phase Lag and Attenuation

This discussion will restrict itself to very small wires (.001 inch and smaller) under the condition of negligible self-heating. When a small wire is exposed to a gas whose temperature is changing, the thermal inertia of the wire and energy absorption and liberation in the boundary layer surrounding the wire will prevent it from exactly following the temperature change. The wire will tend to lag in time (a phase lag) and experience a smaller temperature swing than that of the driving potential (an amplitude attenuation). The smaller the wire for a fixed environmental history, the smaller the boundary layer around it, the lower the inertia, and the smaller the phase lag and amplitude attenuation. It was the intention of the author to use smaller size and faster response instruments than previous investigators, since the methods of compensating for lag and/or attenuation are on the whole not very satis-

factory.

An interesting comparison of resistance thermometer and infrared detector (see page 39 for description of the latter) was presented by H. J. Wienke (51) of the University of Wisconsin. Wienke compared infrared null method gas temperature data of K. C. Tsao and co-workers (52), taken in an unfired CFR diesel engine, with his data, also taken in a CFR head and crankcase with tungsten wire sizes from .001 inch to .00015 inch. Wienke extrapolated peak cycle temperature and peak crankangle linearly with wire diameter, taking the infrared null data to represent a zero diameter wire. This linear extrapolation suggested that the finest size resistance wire tested attenuated the peak gas temperature by about 150°F and lagged the peak crankangle by some five or six crankangle degrees.

Several objections may be presented with regard to the Wienke data and its interpretation. Objections to the infrared null method on the basis of long path length errors are noted elsewhere in this document. The signal is integrated along the entire path length, which includes two cooler boundary layers. Comparison of the "weighted" gas temperature with a locally measured gas temperature must be made with caution.

In the second place, all the data were taken with tungsten wires in an unmodified CFR compression-ignition engine with

oil-lubricated cylinder walls and crankcase. Experience shows that within a few dozen cycles from starting motoring, the air contains minute oil droplets and the metal surfaces of the compression chamber are covered with an oil film. This oil accumulation was the primary cause for the very small wire breakage noted by the experimenter; Schultz (40) had similar troubles during experiments in a Stirling cycle device. The effects of oil and dirt accumulation on the wire are noted by H. P. Grant (53) in an American Society of Mechanical Engineers presentation on anemometry:

> "Foreign matter in the flow gradually accumulates on a hot wire and ultimately changes its calibration (and response) by altering the heat transfer rate. ...At high (fluid) velocity the heat transfer rate is always reduced. ...Without air filtering, cleaning will be required every few hours at velocities below 100 ft/sec., but may be required every few minutes at a velocity about 400 ft/sec. to avoid large corrections for dirt (and oil) accumulation. Tungsten wires must be cleaned with...$K_2Cr_2O_7$ saturated with H_2SO_4." (parentheses added)

With reduced heat transfer rate the dynamic response of the wire is reduced: lag and amplitude attenuation are increased. Thus, wires in a dirty or oily atmosphere will experience response difficulty.

A final consideration is that extrapolations of peak temperature and crankangle should not be made linearly with wire diameter. The classical wire time constant varies with the square of the diameter; the variation of mean heat transfer coefficient about the wire with diameter must also

be taken into account. Based on data presented by Schultz (40) and conversations with several professional persons knowledgeable in small wire work, the index 1.7 was chosen as more appropriate. When Wienke's original data is extrapolated with respect to $d^{1.7}$, a phase lag close to one crankangle degree and amplitude diminutions of 20 F° (at 600 rpm) and 30 F° (at 1200 rpm) are suggested for the 3.81 micron tungsten wire. This is much closer to analytical predictions of lag.

If a wire is in equilibrium with an environment at temperature T_0 and the environment suddenly steps to T_1, then if we ignore capacitance in the boundary layer about the wire and assume the film coefficient to be a constant, the wire temperature at any time is:

$$T = T_1 - (T_1 - T_0) \exp(-hA\tau/Wc) \qquad (5)$$

and the time constant of the wire is:

$$\theta = Wc/hA \qquad (6)$$

where W is the weight of the wire,
c is the specific heat of the wire material,
h is the film coefficient, and
A is the wire surface area.

If we take h as the wire diameter-dependent value calculable from Schultz' (40) data, and define the phase lag as the time period for 63.2% response of the wire, then Fig. 9 gives the phase lag of a platinum wire. These calculations ignore capacitive storage and pressure work

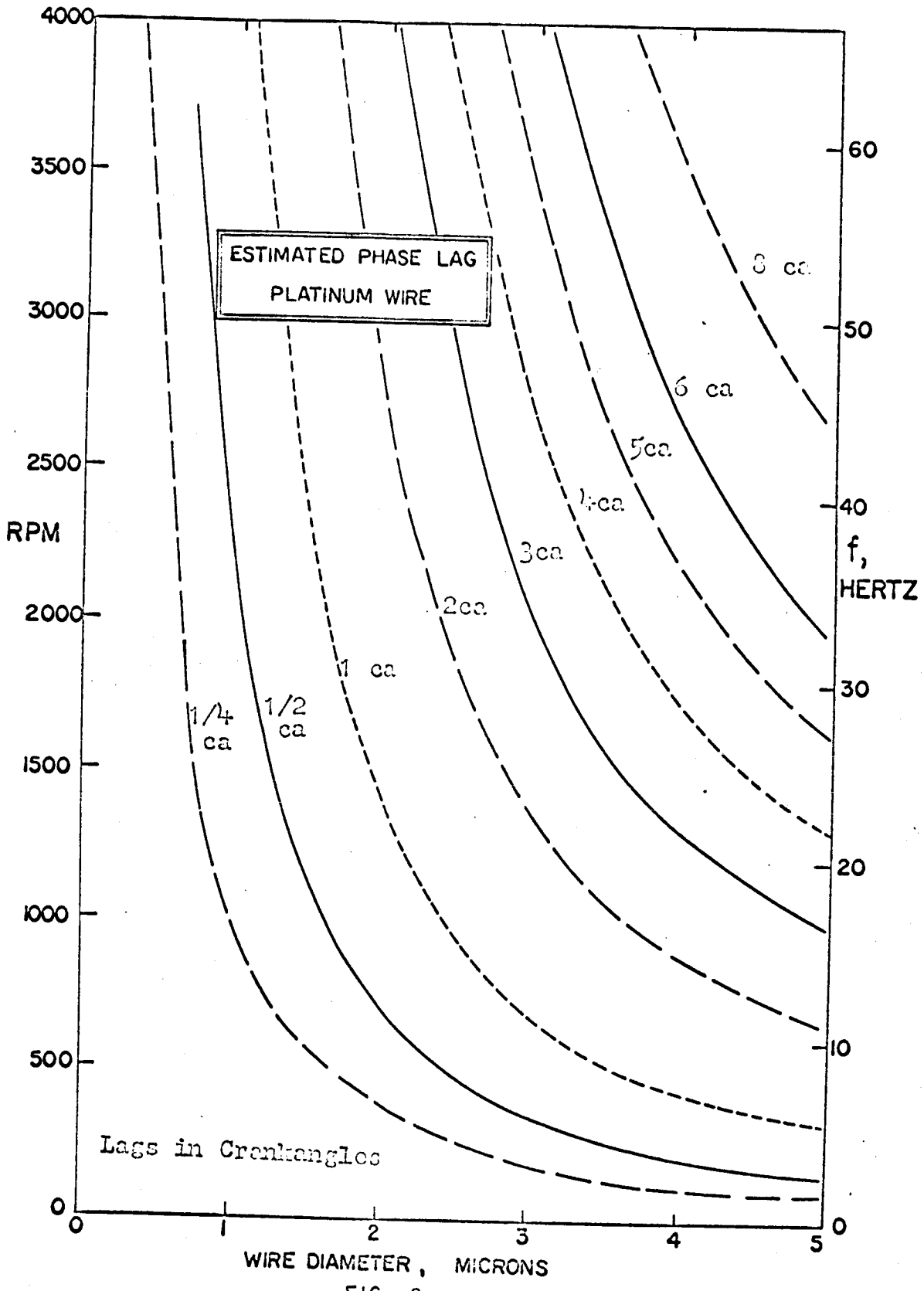
ESTIMATED PHASE LAG
PLATINUM WIRE
1/4 ca
1/2 ca
1 ca
2ca
3ca
4ca
5ca
6 ca
8 ca
Lags in Crankangles
RPM
f, HERTZ
WIRE DIAMETER, MICRONS
4000
3500
3000
2500
2000
1500
1000
500
0
60
50
40
30
20
10
0
1
2
3
4
5

FIG. 9

in the wire boundary layer, and should be taken as an approximate guide only. The analogous plot for tungsten is little different from Fig. 9.

Self-Heating of Wire

It is fundamental in the operation of constant current and constant temperature anemometers that the wire dissipate relatively large I^2R losses to its environment in order that King's Law might be used to calculate the local fluid velocity. The ideal resistance thermometer, however, would exchange no energy with the gas (and consequently the difference $[T_{wire} - T_{gas}]$ would be zero). Since a small current must pass through the wire for sensing purposes, it is necessary to set an upper current limit at which the self-heating is no longer insignificant. Typical operating conditions with a D.I.S.A. 55A35 subminiature probe are as follows:

Diameter of wire = 3.81 microns
Length of wire = 2 millimeters
Resistance of wire = 3 ohms
Mean film coefficient = 30 Btu/hr.°F.ft^2

The last figure represents a conservative estimate of the mean film coefficient around a very small cylinder under compression or expansion gas velocities. The wire area available to dissipate heat is:

$$\text{Area} = \pi DL = \pi(3.81 \text{ microns})\ (2\text{mm}) = 2.58 \times 10^{-7} \text{ft}^2.$$

If we allow a maximum wire-to-gas temperature differential of 1 F°, the maximum allowable energy flux is:

$$\text{Power} = hA(T_w - T_g) = (30)(2.58 \times 10^{-7})(1)/(3.413 \text{ Btu/watthr})$$

$$\text{Power} = 2.26 \text{ microwatts}$$

This means:

$$I_{max} = \sqrt{\frac{P}{R}} = \sqrt{\frac{2.26 \text{ microwatts}}{3 \text{ ohms}}} = 0.87 \text{ ma} \qquad (7)$$

Since our wire current was limited to .48 ma, we have operated within the allowed limit. Under the specified conditions, a current of 0.48 ma would produce a temperature rise of 0.3 F°, a negligible amount compared to a 600 F° gas temperature swing.

Strain Gage Effects

So-called strain gage effects could in principle occur when high fluid velocity causes the wire to bow between its supports. Stretching of the wire would cause its resistance to change; this would look to the electronics like a fluid temperature change.

Weske (54) discusses this effect and suggests that in past experience it has caused little trouble. The fundamental strain gage relation is:

$$\frac{\Delta R}{R_0} = GF\left[\frac{\Delta L}{L_0}\right] \qquad (8)$$

Weske uses a Gage Factor of 1.7 for tungsten and 2.15 for cupronickel; we will take a general GF of 2.5 as a conservative estimate. Deflections observed under the microscope while the probe is exposed to a high velocity air stream suggest a $\Delta L/L_0$ of at most two or three percent. With formula (8) above,

$$\Delta R/R_0 = (2.5)(.03) = .075$$

In a typical data run, the wire temperature swing is on the order of 600 F°. With a temperature coefficient of resistance of .0039 ohms/ohm C° for platinum, the wire resistance swing during a data cycle would be calculated as follows:

$$R(T) = R_0 + R_0\,\alpha(T - T_0)$$

$$\Delta R = R(T) - R_0 = R_0\alpha\Delta T$$

$$\frac{\Delta R}{R_0} = \alpha\Delta T = (.0039/C°)(600F°)(5C°/9F°)$$

$$\frac{\Delta R}{R_0} = 1.60 \qquad (9)$$

Thus the predicated strain gage effect would be less than 5% of the total resistance swing. Experimentally, when the probes were exposed to a jet of 70 psi air exhausting through a .07 inch diameter hole, no perturbations in the bridge output signal could be observed.

According to Weske, a resonant vibration in the wire is

typically started and maintained by the flow, with accompanying cyclic stresses. The frequency of this wire vibration has been experimentally determined to be:

$$f = 0.22\ V_n/d \qquad (10)$$

where V_n is the normal component of stream velocity, and d is the wire diameter in feet.

For an engine with V_n on the order of 100 ft/sec and with 3.81 micron wire (the size most frequently used), the frequency of the vibration, and of the cyclic stress, is 1.8 megaHz. The frequency response of the D.C. amplifiers is such that this signal will be greatly attenuated and will cause no trouble.

Other Considerations

Three other considerations periodically mentioned in the literature pertaining to small resistance wires are aging, wire support end effects, and slip flow conditions.

Aging of the wire means changes in its room temperature resistance due to grain growth, grain boundary changes, and inelastic stretching during the high-temperature portion of its operation. This effect is relatively long-term and is compensated for by recalibration of the wire prior to each data run.

Wire support end effects refer to the influence of the

wire supports as heat sinks on the surrounding fluid. Aftalion (55) claims that fine wire butt-welded thermocouples are five times as sensitive to end conduction effects as are resistance thermometer wires. This effect is deemed negligible for wire L/d ratios in excess of certain somewhat arbitrary limits. Hunt (56), as reported by Meyer (57), calculates a conduction error of less than 1% with an L/d of 52 and "heavy lead wire" supports. Grant (53) gives a lower limit of 100 for small, pointed supports; Thermo-Systems, Inc. (58) states that an L/d of at least 400 is common. For larger support sizes, Schultz (40) maintains an L/d of 2000. An outline of these considerations is given by references 59 and 60. For two styles of Wollaston wire probes, the author fixed the ratio at 1900 and 3200; for the D.I.S.A. 55A35 anemometer probes it was 524, removing support end effects from consideration.

One must consider the possibility of slip flow occurring for very small wires, since a transducer in the slip flow or transition regions will not see its environment as a continuum. According to Otis (61), the transition, slip flow, and "continuum" regions could be approximated by the limits:

$$\text{transition flow:} \quad 0.1 < \frac{d}{\lambda} < 10$$

$$\text{slip flow region:} \quad 10 < \frac{d}{\lambda} < 100 \qquad \text{(11 A,B,C)}$$

continuum region: $100 < \frac{d}{\lambda}$,

where d is the significant transducer dimension (i.e., wire diameter) and λ is the gas molecule's mean free path. A convenient approximate formula for λ is:

$$\lambda \text{ (in centimeters)} = \frac{5}{P \text{ (microns Hg)}} \quad . \qquad (12)$$

Then over a range of 20 psi to 400 psi the gas mean free path varies between 0.048 microns and 0.002 microns. The d/λ ratio for the 3.81 micron wire used varies from 80 to 1600. Thus on the whole the flow past the wires used was continuous; however, for smaller wires and/or lower pressures, care would have to be taken in interpreting the data.

MULTIPLE WIRE METHODS

In an attempt to circumvent the problems of phase lag and amplitude errors caused by wire and boundary layer inertia, some experimenters have proposed multiple wire schemes in which simultaneous temperature measurement with two or more transducers of differing inertia would yield a solution for instantaneous gas temperature.

Pfriem (62) made use of energy considerations in an early work to correct the temperature indications of several sizes of resistance thermometer. Rounthwaite (63) em-

ployed a two-wire resistance thermometer in the study of temperatures in explosions of gases.

Aftalion (55) of Sulzer used two very large (50 and 100 micron) butt-welded thermocouples to study exhaust gas temperatures in a huge stationary diesel engine. Recording his data on a Siemens Oscillograph (the frequency response of that instrument must have restrained the useable cyclic frequency of the engine to a few hundred rpm) and correcting for radiation, convection, and capacitive inertia by means of a nomograph, Aftalion came up with some unusual calculated gas temperatures. A sample of his calculated and measured temperatures is reproduced at right.

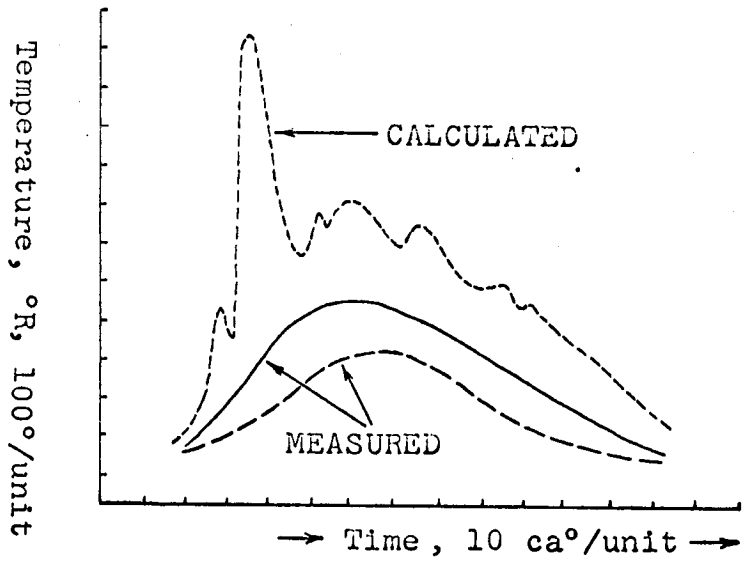

AFTALION DATA

According to Aftalion, because of the combustion, "a fine deposit of soot is expected (on the wires) after a very short period of operation". This soot will increase the local heat transfer coefficient and the area available for convection (see page 56

for the effect of dirt and oil on calibration); this effect was not considered by Aftalion.

Aftalion measures wire temperature swings of 245 F° and 380 F° with the two large wires and from the slopes of these data computes a gas temperature curve with a swing of 930 F°. An accuracy figure of 2% is claimed, and various physical interpretations are given the oscillations in the computed curve.

A simplified two-wire technique is advanced by W. E. Meyer (57) in the Society of Automotive Engineers Transactions. Equating the convective heat transfer to a thermocouple wire to its rate of change of internal energy, for each of two thermocouples, A and B (subscripts),

$$(\rho cd/4)(T' - T) = h(T_{gas} - 1/2[T' + T])\Delta\tau \qquad (13\ A,B)$$

where ρ is wire density,
c is wire specific heat,
d is wire diameter,
h is the film coefficient of heat transfer,
T_{gas} is the average gas temperature for the period $\Delta\tau$, and
T, T' are junction temperatures at beginning and end of the time period $\Delta\tau$.

This equation is reproduced here because the many printing errors in the Transaction version may cause confusion. Designating the two thermocouples by the subscripts A and B, we write Nusselt's expression for each thermocouple:

$$\left[\frac{hd}{k}\right]_A = \left[\frac{\rho V d}{\mu}\right]_A^n \left[\frac{c_p \mu}{k}\right]_A^m \tag{14}$$

$$\left[\frac{hd}{k}\right]_B = \left[\frac{\rho V d}{\mu}\right]_B^n \left[\frac{c_p \mu}{k}\right]_B^m . \tag{15}$$

Taking the ratio of these relations to eliminate common, but unknown gas properties, we get:

$$\frac{h_A}{h_B} = \left[\frac{d_B}{d_A}\right]^{1-n} \tag{16}$$

Combining Eqn. 16 with Eqns. 13 A, B, and solving for gas temperature, we get an expression for gas temperature as a function of the unknown n and a number of known quantities:

$$T_{gas} = f(n). \tag{17}$$

Meyer proposes to solve for the unknown T_{gas} from among the <u>four</u> unknowns T_{gas}, h_A, h_B, and n with the simultaneous solution of <u>three</u> independent equations (note that [17] above is not independent):

$$h_A = f_1(T_{gas}) \qquad \text{(or Eqn. 13A)},$$

$$h_B = f_2(T_{gas}) \qquad \text{(or Eqn. 13B)},$$

$$n = f_3(h_A, h_B) \qquad \text{(or Eqn. 16)}.$$

The technique given is to assume an n (aided by values from McAdams' book [64], which are based on early data of L. V. King, the formulator of King's Law of Anemometry), calculate a T_{gas}, solve for h_A and h_B with Eqns. 13 A, B, and verify the assumed n with Eqn. 16. This calculation is clearly not possible; any choice of n at all will work equally well. Even then, it is not clear that the Nusselt relation, measured in steady-state gas flow, is valid for cylinders only a hundred times a mean free path in diameter in a very unsteady gas environment.

Somehow using this method, Meyer calculates a smooth gas temperature from data taken in a motored diesel engine at 100 and 150 rpm and finds it to be only a few degrees above the indicated thermocouple temperatures at top dead center for 20 and 13 micron thermocouple wires. At these frequencies (less than 3 Hz) the thermocouple errors are so small (3% at most) that the correction, regardless of how it was obtained, is trivial, and does not affect the validity of the conclusions Meyer drew from the data.

A three-wire method expounded by Benson is being used by G. A. Morgan (65) of the University of Adelaide in Australia in a work similar to this one. Benson's differential equation reduces to:

$$T_{gas} = T_{wire} + d^{2-m} \left(\frac{dT_{wire}}{d\tau}\right) \left[\left(\frac{\nu_g}{V_g}\right)^m \cdot \frac{\rho_w c}{4A\lambda_g}\right] \qquad (18)$$

with the various constants being evaluated from the three-wire data. Benson comments that d^{2-m} is not sensitive to small changes in m, as m is much smaller than 2. An extension of Benson's work by Daft shows that three wires enable m and all of the bracketed terms to be treated as unknowns and eliminated in the solution for T_{gas}.

Multiple wire methodologies generally depend on the slopes of experimental data and are subject to scatter; in addition, they ignore the capacitive and pressure work phenomena thought to exist in large-wire boundary layers and their effect on wire signal lag and attenuation.

In view of these uncertainties, multiple wire techniques were not used in this work, and emphasis was placed on obtaining repeatable signals from the finest diameter resistance wire possible, consistent with the requirement of moderate durability.

VI. CALIBRATION

PRESSURE RECORDING SYSTEM

The pressure pickup used was a Kistler 601H piezoelectric transducer. A Li-Draper catenary diaphragm (strain gage) pickup was originally used, but the Kistler diameter is less than that of the Li, and using it allowed more flexibility in instrument placement.

The Kistler pressure pickup was calibrated under static conditions in a dead weight tester and its output was found to be essentially linear over the range -11 psig to 600 psig; with an average output coefficient of 1.078 pcb/psi over this range, the transducer output was about 8% above the nameplate output of 1.000 pcb/psi. The pickup output was calibrated on the display by noting the zero gage pressure level on the oscilloscope before and after the data run with the charge amplifier in short time constant operation.

SURFACE THERMOCOUPLE

The surface thermocouple was calibrated as follows: placed in a lucite block which protected all rustable surfaces, the thermocouple was connected in series with a cold junction and a Leeds and Northrup potentiometer and was immersed in stirred distilled water of different temperatures from

0°F to 212°F. Fig. 10 shows the result of this calibration; the outputs were closely linear, and the most representative slope was taken to be .0298 mv/F° for iron-constantan thermocouples and .0170 mv/F° for iron-nickel thermocouples. Eleven thermocouples were calibrated, including four pre-1960 and four newly purchased iron-nickel thermocouples.

Knowing the thermocouple gain, d.c. amplifier gain, and Tektronix oscilloscope gain (individually and collectively calibrated), it was necessary to know the temperature at one time on the oscilloscope display or on an exposed drum camera film to fix all the head surface temperatures. Previous investigators used automotive breaker point assemblies connected to camshaft or other geared-down power takeoffs. In keeping with this philosophy, the author spent some time designing and constructing a similar assembly to run at the crankshaft speed and provide adjustable intervals in each engine cycle during which known voltages could be superimposed upon the various traces. Because this mechanism had to run up to 3600 rpm (as opposed to 800 or 900 rpm for previous CFR camshaft-driven setups), and because the present signal levels were very low, finding the signal amidst the noise was difficult.

A simpler technique suggested by G. Ebersole (66) was then adopted, wherein a Leeds and Northrup type 778746 potentio-

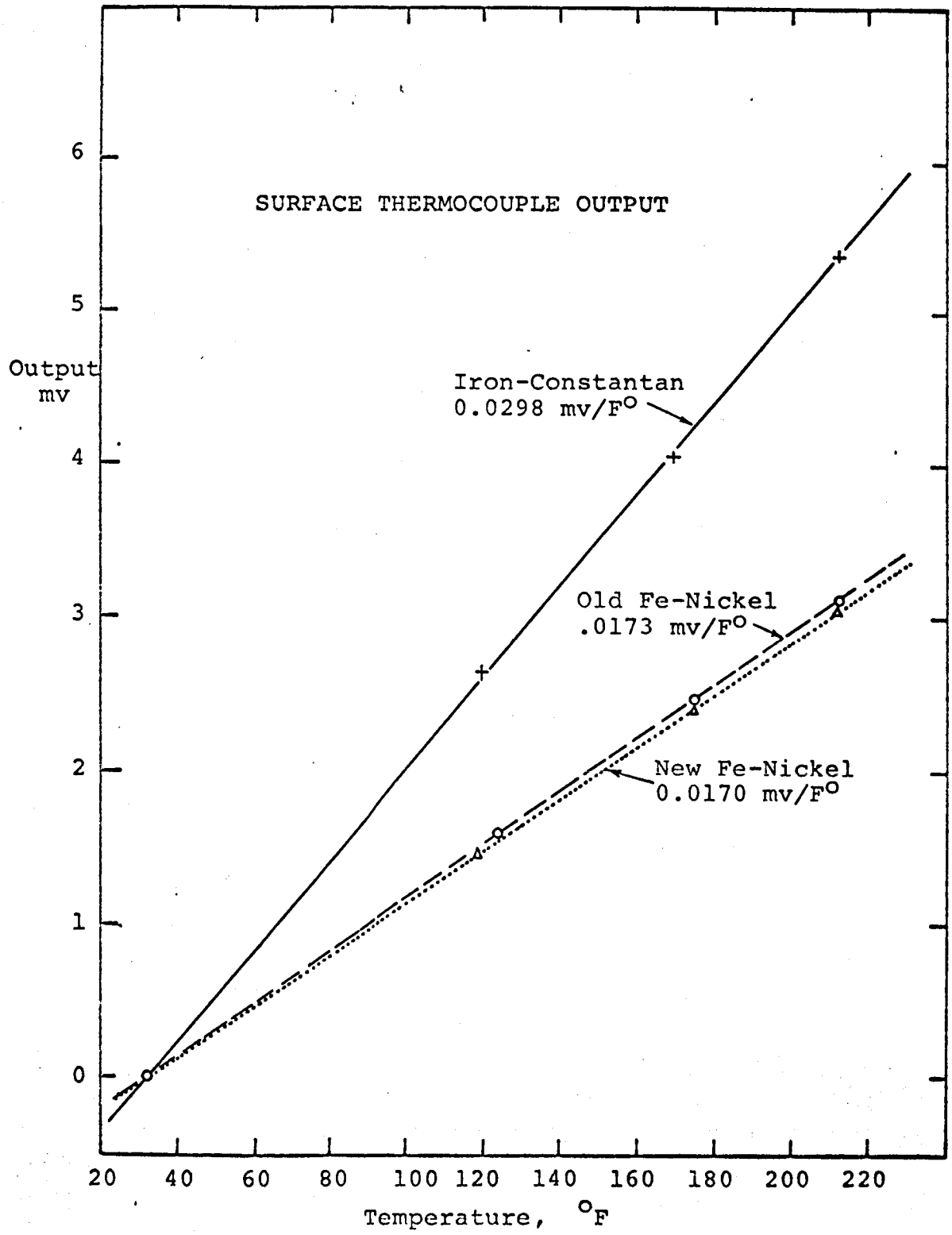

Fig. 10 Surface Thermocouple Calibration

meter was used to measure the time-averaged head surface temperature; this temperature was used as the first term in the Fourier breakdown of the surface temperature trace. This technique is much easier and faster to use than the previous method, and it doesn't require sending low level, high frequency signals through automotive breaker points, significantly improving the signal/noise ratio.

RESISTANCE THERMOMETER

The resistance thermometer calibration posed some problems. The probe was sealed inside the compression chamber with piston at bottom dead center and hot air was circulated about the cylinder and head from an external blower and bank of heaters, the air system of which is shown of Fig. 1. When the system had reached equilibrium at a known temperature, the bridge output for a given bridge voltage was recorded. Many times, however, an expensive resistance wire which could withstand compression and expansion heating and gas velocities would break under this gentle external heating. Greater success was achieved when the heating method was changed: hot air was blown through the makeup holes in the lower cylinder wall, across the wire, and exhausted through a port in the head. It is postulated that uneven wire support expansion snapped the wires in the previous method.

Fig. 11 shows bridge output as a function of wire tempera-

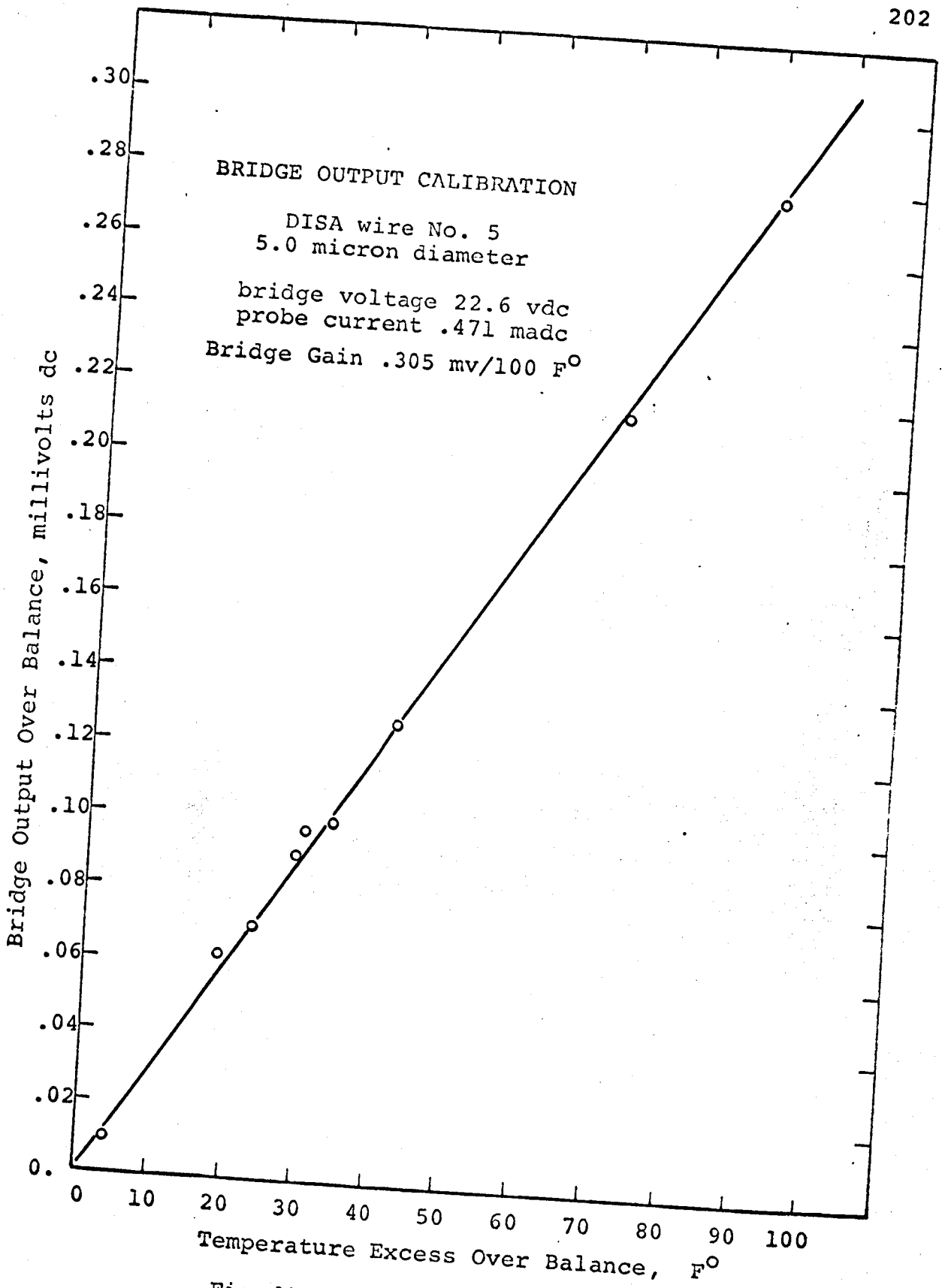

Fig. 11 Resistance Wire Calibration

ture for a typical D.I.S.A. probe; the relationship was linear through the 70°F - 190°F test range and was assumed to be linear over the whole range of operation.

Resistance thermometer output was calibrated on the display by noting the vertical location of the room temperature line on the oscilloscope just before operation and setting this abscissa equal to room temperature.